An Investigation on the Critical Degree of Saturation of Half Brick Samples via the Frost Dilatometry Methodology

by

Javeriya Hasan

Master of Structural Steel Design and Sustainable Development, Imperial College London, 2009

A Major Research Project

presented to Ryerson University

in partial fulfillment of the

requirements for the degree of

Master of Building Science

In the Program of

Building Science

Toronto, Ontario, Canada, 2019

AUTHOR'S DECLARATION

I hereby declare that I am the sole author of this MRP. This is a true copy of the MRP, including any required final revisions, as accepted by my examiners.

I authorize Ryerson University to lend this MRP to other institutions or individuals for the purpose of scholarly research.

I further authorize Ryerson University to reproduce this MRP by photocopying or by other means, in total or in part, at the request of other institutions or individuals for the purpose of scholarly research.

I understand that my MRP may be made electronically available to the public.

Abstract

An Investigation on the Critical Degree of Saturation of Half Brick Samples via the Frost Dilatometry Methodology

By Javeriya Hasan

Master of Building Science in the Program of Building Science 2019

An assessment of freeze-thaw deterioration of bricks necessitates predicting the moisture content at which frost decay occurs, whereby this is called the critical degree of saturation (S_{crit}). The study involved performing frost dilatometry testing of eight half-brick samples. Strains along the x, y and z axes of samples were measured, whereby the results show that trends of frost decay were non-uniform along certain axes. However, along the z-axis, brick sample types 305-EB4, 295A-F4, 297-EB2 showed S_{crit} values of 81%, 90% and 77.5% respectively, which were comparable to the slices' S_{crit}, which were at 84.4%, 88.1% and 77.5% respectively. Similarly, for brick sample type 349-ER1, the S_{crit} at its x-axis was 92%, which was near to its slice's S_{crit}, at 87.3%. Sample types 60 and 295-F2 showed differences as high as 17% in their S_{crit} values, at 56% and 88% respectively, compared to their slices, which were at 73.4% and 78.4%.

Acknowledgements

I would like to express my immense gratitude to Dr. Russell Richman for his guidance and support in my research endeavors. I would like to thank Dr. Randy Van Straaten for his overview on frost dilatometry testing of brick masonry. I would like to thank Mr. Greg Labbé, who has always been there to support me with equipment, supplies, and most importantly, I have been motivated by our brainstorming sessions on laboratory testing and the likes. I would like to thank Dr. Miljana Horvat for her feedback on a draft version of this report.

Finally, I would like to thank my parents, my sisters, Inam and Asher for being a constant source of motivation for me.

Table of Contents

List of Figures

List of Tables

List of Abbreviations

ASTM – American Society for Testing and Materials

A-value – Capillary water uptake coefficient

BET - Brunauer–Emmett–Teller

CSA – Canadian Standards Association

MIP - Mercury Intrusion Porosimetry

OP – Open Porosity

PSD – Pore size distribution

RH – Relative Humidity [%]

S_{crit} – Critical Degree of Saturation

SEM - Scanning Electron Microscopy

WUFI – Wärme und Feuchte Instationär (“Transient Heat and Moisture Transport”)

X-ray micro CT – X-ray micro computed tomography

1 INTRODUCTION

The 1970s global oil crisis propelled the need to re-evaluate the status quo approach on looking at energy consumption in the construction sector. There was a subsequent move towards energy efficiency, whereby policymakers looked at phasing out the reliance on fossil fuel for meeting heating and cooling needs in buildings. Much progress was made in the era between the 1970s and 1980s, where the industry focus shifted on the materials constituting the building envelope and how they could be made more robust and durable. In contemporary times, there has been increasing attention on the behavior of brick masonry under extreme exposure conditions. As a corollary to the global drive towards increasing energy efficiency in the built environment, many historical brick masonry buildings in cold climatic regions undergo envelope retrofits. In recognition of the need to preserve the architectural outlook of such buildings and simultaneously improve the performance of the building envelope, designers typically opt for introducing insulation on the interior side. Insulation on the exterior, on the other hand, would provide the benefits of reducing instances of thermal bridging and would effectively protect brick masonry from wind and rain events. Studies have now shown that adding insulation on the interior has the disadvantage of reducing the ability of the wall to dry inwards, resulting in the disruption of the moisture balance that previously existed (Straube, Schumacher, & Mensinga, 2010). This new wall condition, in turn, exacerbates the risk of freeze-thaw damage to brick masonry, as the internal moisture content may potentially increase beyond a threshold that the brick can sustain. Therefore, certain exposure conditions during the year may initiate the process of decay in brick masonry. It is important to understand that the porosity and pore size distribution (PSD) are critical determinants of the physical and mechanical attributes of brick masonry. These characteristics influence brick masonry resistance to weathering and freeze-thaw damage (Cultrone et al., 2004). It is now well understood that the current criteria on freeze thaw assessment is unreliable in the prediction of brick performance in-situ (Davison & Sereda, 1978). Litvan (1973) states that “no material can be inherently frost resistant”, whereby analogizing that to the concept of limit state design, a metric of critical degree of saturation (S_{crit}) that predicts the onset of failure in brick masonry has been proposed for the assessment of brick durability. The frost dilatometry methodology has become widely known as a reliable technique in ascertaining the S_{crit} point of porous materials such as concrete and brick masonry (Fagerlund, 1977). It is thus important to be able to predict the moisture content of bricks present in-situ, which is why in contrast to previous research that looked

at the determination of S_{crit} of brick slices, this study investigates the S_{crit} of a sample of half-brick specimens as well as discusses how the current approach to frost dilatometry testing could be adjusted to accommodate larger sized test specimens.

1.1 RESEARCH AIM AND OBJECTIVES

Based on the need to preserve the integrity of brick masonry walls, which are exposed to extreme exposure conditions, frost dilatometry testing is done to predict the onset of frost decay. Therefore, the aim of this research was to assess the freeze-thaw resistance of brick masonry by performing frost dilatometry testing of half-brick samples. This was accomplished with the following objectives:

1) Undertake a literature review on existing knowledge pertaining to the freeze-thaw deterioration of porous materials like clay brick masonry.
2) Conduct frost dilatometry experiments and produce experimental data pertaining to the response of test samples under predetermined exposure conditions (moisture content and freeze-thaw cycles).
3) Evaluate the evolution of resultant strains across the test conditions.
4) Infer the reasons behind the peculiar behavior of clay brick masonry under the considered conditions.
5) Make recommendations on improving the current approach to testing brick masonry.

Therefore, the scope of this MRP project was to determine the variation (if any) in the magnitude of the critical degree of saturation, S_{crit}, between slices and 'half-brick' sized specimens of historic bricks. The values of S_{crit} of brick slices were obtained from earlier tests; whereby, parts of the bricks that remained were selected for the project testing.

Eight samples of bricks from different locations in Location A and Location B in Ontario underwent testing that included drying, vacuum saturation, freeze-thaw cycling, and dilation measurements. The exact age of the brick masonry used in the tests in this study is currently unknown; given their texture and appearance, they may be assumed to date back to the GEO1800s. The incidence of strain in the brick samples (the threshold value being 100 microstrains) was reflective of the initiation of freeze-thaw damage in the brick samples, and the point at which this

occurs has been interpreted as S_{crit}. It is understood that the range of S_{crit} values obtained from testing varied greatly, maybe owing to the impact of physical properties and mineralogical composition peculiar to the type of brick considered, however this aspect of brick masonry durability has not been explored.

1.2 RESEARCH QUESTION

As a continuation of the frost dilatometry work undertaken by Mensinga (2009) and Williams (2015), literature review on the subject points to a dearth of research done on the determination of the critical degree of saturation, S_{crit}, of half-brick (or larger-sized) samples, which are typically 110mm x 86mm x 60mm. Owing to an understanding that larger-sized samples may contain a relatively more extensive network of pore spaces compared to brick slices, there may be differences in the way moisture distribution and storage occurs in former. It is inferred that this may potentially influence the point at which a sample deteriorates under certain exposure conditions. Therefore, considering the current approach to frost dilatometry, it is important to ascertain if the size of the test samples has a bearing on the S_{crit} metric or not. Similarly, the assessment of the critical degree of saturation of whole bricks in-situ can be better approximated with the determination of S_{crit} values of half-brick samples, which are relatively a better representation compared to slices. Based on earlier tests on slices (from a whole brick), results pertaining to the physical characteristics of the specimens were established. However, it was also important to understand if larger sized samples hailing from the original specimen produced the similar results when the same type of testing was performed on them. The following research question forms the backdrop of this study:

How do the values of critical degree of saturation of half-brick (or larger sized) samples differ (or not) from that of brick slices (~10mm thick)?

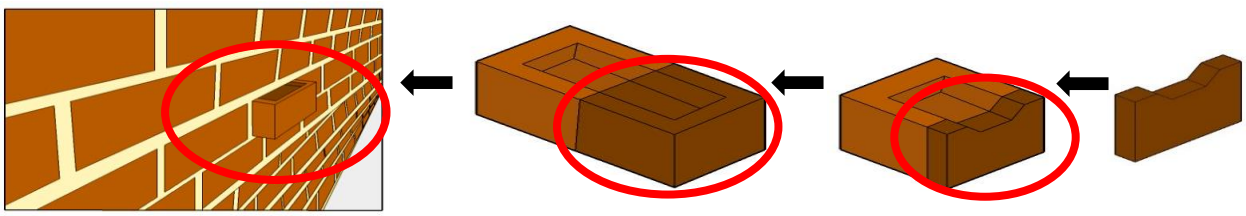

FIGURE 1-1: A SCHEMATIC SHOWING A BRICK WALL, WHOLE BRICK, HALF-BRICK AND BRICK SLICE AS THE BACKDROP OF THE RESEARCH QUESTION.

2 BACKGROUND

2.1 EXISTING STANDARDS VS THE CONCEPT OF S_{CRIT}

In 1977, Robinson and Holman investigated the relationship between the physical properties and durability of 5217 brick specimens. The methodological approach involved testing for the properties such as the "initial rate of absorption, room temperature absorption, saturation coefficient, freezing and thawing tests (*resistance*) and compressive strength" (Robinson & Holman, 1977, p. 1071). In order to determine the impact of the properties on brick durability, "statistical analyses" (p. 1072) were undertaken and this entailed establishing a discrimination factor, which was a value that helped ascertain if brick specimens were accurately assigned the pass-fail classification based on tested properties. According to Robinson and Holman (1977) the 'discrimination factor' is a ratio between the percentage of failed specimens due to a specific property against the percentage of passed brick specimens. The range of values for the 'discrimination factor' lied between 0 and 100, wherein 0 referred to there being no differentiation between "good and bad brick" (p. 1073) and 100 was "perfect selection" (p. 1073). The results showed that as per the durability stipulations in 'ASTM Standard C62 for Grade SW Building Brick', bricks that were durable were incorrectly rejected and vice versa. According to Robinson and Holman (1977), "the present specification is not very effective in discriminating between good and bad brick" (p. 1074) if the pass-fail criterion was based on the durability against a single property. However, it was found that a combination of properties such as <8% cold absorption and >55.2 MPa (8000 psi) compressive strength, were better indicators of the resistance to freeze thaw damage, such that the discrimination factor was greater in magnitude compared to <8% cold absorption only. Similarly, the saturation coefficient of 0.78 (as stipulated in the ASTM Standard C62) provided a better discrimination factor (i.e. a higher value) of 45.7%.

Similarly, in 1984, Crawford looked at the frost durability of clay bricks and relevant criteria that govern the overall quality and integrity of such materials. The study categorically emphasized that existing tests to investigate the performance of bricks were generally deemed unreliable (Crawford, 1984). With regards to CSA A82.1, Crawford (1984) pointed out that "although the saturation coefficient criterion (*which is a prescribed durability criterion mentioned in CSA*

A821.1) has some merit, it fails, by itself, to take into account the variation in the critical saturation coefficient from one raw material to the other" (p. 15).

In this context, it is also important to consider a case study by Anderson (1999) that investigated brick spalling on the exterior face of newly constructed walls in an educational facility in the USA. The research question was whether only one unique factor could be attributed to be the prime reason for the freeze-thaw deterioration of bricks. Three theories were proposed to explain the phenomenon of brick spalling: water ingress inside the building, the inadequacy of the type of brick used in the wall assembly and vapor pressure from inside the building. The methodological approach involved conducting a combination of field and laboratory investigations of the affected areas. Despite the conformance of bricks to the durability stipulations laid out in ASTM C-216, additional laboratory testing on half brick samples under freeze-thaw conditions indicated that they had failed. The study concluded that brick spalling was more pronounced at certain parts of the building than others, due to a combination of several factors i.e. poor workmanship, water ingress through multiple points, vapor pressure from inside and treated bricks unsuitable to be used in that climate. Based on the results, Anderson (1999) recommended that conformance to ASTM C-216 is not enough to select bricks for wall construction, whereby they need to undergo freeze-thaw cycling tests to assess their suitability for use. Albeit being a case-study only, this brought to light the importance of testing for freeze-thaw resistance in bricks to ensure their integrity under field conditions.

Currently, durability assessments of brick masonry involves meeting performance criteria stipulated in ASTM C62-17, ASTM C216-07a, ASTM C67- 19 and CSA Standard A82- 06 (Straube et al., 2010). ASTM C62-17 is the Standard Specification for Building Brick (Solid Masonry Units made from Clay or Shale); ASTM C216-07a is the Standard Specification for Facing Brick (Solid Masonry Units made from Clay or Shale), ASTM C67-19 is the Standard Test Methods for Sampling and Testing Brick and Structural Clay Tile and CSA Standard A82-06 is the standard for Fired Masonry Brick Made from Clay or Shale.

ASTM C62-17 prescribes acceptance criteria such as a minimum compressive strength, maximum water absorption by 5-h boiling and maximum saturation coefficient that bricks classified as either Severe Weathering (SW), Moderate Weathering (MW) or Negligible Weathering (NW) meet. As

per ASTM C62-17 Clause 5.1.2 “Absorption Alternate”, the saturation coefficient of brick masonry does not need to be evaluated if the 24-hour cold water absorption of five samples of the brick does not exceed 8.0%. Similarly, Clause 5.1.3 “Freezing and Thawing Alternative” of the standard states that if brick masonry meets the compressive strength limits and passes the freeze-thaw tests stipulated in ASTM C67-19, testing for 5-h boiling water absorption and saturation coefficient is not required. ASTM C67-19 stipulates tests for the evaluation of modulus of rupture (flexure), compressive strength, abrasion resistance, absorption, freezing and thawing, initial rate of absorption and efflorescence, etc. In the freeze-thaw test outlined in ASTM C67-19, the assessment done to investigate the extent of freeze-thaw damage in brick masonry involves examining the crack length and mass loss, which would need to be above a threshold limit specified for a certain brick classification. It is pertinent to mention here that different types of bricks, particularly old or new, may behave differently under the test conditions.

The major drawback of the standards mentioned above is that they cannot be relied upon for accurately predicting the in-situ performance of brick masonry. The performance limits stipulated are based on the assumption that bricks can be “freeze thaw resistant” (Straube et al., 2010, p. 2). Like other construction materials, bricks can fail under certain exposure conditions. Durability assessments of brick masonry are determined either by the abovementioned “acceptance criteria” or freeze thaw tests, whereby other important factors are not taken account. According to Straube et al. (2010), the ASTM and CSA standards provide an “incomplete understanding of the physics of freeze-thaw damage, an oversimplification of field exposure conditions, and testing that focus on unit, not material, response to freeze-thaw cycling.” (p. 3).

Earlier, in 1977, Fagerlund had proposed a new approach to assessing the performance of concrete (a porous material like clay brick masonry) under freeze-thaw exposure conditions. The method was based on the need to produce results that could be replicated again; specimen performance could be hierarchically categorized and the experimental conditions would be similar to what would be experienced by the material when in-situ (Fagerlund, 1977). Therefore, the method introduced the concept of a metric known as the critical degree of saturation, also known as S_{CR} or S_{crit} (this term has been used in subsequent sections), which is essentially the moisture content above which a material can experience irreversible damage under freezing conditions. It is important to understand that S_{crit} is inherently a material property that does not vary depending

upon the exterior climate. The process of S_{crit} determination involves drying brick specimens to a certain temperature and then subjecting them to vacuum saturation. Fagerlund (1977) stated the freeze-thaw resistance of a material can be represented as follows:

$$F = S_{CR} - S_{ACT}$$

- S_{ACT} is the actual degree of saturation and can be interchangeable with S_{CAP}, which is the capillary degree of saturation.
- S_{CR} is the critical degree of saturation

The degree of saturation, S, is indicated by the following relationship:

$$S = \frac{V_w}{V_p}$$

- In case of complete saturation (possibly through the vacuum method), $S = 1$
- V_w is the total water volume that is evaporated when the brick is dried to 105°C
- V_p is the cumulative volume of all the pores before the onset of freezing

With regards the test to determine the S_{CR} (or S_{crit}), Fagerlund (1977) states that:

> …the value of S_{CR} gives information of the maximum admissible water-filling of the air-pore system; the value of S_{CAP} gives information of the susceptibility to water absorption in the same pore- system (Fagerlund, 1977, p. 218)

In the freeze-thaw experiments that Fagerlund (1977) performed on concrete, strain vs temperature graphs were plotted for a specimen that had been subjected to one freeze-thaw (from 10°C to -20°C) cycle over the course of twenty-four hours. The findings of the experiments were as follows:

1) Curve A on the strains vs temperature graph indicated that at moisture contents less than the S_{crit} value, the specimen underwent shrinkage (manifested as negative microstrains) at temperatures from 0 to -20°C (see Figure 2-1a).
2) Curve B on the strains vs temperature graph indicated that at moisture contents greater than the S_{crit} value, the specimen underwent expansion (manifested as negative microstrains) at temperatures from 0 to -20°C (see Figure 2-1a).

3) In the study, the moisture content (% saturation) at which the strains at -20°C were equivalent to 0 was the critical degree of saturation, S_{crit} (see Figure 2-1b).

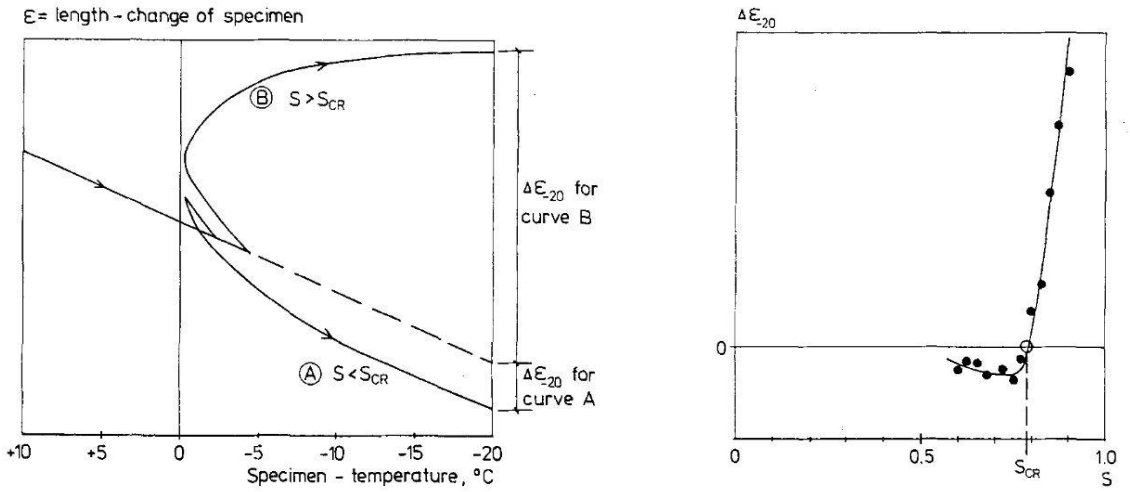

(a) (b)

FIGURE 2-1: (A) A STRAINS VS TEMPERATURE GRAPH INDICATING THE EXPANSION AND SHRINKAGE STRAINS AT TEMPERATURES FROM 0 TO -20°C. (B) STRAIN VS MOISTURE CONTENT GRAPH INDICATING THE ONSET OF FROST DECAY (FAGERLUND, 1977).

As these experiments had been performed on concrete, the same approach has formed the basis of assessing the freeze thaw damage of other materials such as clay brick masonry (Mensinga, 2009). Thus, this seminal research was the basis of the frost dilatometry methodology that assesses freeze thaw deterioration of porous materials like clay brick masonry. This has been widely considered as an improved yet reliable technique for testing the durability of bricks.

2.2 PROPERTIES OF BRICK

In 1921, the need for an improved understanding of porous materials led Washburn to describe a method to measure the size and distribution of pores in such materials via the intrusion of mercury at high pressure. The relationship between pressure and pore diameter was indicated by the following formula (Washburn, 1921):

$$\text{Pressure} = \frac{-2\gamma\cos\theta}{r}$$

Where:

γ is the surface tension

θ is the angle of contact

r is the capillary pore radius

To undertake the test, a porous material was subjected to a vacuum in a steel pressure vessel. Mercury was then poured in at different pressures, wherein subsequent measurements for pressure and volume were done. The volume difference (correlating to a decrease pore radius, Δr) corresponded to a pressure difference, Δp, indicating the distribution of pores with radii in a certain range (Washburn, 1921).

Properties of clay brick masonry are influenced by factors such as their mineralogical constituents, type of manufacturing process, the variation of kiln heating temperature and particle size (Crawford, 1984). Brick properties can be characterized as follows (Crawford, 1984, p. 2):

i) Saturation coefficient:
   This metric, which is a ratio between the 24-hour cold soak and 5-hour boiling absorption value, provides an indication of the clay brick capacity to internally withstand the "expansive pressure of freezing of water" (p. 15).
ii) Pore structure
   a. Total porosity
   b. Pore size distribution
iii) Specific surface area
   For a porous material, this metric is a ratio between the total surface areas (internal and external) and its weight.
iv) Modulus of elasticity

The specific surface area is influenced by the size of the particles and porosity of the material. Therefore, a smaller particle size and greater porosity indicates a higher specific area of the clay brick. For example, a well-fired brick has well-developed bonds between the particles, thereby the specific surface area is lower compared to that of unburnt bricks. The durability of clay bricks can be assessed via the specific surface area, which in turn is affected by the type of raw material

constituents. It is important to note that the porosity and pore make-up impact the strength, hardness, permeability, wetting and drying of a clay brick (Crawford, 1984).

The wetting and drying potential of bricks is influenced by the pore sizes: coarse, intermediate and small. Coarse pores (<1 micron) can fill quickly with water, however, can dry out. On the other hand, small pores fill with water with great difficulty and can only be susceptible to frost damage at below-freezing temperatures. Conversely, bricks with intermediate pores (approximately between 0.1 and 1 microns) have a greater risk of freeze-thaw damage (Crawford, 1984).

According to Crawford (1984), the forming process of brick masonry affects its pore distribution. It is explained that:

> The greater the consolidation force during forming, the higher the percentage of smaller pores. Thus, stiff extrusion produces bricks with high volume of smaller pores in green state and dry press results in a more uniform and wider range of pore sizes. It is also safe to conclude that the greater the power of the extruder, the larger the volume of smaller pores (Crawford, 1984, p. 17).

Similarly, firing temperature impacts the distribution of pores and porosity in brick masonry. When a brick is fired, there is "grain growth" (p. 18) and the linkages between particles are developed. This reduces the spaces that exist between particles, thereby reducing the overall porosity (Maage, 1984). In regards the effect of firing temperature on brick characteristics, Maage (1984) states that:

> Both tensile strength, porosity, and pore size distribution are influenced by the degree of burning. Increasing degree of burning results normally in higher tensile strength, lower porosity and bigger pores (Maage, 1984, p. 348).

There is a relationship between porosity and the saturation coefficient of brick masonry. The higher the porosity, the higher the saturation coefficient. The capillary uptake of water in bricks depends on the porosity of brick masonry. Crawford (1984) investigated the level of water saturation in a sample of bricks that were subjected to one-hour soaking in water. The results of the test indicated that different bricks saturate to varying levels, whereby this can also be attributed to different firing temperatures. This has significant implications in terms of the risk of bricks to frost damage.

The irreversible expansion experienced in bricks after a freeze thaw cycle is basically the difference between the effect of "freezing expansion and thawing shrinkage" (see Figure 2-2Figure 2-2) (Crawford, 1984, p. 30). Manufacturing methods have an impact on the risk to freeze thaw deterioration, such that bricks that have been form through extrusion process tend to have a higher "increase in freezing expansion" when water saturation exceeds the S_{crit} threshold (Crawford, 1984, p. 30). Extrusion process results in the formation of a large pore volume in brick masonry, which explains the reason why freezing expansion is more pronounced compared to bricks formed from other processes.

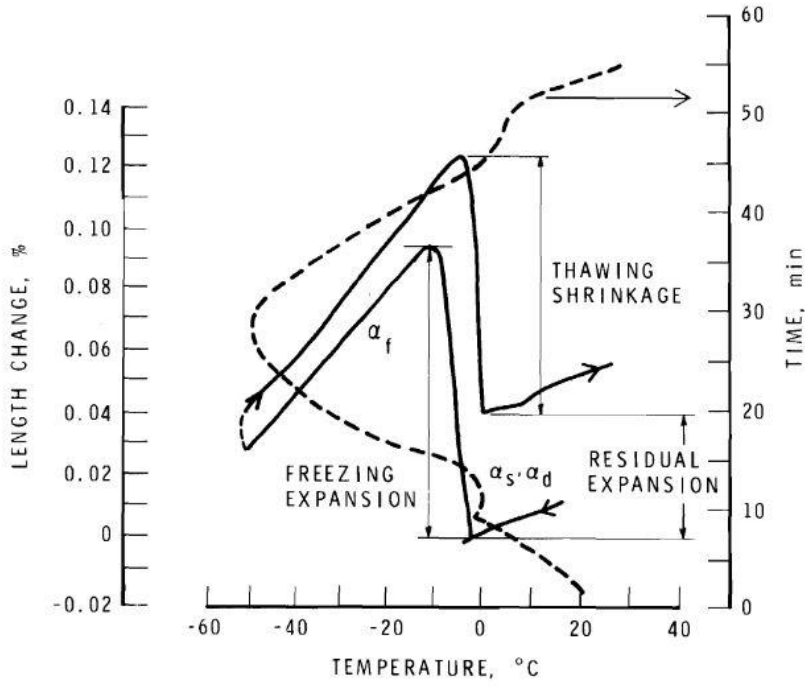

FIGURE 2-2: RESIDUAL EXPANSION AS A DIFFERENCE BETWEEN FREEZING EXPANSION AND THAWING SHRINKAGE IN CLAY BRICK MASONRY (CRAWFORD, 1984)

Firing temperature also improves the durability of clay brick masonry, wherein a higher temperature corresponds to a lowering of the total surface area of the brick and a lower saturation coefficient. Furthermore, the presence of certain compounds such as SiO_2, Al_2O_3, and CaO require higher firing temperature for brick masonry to achieve a certain level of resistance against freeze-thaw damage.

2.3 EFFECT OF THE MINERALOGICAL COMPOSITION ON BRICK MATERIAL PROPERTY

An assessment of brick masonry necessitates an understanding of its risk to freeze thaw damage, which is the primary durability concern in walls. It is for this purpose it is important to understand the specific "physical and mineralogical properties" of different types of brick masonry to predict how they would perform in-situ (Crawford, 1984). Cultrone et al. (2004) investigated the relationship between the mineralogical content of brick masonry; the temperature at which it was fired; porosity and pore size distribution (PSD). It is understood that porosity and pore size distribution affect the ability of the fluid to be stored and redistributed in brick masonry. The extent of porosity and PSD in turn influence brick masonry durability, and its susceptibility to freeze-thaw deterioration. The methodology of the study involved testing the porosity of two different types of clay brick masonry i.e. one that was largely composed of carbonates and the other with phyllosilicates (and no carbonates). The bricks with carbonates had a notably higher concentration of calcite ($CaCO_3$) and dolomite ($CaMg(CO_3)_2$). It is important to understand that the mineralogical composition of the brick masonry tested was what is typically found in the construction industry (Cultrone et al., 2004). The brick specimens were fired at a rate of temperature increase of 3°C to between 700°C and 1100°C. An X-ray diffractometer was used to analyse the different phases in which the minerals existed. Similarly, scanning electron microscopy (SEM) helped in evaluating the textural changes that occurred in the specimens over the course of the firing. A digital image analysis (DIA) helped in determining the "pore shape, spatial distribution, and connectivity", especially the distribution of macropores ($r > 1\mu m$) of the brick specimens (Cultrone et al., 2004, p. 549). Additionally, hydric tests were done to measure parameters such as absorption coefficient, capillary uptake and rate of drying. This would help in the evaluation of the degree of pore interconnectivity, Ax, which is a function of free water absorption (Al) and forced water absorption (Af). A higher Ax denotes a greater proportion of pores that are "not easily accessible under natural conditions (only under forced water absorption)" (p. 553). The hydric tests also enabled in analysing the absorption coefficient (Ac) and drying index (Di) of the bricks, whereby the former explains the rate at which water is absorbed and the latter is the rate of drying. The technique of Mercury Intrusion Porosimetry (MIP) (also discussed earlier) was adopted to gauge the porosity and PSD of specimens at different firing temperatures,

such that there were graphical representations of locations of pores of a specific size. An ultrasound propagation velocity was used to measure the variation in porosity during the firing process. The results of the study showed that the types of mineralogical content (with carbonates and lack thereof) explained the variations in brick porosity, as the firing temperature progressed from 700°C to 1100°C. A progressive increase in temperature either leads to the formation, changes in state, disappearance and increased concentration of clay minerals in the two types of bricks. This phenomenon varies depending upon the type of bricks considered, such that calcareous bricks have a higher concentration of the non-crystalline phase at low temperatures (<900°C). Phyllosilicates in bricks vitrify (melt) at higher temperatures, leading to the joining together of pores and an overall reduction in porosity. It is also important to mention that the rate of drying of bricks was almost constant for such type of bricks, whereas it decreased for the carbonates bricks. Ax was higher for the non-carbonate bricks, due to "a good development of the vitreous phase" (p. 553), as opposed to lower values for carbonate bricks for temperatures between 800°C and 1000°C. According to C, this is because calcareous bricks experienced "lime blowing" (p. 560), which happened when calcite ($CaCO_3$) and dolomite ($CaMg(CO_3)_2$) decomposed and later hydroxylated to form portlandite ($Ca(OH)_2$) and brucite ($Mg(OH)_2$). This leads to greater pore interconnectivity, a higher number of pores with r<1μm and propagation of micro-cracks (as shown by SEM) within the internal structure of bricks. This augments the brick porosity leading to a higher Ac and lower Di, eventually compromising the durability of the calcareous bricks (see Table 1).

TABLE 1: RESULTS OF THE CULTRONE ET AL. (2004) STUDY SHOWING THE VARIATION IN THE LEVEL OF POROSITY AND DURABILITY OF BRICK TYPES THAT EITHER CONSITUTE CARBONATE OR ARE WITHOUT CARBONATES

Brick type	Mineral phases	Porosity	Durability
With carbonates	• Ca (Mg) silicates • limited melt (900–1000 °C)	• ↑ Micropores (< 1 μm) • ↑ Cracks ("lime blowing")	• ↓ Resistance to salt weathering and freeze–thaw cycles • Loss due to ↑ micropores ($\Delta P = 2\gamma/r$)
Without carbonates	• ↑ Mullite + melt • 1st melt at 900 °C • Melt ↑↑ 1100 °C	• ↑ Macropores (> 1 μm) • Porosity ↓ as T ↑ • ↓ Pore interconnection	• Extensive melting = isotropic/homogeneous texture = absence of weak planes • ↑↑ Durability due to limited amount of micropores

↑ = high/abundant; ↑↑ = very high/very abundant; ↓ little/reduced; ΔP = crystallisation pressure (of a salt or ice in a pore of radius r), γ = interfacial energy.

When calcium carbonate ($CaCO_3$) in brick masonry decomposes, it forms calcium silicate, which increases the capillary coefficient, K_s. Another phase change that can occur is when there is "an

incomplete rearrangement of clay minerals, together with the low sintering degree", which results in a lower porosity (Raimondo et al., 2009, p. 2628). The type of elements present in brick masonry impact brick properties, such as length dilation occur under certain exposure conditions (Hughes & Bargh, 1982). According to Hughes and Bargh (1982), "the firing process probably the most important step in determining the eventual strength, durability, permeability, color, and texture of a brick" (p. 3). Depending upon the firing temperature and duration, there is a risk of development of cracks, faults and points of weakness within the brick's internal microstructure. These are coincidentally the locations where there is a "high porosity", and freeze-thaw damage is likely to occur (Hughes & Bargh, 1982, p. 5). The durability of bricks against frost damage also depends upon the capillary uptake, such that moisture entry in a uniform manner would pose less compared to localized areas of high permeability, which would lead to erratic movement of moisture into the brick. Comparing brick masonry to stones would help put to perspective the behavior of bricks under certain environmental conditions.

2.4 FREEZE THAW CYCLING OF CLAY BRICK MASONRY

In 1968, Ritchie did seminal research on the impact of freezing-thawing conditions on a number of brick samples. The investigation involved the determination of parameters that influence the onset of damage (manifested as a crack) in bricks. The methodology involved prepared test samples which were a "square-inch in cross-section" and were about "two and a quarter inches long" (Ritchie, 1968, p.1). The samples were then placed in a freeze-thaw chamber, where they were subjected to temperatures ranging from -15ºF to -20ºF (~ - 26.1ºC to -28.9ºC). The results of the study were that increased brick moisture, increased rate of change of temperature content and the surface from which the cooling onset takes place are important factors that can potentially enhance the risk to freeze-thaw damage.

Past studies on brick durability have underpinned the basic understanding that freeze-thaw failure in bricks is not just because the brick is fully saturated with water or has undergone freeze-thaw cycles when the moisture content is below a critical value (Fagerlund, 1977; Litvan, 1973). It is, in fact, a combination of factors that initiate the failure mechanism in the brick.

It is in this this context that in 1973, Litvan analogized frost damage in bricks to frost heaving in soil, which is affected by "soil particle, size, and percentage of voids, amount of water available

and cooling rate" (p. 2). It is linked to a build-up of mechanical pressures in the brick pore system as a result of the water freezing, whereby there tends to be a concentration of water in weak areas such as micro-cracks and faults. According to Litvan (1973), intermediate-sized pores (typically between with radii between 300 to 40μm) are prone to the effects of frost damage. Larger pores in bricks act as buffers against the capillary water expansion, which would occur at low temperatures. Similarly, water held in the smaller pores can only initiate frost related damage at low temperatures. It is evident that pore size impacts the ability of a brick to resist freeze-thaw deterioration, such that the relationship of the former parameter is "inversely proportional" to that of the S_{crit} value of a brick (Litvan, 1973, p.7). Therefore, the durability of brick masonry is a function of its ability to redistribute internally held moisture via a network of pores that it is constituted of. The critical degree of saturation, S_{crit}, depends upon material properties such as "absorptivity, pore-size distribution, and permeability", which in turn having a bearing on the total surface area of brick masonry (Litvan, 1973, p.8).

Litvan (1973) investigated 27 types of brick masonry for their resistance to frost damage. The test methodology involved subjecting the bricks the BET (Brunauer-Emmett-Teller) nitrogen exposure for the purpose of ascertaining their surface areas. Brick masonry durability was based on classifications that were already established given their in-situ performance in a duration of time. The classifications were durable, questionable and unsound. The results of the investigation showed that bricks with a larger surface area (i.e. higher porosity and small pore-size), which was between say 1.14 m^2g^{-1} and 8.25 m^2g^{-1} were categorized as "unsound" (Litvan, 1973, p.9).

Davison and Sereda (1978) investigated the linear expansion in bricks due to freezing via an instrument known as extensometer. As per the test approach, saturated brick specimens with dimensions that were approximately 13m by 13mm by 76mm were placed in the extensometer chamber (bath) and subjected to freezing and thawing conditions. The temperature inside the bath was controlled to achieve a specific rate of freezing and thawing. The states of freezing and thawing led to expansion in the brick specimen and this was measured via the dial at the top of the instrument. A thermocouple was also placed on the surface and the center of specimen, in order to confirm that the temperature in the specimen uniformly followed the temperature of the bath. The results of this test experiment showed that repeated freezing and thawing cycles decreased the difference in expansion and shrinkage in the specimen at each ascending cycle. Similarly, there

was a “temperature differential” (p. 146) at the surface and center of the brick specimen, which occurred at the same time of freezing and thawing. The permanent expansion of the brick is the difference of the reading at the start of the test and after thawing is complete. This study provided an insight on how dimensional variability, particularly irreversible changes after freezing and thawing, could explain brick durability in-situ.

2.5 POROUS MATERIALS

When assessing porous materials, it is important to understand key properties such as total hydraulic potential and hydraulic conductivity, which dictate the movement of moisture through them. An understanding of the internal microstructure of porous materials would throw light on how moisture movement occurs. As Hall (1977) states:

> The complementary microscopic approach attempts to relate permeability and associated properties to pore size distributions and pore structures. This has been pursued successfully in the analysis of certain problems, notably the flow of liquids in saturated porous solids, water content hysteresis, and indeed the fluid microdynamics of porous solids generally (Hall & Hoff, 2009, p. 118).

The pores in porous materials can be categorized according to the pore diameter. Macropores have diameters greater than 1mm; micropores have diameters between 1mm and 0.1μm and nanopores have diameters less than 0.1 μm (Charola & Wendler, 2015). All pores are interconnected with smaller diameter capillaries, which aid in the transfer of moisture internally. The characteristics of porosity and pore size distribution have a bearing on the tensile strength of porous materials, which in turns affects the resistance to freeze-thaw deterioration.

In this regards, it is pertinent to mention a study by Maage (1984) who investigated the relationship between the frost resistance of brick masonry, the porosity and pore size distribution. In order to determine the freeze-thaw deterioration of brick masonry, Maage (1984) adopted the approach of determining the critical degree of saturation, S_{crit}, which indicated the onset of damage. The experimental objectives entailed performing Mercury Intrusion Porosimetry (MIP) to identify the pore size, pore distribution and pore volume of the brick masonry tested. Through the measurements via MIP and scanning electron microscopy (SEM), “the surface area of the material,

the bulk specific density, the absolute specific density, and the porosity can be calculated" (see Figure 2-3 & Figure 2-4) (Maage, 1984, p. 347).

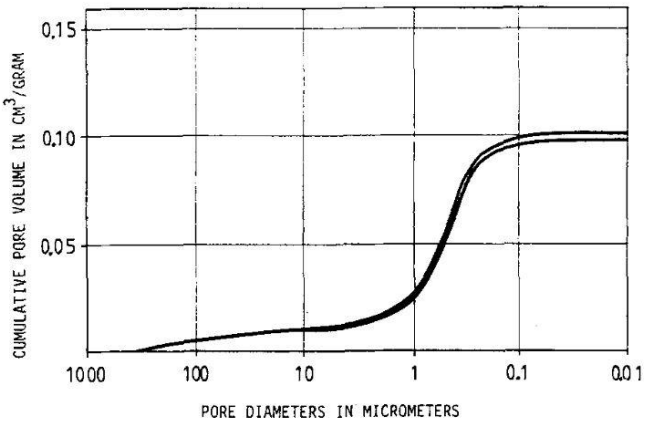

FIGURE 2-3: PORE SIZE DISTRIBUTION IN A GIVEN TEST SPECIMEN (MAAGE, 1984)

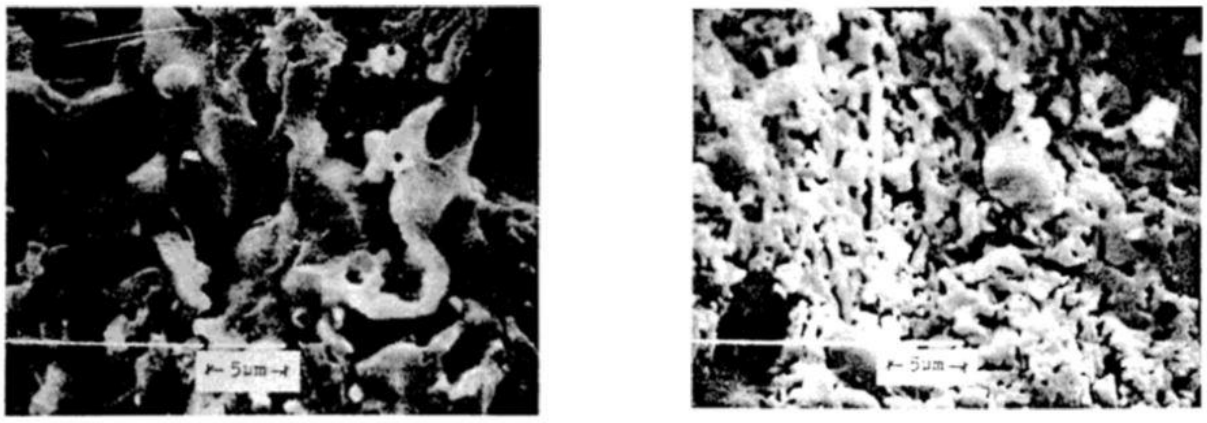

(a) (b)

FIGURE 2-4: SEM IMAGES OF TWO DIFFERENT TYPE OF BRICK SPECIMENS. (A) AND (B) HAVE THE SAME POROSITY, HOWEVER THE MEDIAN PORE DIAMETER VARIES. (A)'S MEDIAN SIZE PORE DIAMTER IS GREATER THAN (B) (MAAGE, 1984)

Maage (1984) found that the bricks tested varied greatly in their porosity and pore diameters, which resulted in their differing levels of resistance to freeze-thaw deterioration. The results of this study showed that resistance to freeze-thaw deterioration is inversely proportional to the pore volume; however, the resistance is proportional to the "percentage of pores with diameters bigger than 3μm" (see Figure 2-5) (Maage, 1984, p. 349).

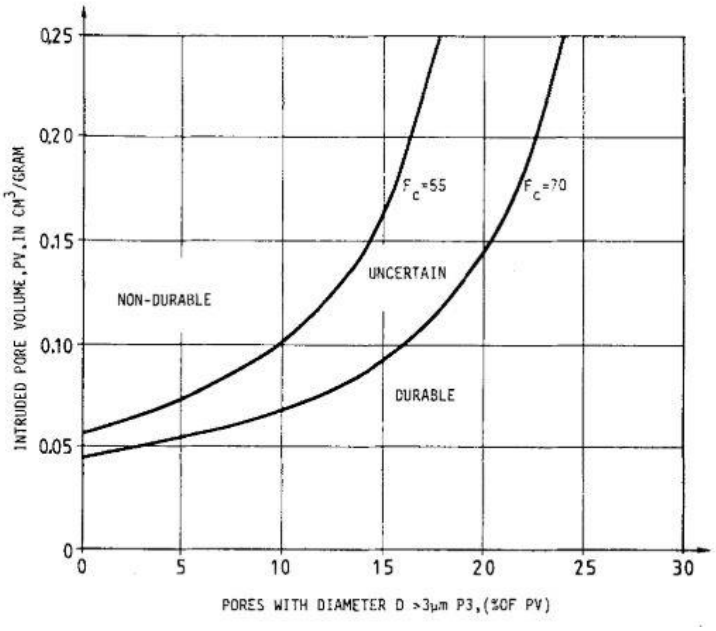

FIGURE 2-5: RELATIONSHIP BETWEEN FROST RESISTANCE, PORE VOLUME AND PORE DIAMETER (MAAGE, 1984)

Capillary suction of moisture typically occurs in brick masonry, particularly due to microstructural characteristics intertwined to their porosity. This characteristic of the porous materials can be distinguished by the "amount, size and shape of pores" (Raimondo, Dondi, Gardini, Guarini, & Mazzanti, 2009, p. 2623). It is therefore important to understand the notion of the capillary coefficient, which is related to the amount of water absorbed per area of a porous material (m) and time in the following way (Raimondo et al., 2009):

$$m = K_s t^{1/2}$$

Where:

m is the water absorbed by a porous material per unit surface of an area

t is time

K_s is the capillary coefficient, and can be denoted as follows:

$$K_s = C \cdot \frac{\varepsilon}{\lambda} \cdot {r_0}^{1/2}$$

Where:

ε is the effective porosity

r_0 is the median pore size

λ is the pore tortuosity of the solid (non-dimensional parameter)

This capillary coefficient is the same as the 'liquid absorption coefficient' (or the A-value), which is responsible for the capillary suction of moisture in a porous material like brick masonry. The magnitude of the capillary coefficient, K_s, has been further linked to "the density, the surface tension and the viscosity of the liquid" and "effective porosity", "median pore size", "pore tortuosity" and the "liquid-brick contact angle" (Raimondo et al., 2009, p. 2624). It is, however, noteworthy that the liquid properties are assumed to be constant in the experiment.

Raimondo et al. (2009) investigated the phenomenon of capillary action in brick masonry including an examination of its relationship with the physical properties of the porous material. 15 samples of brick masonry, which were obtained from different manufacturers, were tested. The methodology involved the determination of the open porosity (as per ASTM C373), pore size distribution (through Mercury Intrusion Porosimetry) and pore specific surface (through nitrogen absorption based on the BET theory) of the test samples. For the pore size distribution, the following variables were determined (Raimondo et al., 2009):

1) Mean pore radius
2) The proportion of micropores (P50 whereby the diameter, $\varphi < 0.05\mu m$ i.e. 50nm)
3) The proportion of macropores (P3 whereby the diameter, $\varphi > 3\mu m$)

The results of the study showed that there was variation in the physical properties of the different brick samples, which manifested with differing levels of "resistance" to "capillary suction" (see Figure 2-6) (Raimondo et al., 2009, p. 2625).

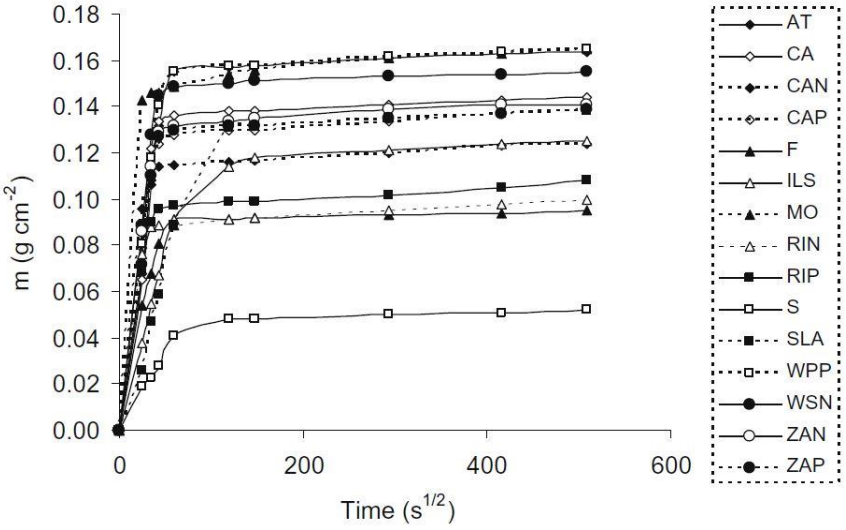

FIGURE 2-6: THE DIFFERENT TYPES OF BRICK SAMPLES TESTED HAVE DIFFERENT VALUES OF CAPILLARY COEFFICIENT (OR A-VALUE) (RAIMONDO ET AL., 2009)

It can be inferred from the results that the total amount of liquid uptake in a sample essentially correlated to its porosity and the proportion of micropores (P50) but not mean pore size. The study also shed light on the following findings (Raimondo et al., 2009):

1) Pore size does not have an impact on capillary suction in the brick, and this is evident in the cases of samples S and MO, which differ greatly in their capillary coefficients, Ks (0.6 and 5.9 respectively), however, the magnitude of difference between their mean pore radii is relatively insignificant (r_0 = 0.61μm and 0.43μm respectively).
2) A large proportion of micropores (P50), such as 13.4% in the brick sample S, resulted in a lower magnitude of liquid intake through capillary action and a lower capillary coefficient (or A-value), K_s.
3) There is no significant correlation between larger pores (P3) and the capillary coefficient.
4) A higher material porosity would result in a higher capillary coefficient (A-value) and total moisture absorbed by a porous material.

K_s can also be expressed as the following:

$$K_s = 2.915 \frac{OP}{\lambda} (r_0)^{1/2}$$

Where

OP is the Open Porosity of the material

It can be seen from Figure 2-7 that increasing the mean pore radius and decreasing the pore tortuosity factor at the same level of porosity (of the different test samples) has the effect of reducing the capillary coefficient, K_s.

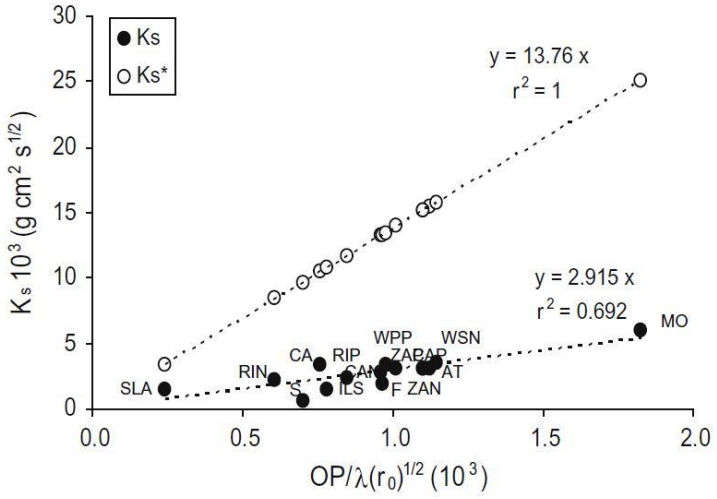

FIGURE 2-7: THE RELATIONSHIP BETWEEN KS, PORE TORTUOSITY FACTOR AND PORE RADIUS OF THE DIFFERENT BRICKS SAMPLES (WHILE THE POROSITY REMAINS THE SAME) (RAIMONDO ET AL., 2009).

2.6 MOISTURE MOVEMENT IN BRICK MASONRY

The peculiar behavior of bricks to absorb, store and release moisture, depends essentially on their properties, which are unique to their microstructure. Porosity in bricks is a culmination of factors such as mineralization of constituent particles due to “high-temperature sintering” (p. 2), which causes pores to “merge and coarsen” (Hall & Hoff, 2009, p. 2). The brick property of porosity has an inverse relationship with bulk density (see Figure 2-8), and as a consequence, impacts the nature of moisture movement internally (Hall & Hoff, 2009; Mallidi, 1996).

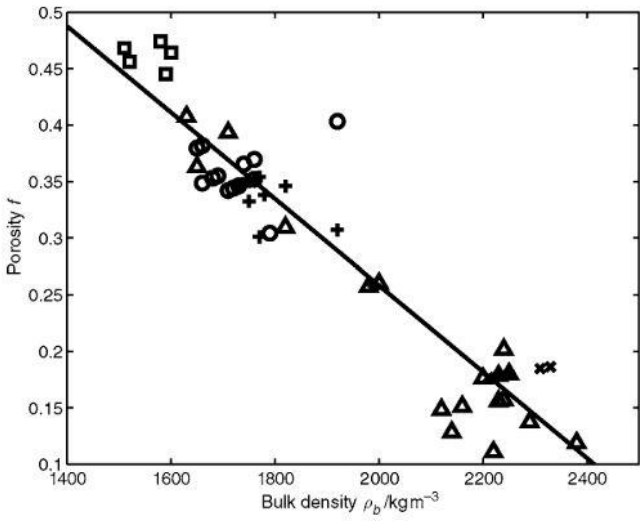

FIGURE 2-8: THE VARIATION OF THE POROSITY WITH BULK DENSITY OF BRICK MASONRY (HALL & HOFF, 2009)

Similarly, as bricks are porous materials and are basically characterized by the extent of their porosity, their total internal surface area impact their ability to store and redistribute moisture. A microscopic examination of bricks reveals that there is great variation in the pore sizes and distribution, and is typically non-uniform (Hall & Hoff, 2009). Moreover, the pores in a bricks can be categorized broadly as "open interconnected" and "closed dead-end" pores that are linked to the outside environment, whereas "closed or sealed" pores are so-called because they don't possess such a connection (Straube & Burnett, 2005). Similarly, when evaluating the porosity of brick masonry, the open porosity is the subject of focus, which is primarily based on the open interconnected pores. Therefore, Straube and Burnett (2005) state that

> some porous building materials (*like bricks*) can store their own weight in water in their internal pore volume with one-quarter of this amount as adsorbed water vapor on the pore walls at high relative humidities (Straube & Burnett, 2005, p. 294).

As bricks are hygroscopic materials, there are fundamentally three "regimes" (p. 323) by which moisture movement occurs in bricks (see Figure 2-9) (Straube & Burnett, 2005):

1) The hygroscopic regime
2) The capillary regime

3) The over-saturated regime

The way moisture storage in brick masonry varies with the exterior relative humidity (RH) is different from other materials such as wood or concrete. As seen in Figure 2-9, the sorption isotherm for bricks indicates both wetting and drying and consists of the regimes outlined above. Due to the types of pores that exist in clay-fired brick masonry, they absorb "moderates amounts of water at low and intermediate relative humidities" (p. 64) in the hygroscopic regime (Hutcheon & Handegord, 1995). The hygroscopic regime, where moisture exists either in the vapor phase or are adsorbed in the porous material, is further sub-categorized as follows (Mensinga, 2009; Straube & Burnett, 2005):

1) One-layer thick water molecules form on all the pore walls inside the brick
2) Multiple layers of water molecules from on all the pore walls inside the brick
3) Capillary condensation occurs inside the pores due to moisture build-up

However, as the relative humidity exceeds a certain threshold metric (the critical degree of saturation, S_{crit}, or W_{crit}, as shown in Figure 2-9), the moisture content enhances drastically with minute increases in RH (Hutcheon & Handegord, 1995). This is indicative of the capillary regime, where there is a phase change from vapor to liquid, resulting in the movement of liquid water in the brick (Hall & Hoff, 2009; Mensinga, 2009). Finally, the supersaturated regime occurs under certain controlled external conditions (vacuum or boil saturation), wherein all the pores are filled with water and any hitherto moisture content increases happen "independent of RH (Straube & Burnett, 2005).

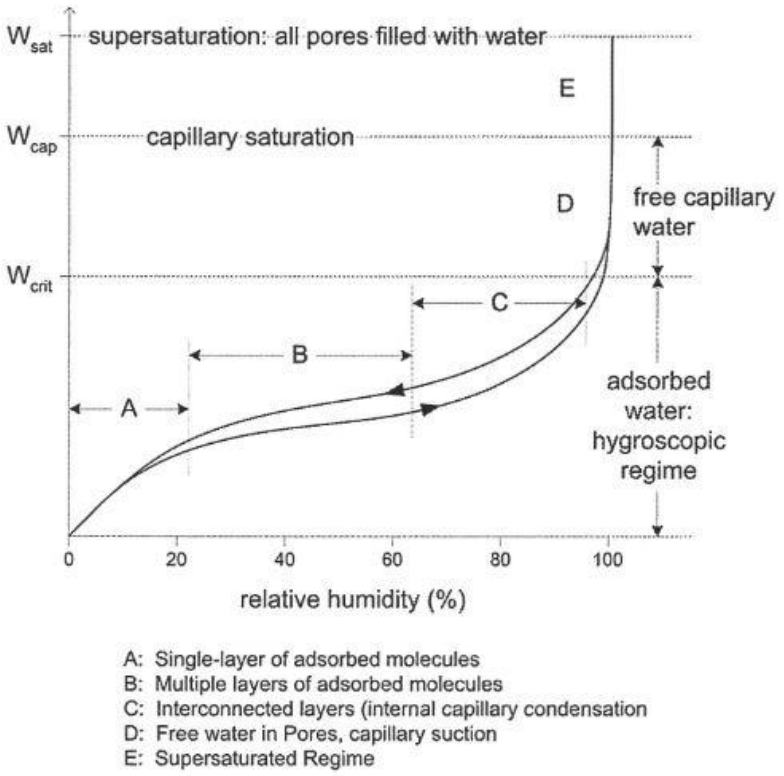

FIGURE 2-9: MOISTURE MOVEMENT IN BRICK MASONRY CAN BE EXPLAINED IN TERMS OF THE HYGROSCOPIC, CAPILLARY AND OVER-SATURATED REGIMES (STRAUBE & BURNETT, 2005)

In contrast to moisture storage, moisture transport in brick masonry happens by mechanisms such as "vapor diffusion, surface diffusion and capillary conduction" (Mensinga, 2009, p. 10). The type of mechanism that dominates basically depends upon the pore size and distribution of brick. It is noteworthy that these transport mechanisms do not occur independent of one another, rather there is a transition between the phases (Charola & Wendler, 2015).

In 1998, Brocken had discussed the Philip and de Vries theory, which he attributed to "the simultaneous transport of liquid water, water vapor, and heat governed by gradients of moisture content and temperature" (p. 12). Vapor diffusion in porous materials is governed by Fick's Linear Law for the macroscopic vapor flow (Hall & Hoff, 2009) and is given as follows:

$$J_w = -D_v \frac{dp_w}{dx}$$

Where:

J_w is the mass vapor flux

D_v is the water vapor permeability

$\frac{dp_w}{dx}$ is the gradient of water vapor pressure

The above equation explains water vapor movement inside a porous material primarily by a mechanism of diffusion, which occurs due to an existing vapor pressure gradient. The water vapor molecules are closely bonded to the pore walls of the material. Vapor molecules that have been caught in the cylindrical pores in a porous material encounter a lowered internal pressure, thereby transforming phases to become liquid. These liquid molecules that are initially adsorbed onto the pore surface, form a curved meniscus owing to the capillary pressure. Therefore, the Laplace-Young equation defines the relationship between the capillary pressure and pore radius and essentially accounts for the movement of moisture between pores and capillaries in brick masonry (Hall & Hoff, 2009; Mensinga, 2009; Straube & Burnett, 2005).

$$\Delta p = 2\sigma/r$$

Where:

Δp is the pressure difference between the liquid phase and air in the pore

σ is the surface tension

r is the radius of the meniscus formed by the liquid in the cylindrical pore

It has been pointed out by Brocken (1998) that in reality, the vapor flow in porous materials may be dominated by surface diffusion and capillary suction. Surface diffusion occurs when the thin film of adsorbed molecules, which were initially formed through vapor diffusion, accumulate to form several layers (Mensinga, 2009; Straube & Burnett, 2005). This occurs due to an increase in ambient RH, which causes more moisture influx into the porous material. Water molecules can form an adsorbed layer on the pore surface as the "attraction between the substrate (*brick pore surface*) and the water molecules is higher than the attraction of the water molecules for each other in the liquid form" (Charola & Wendler, 2015, p. 57). In this situation, surface diffusion "is a

diffusion process since the flow is driven by the mass density gradient of adsorbed water molecules" (Straube & Burnett, 2005, p. 342). Surface diffusion, as is evidenced by studies on porous materials, is commonly found in intermediate-sized pores.

The third important mechanism of moisture transport in bricks is capillary condensation, which occurs in small pores (Hall & Hoff, 2009; Straube & Burnett, 2005). Referring to capillary condensation, Hall and Hoff (2009) state that:

> Once initiated by nucleation, water vapour continues to diffuse into the pores and condense on existing menisci until the internal and external water vapor pressures come into balance and equilibrium is reached (Hall & Hoff, 2009, p. 59).

The Kelvin equation denotes the occurrence of capillary condensation inside the pore spaces (Hall & Hoff, 2009):

$$\ln\left(\frac{p_v}{p_{vs}}\right) = -\frac{2\sigma\gamma_1}{RT}\frac{1}{r}$$

Where:

P_v is the vapor pressure

P_{vs} is the saturation vapor pressure

R is the gas constant

T is the absolute temperature

According to Brocken (1998), "water sorption due to capillary condensation in a porous material is related to this relative humidity (*indicated as the P_v/P_{vs} ratio in the Kelvin equation*)" (p. 11). It is believed that capillary condensation also aids in vapor diffusion to the pores inside the brick (Straube & Burnett, 2005). Therefore, the movement of moisture through capillary condensation depends upon moisture content and RH. Moisture is constantly distributed in a porous material as they move from higher concentrated areas (water-filled pores) to dryer regions, wherein the pores are empty.

It is likely that smaller diameter pores contain moisture, as compared to those with larger diameters, which experience evaporation more quickly. Micropores (1mm < φ < 1μm) tend to experience capillary conduction whilst smaller pores (φ < 1μm) undergo vapor and surface diffusion (Charola & Wendler, 2015). The network of capillaries that exists in brick masonry helps develop the requisite force i.e. surface tension, to be able to pull liquid through capillary action into the material (Raimondo et al., 2009).

TABLE 2: THE VARIATION OF MOISTURE TRANSPORT MECHANISMS DEPENDING UPON THE PORE SIZE (ADAPTED FROM CHAROLA AND WENDLER (2015), P. 62)

<table>
<tr><td>Macropores</td><td colspan="3">Micropores</td><td colspan="2">Nanopores</td></tr>
<tr><td>$\emptyset > 1$mm</td><td>1mm –10μm</td><td>10μm – 1μm</td><td>1μm – 0.1 μm</td><td>100nm – 10nm</td><td>$<$ 10nm</td></tr>
<tr><td>Liquid water flow</td><td colspan="2">Capillary absorption</td><td colspan="3">Water vapor adsorption and surface diffusion</td></tr>
<tr><td colspan="4">Water vapor diffusion</td><td colspan="2">Capillary condensation</td></tr>
</table>

In summary, the moisture movement and transfer to all pore spaces within a porous material such as brick masonry can be outlined in stages as below (see Figure 2-10) (Torraca, 2006):

1) Level 1

The pore spaces are devoid of any moisture content as the material is in a completely dry state

2) Level 2

The smaller diameters pores and capillaries are filled with moisture, whereas the adjacent larger diameters pore may be dry.

3) Level 3

Whilst capillaries are full of moisture, the surfaces of larger diameter pores are covered by a think film of moisture.

4) Level 4

Finally, the capillaries and interconnected pores are completely full of water.

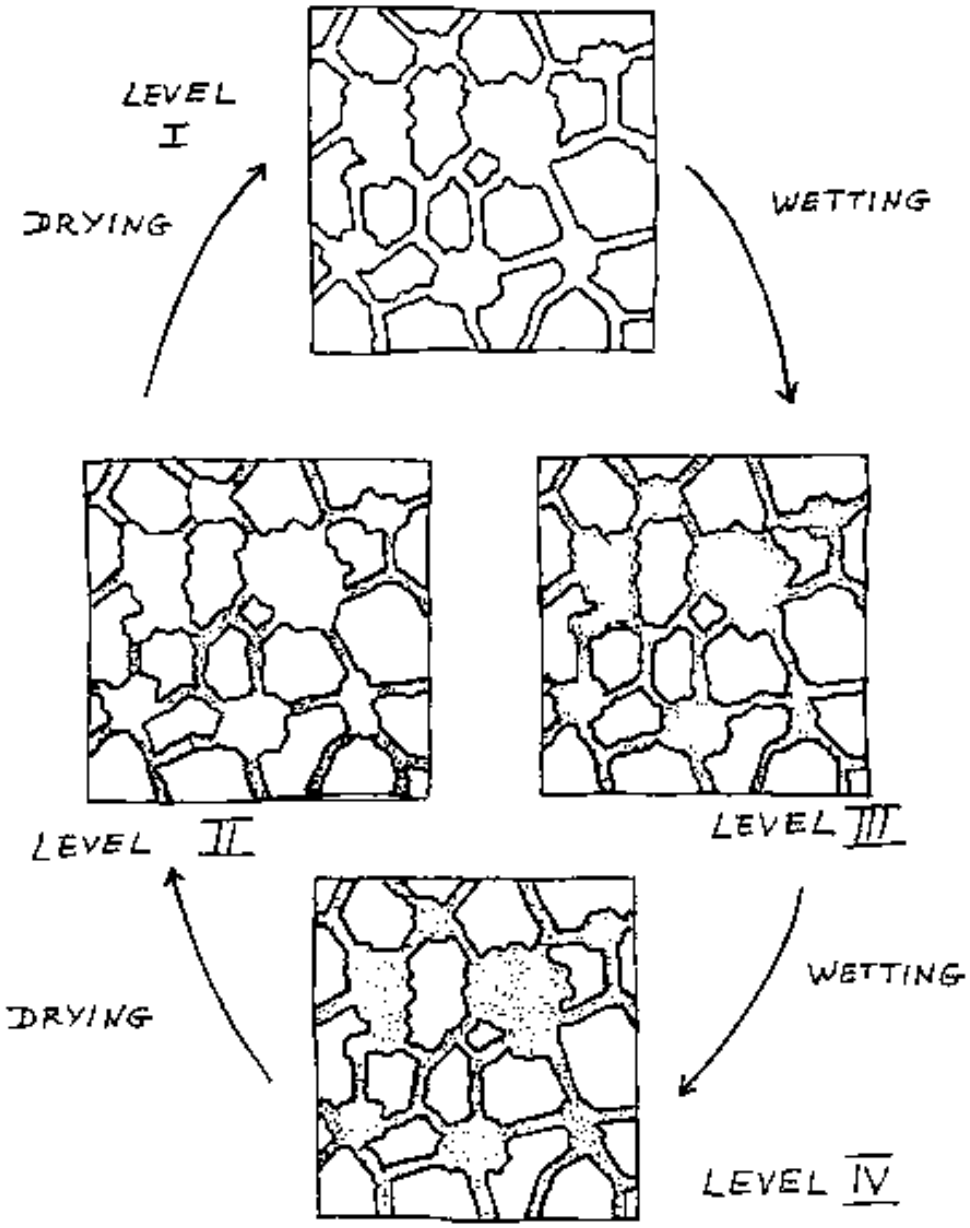

FIGURE 2-10: MOISTURE DISTRIBUTION IN THE CAPILLARIES AND PORES OF A POROUS MATERIAL SUCH AS CLAY-FIRED BRICK MASONRY (TORRACA, 2006)

The sorptivity of porous materials is an important factor by which water uptake happens through capillary action and "distributes itself in the material" (Hall, 1977, p. 117). This is an intrinsic material property, which is not impacted by changes in state of the material (whether it is dry or wet). The sorptivity parameter varies between bricks, irrespective of the mineralogical content

(Gummerson, Hall, & Hoff, 1980). Regarding the sorptivity of a porous material, Gummerson et al. (1980) point out that it "provides a much better measure of the comparative suctions of different bricks over a sensible time scale" and that it "demonstrates clearly the differences in suction between different materials" (p. 106).

Supersaturated flow in porous materials occurs due to boiling or vacuum saturation. The driving force behind the moisture movement is typically mechanically applied air pressure (Straube & Burnett, 2005). In this case, "capillary transfer changes into fluid flow process, i.e. Darcy flow, particularly for pores with diameters around and above 1mm" (Charola & Wendler, 2015, p. 62). Darcy's flow in a saturated porous material happens as a result of the "hydraulic potential", or pressure head (Pa), and is expressed as the following equation (Straube & Burnett, 2005, p. 347):

$$q_1 = k_1 . \Delta P$$

Where:

q_1 is the mass flux density of liquid water flow

k_1 is the hydraulic conductivity

P is the pressure

Moreover, hysteretic effects that arise due to desorption of moisture from pore surfaces inside a brick can be explained by the "ink bottle effect" (Funk, 2014, p. 228). This arises due to a difference in energy between pores and capillaries, which gives rise to a condensation potential at certain RH and moisture content that can support the desorption process. Therefore, depending upon the diameter of the interconnected capillaries and pores considered, the moisture can transfer out of the pore spaces (Funk, 2014).

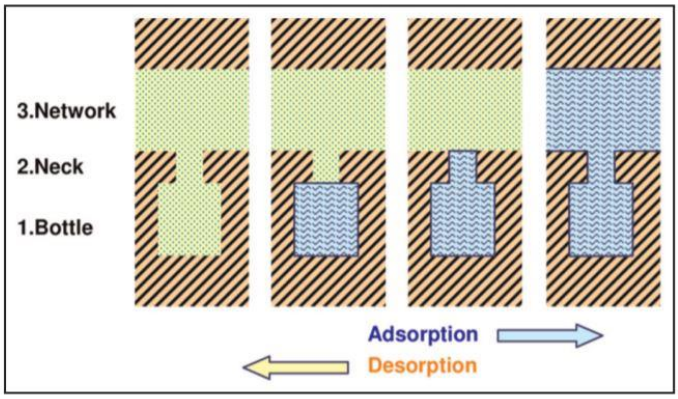

FIGURE 2-11: HYSTERETIC EFFECTS SCHEMATIZED THROUGH THE DESORPTION PROCESS IN THE CAPILLARY-PORE NETWORK (FUNK, 2014)

2.7 FREEZE-THAW DETERIORATION

According to Everett (1961), frost damage in a porous material is initiated when the pressure exerted by ice crystallization exceeds the material's mechanical strength. This is delineated with an idealised model consisting of two cylinders, A and B, that contain water; are sealed with movable pistons and relate to a relatively thinner diameter capillary tube. It is noteworthy that this setup is analogized to pore distribution within a porous material, and the connection of larger pores to finer capillaries. The ambient temperature is dropped for B, which then initiates the process of ice crystallization therein. Once ice crystallization is complete in B, the plausible route of movement of water in the capillary tube is from A to B, if the piston on the top immovable. In other words, a material consisting of coarse pores that interconnected with finer capillaries, would draw out water (high energy potential) to consolidate growth of ice crystals (low energy potential). As a result, bulk-ice build up in B would create stress that could exceed the strength of the walls, possibly leading to the incidence of freeze-thaw damage (in the likes of brick masonry) (Everett, 1961).

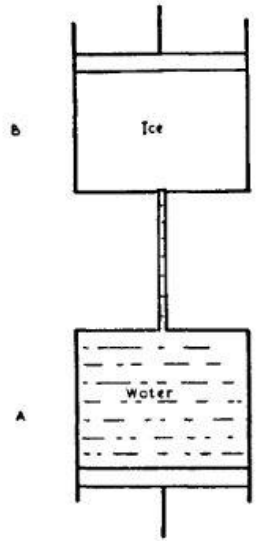

FIGURE 2-12: THE THEORY OF ICE-CRYSTALLIZATION IS EXPLAINED BY AN ANALOGY OF TWO CONTAINERS, A AND B, SEALED WITH MOVABLE PISTONS AND CONNECTED WITH A CAPILLARY TUBE, TO PORE SYSTEMS IN POROUS MATERIALS (EVERETT, 1961).

Porous materials have great propensity to undergo freeze-thaw deterioration (also known as frost damage). A combination of pore changes and increased moisture content have been attributed to frost damage in clay-brick masonry. It is important to understand that such materials experience permanent damage, when there is an internal pressure build-up, due to ice-crystallization. The pressure may be augmented when the crystals grow in the pore space, whereby they are near internal flaws, and may potentially compromise the strength of the material with their gradual expansion. A number of factors delineate the onset of damage due to ice-crystallization, namely (Scherer, 1999):

1) The shape of the crystal that is growing into a cylindrical pore space. If the contact angle, θ, between the crystal and pore space is greater than 90^{o}, then there is no further crystal growth into the pore space. Conversely, if θ is less than 90^{o}, the crystal will propagate into the pore space and possibly initiate damage in the material's microstructure.

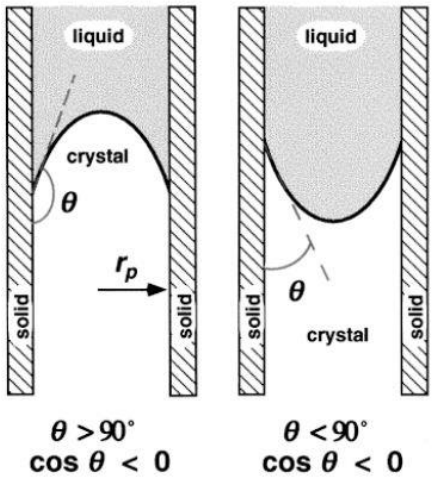

FIGURE 2-13: THE CONTACT ANGLE BETWEEN THE ICE CRYSTAL AND THE PORE WALL (SCHERER, 1999)

2) The crystal, in the presence of a liquid in the pore space, will develop capillary pressure that will need to be countered by the pore walls. Therefore, the wall would exert a "tensile radial stress", which may eventually contribute to the initiation of freeze-thaw damage in the material (p. 1353).
3) The growth of ice-crystals requires cooling of a liquid in a porous material to very low temperatures (like -37°C). Therefore, for nucleation of crystals in porous materials to occur at higher freezing temperatures (say -7°C), nucleation is favored in "cracks and pits" (p. 1354), where there is a greater surface area of the porous material exposed to the liquid at the onset of its freezing.
4) When crystals grow inside a pore, there is a significant build up of stresses. However, given the overall volume of the material considered, these stresses may not be large enough to cause permanent damage therein. On the other, if the crystals were to grow in a manner to initiate damage, there must be a "driving force" to advance ice crystallization into the internal flaws.
5) The stress exerted by a growing ice crystal is lower in pores of larger size.

The behavior of such brick masonry, when subjected to freeze-thaw cycles, has typically been likened to frost heaving in soil. Studies on silty-clay soil have shown that application of an increasing number of freeze-thaw cycles at temperatures as low as -15°C, can significantly alter increase pore volume and diameters, thereby leading to microstructural changes in the tested

material (Chen, Chen, Li, Li, & Ma, 2019). Likewise, tests on other porous materials such as concrete and rock, have indicated the material property of the critical degree of saturation (S_{crit}), as an important metric in the determination of the onset of freeze-thaw damage in a material. This, in turn, relates to the moisture content above which the material would undergo permanent deformation (Fagerlund, 1975). Therefore, the onset of freeze-thaw deterioration has been explained by theories, which have been corroborated by studies on different porous materials. The impact of freezing and thawing cycles on masonry properties was derived from three potentially relevant theories as mentioned below (Uranjek & Bokan-Bosiljkov, 2015)

1) The theory of hydraulic pressure building up inside brick masonry due to the formation of ice crystals within the porous structure.
2) The theory of impact of frost damage on the concrete masonry, due to the internal build up of hydraulic pressure. The theory analogizes the material model of the concrete masonry to be a 'closed container'.
3) The 'ice lens' theory about cement-based construction materials, which refers to aggregate particles and inter-connected pores.

It is pertinent to mention a study done by De Kock et al. (2015), who investigated the chronological evolution of freeze-thaw damage in a type of limestone with a scanning technique involving X-ray micro-CT. The methodological approach for the study involved capillary saturating the test material and then subjecting it to two different types of cycles: at freezing temperatures of -5°C and -15°C for a six-hour period. The test material contained mostly micropores ($\varphi < 16.2\mu m$), which are especially important for capillary transfer of moisture. It had also had a good ability to absorb moisture, which is due to interconnectedness of all the pores (De Kock et al., 2015). The results of the study showed that with an increase in the number of freeze-thaw cycles, there was micro-crack propagation along already existing internal fault lines in the materials, thereby leading to an increase in linkages between pores. In addition to enhancing the ability for capillary absorption in the test material, the structural changes that ensued after the freeze-thaw cycles, led to a decrease in the compressive strength of the material. An examination of the scans of effect of freeze-thaw cycles (at a freezing temperature of -15°C) on the fracture propagation throws light on the following (De Kock et al., 2015):

1. Fracture development increases with the number of cycles and is particularly evident of scans of the material in the freezing period, whereas upon thawing, the fracture seals.

2. After a threshold number of cycles (5), there is development of irreversible expansion within the material due to the propagation of the internal fractures. This has implications on the intactness of the material, such that in thawing, the fracture does not seal as in the case of earlier cycles.
3. Finally, after the sixth cycle, the overall volume of the fractures increases due to increasing linkages between one another.
4. Nucleation for ice-crystals were initiated in the smaller sized pores.

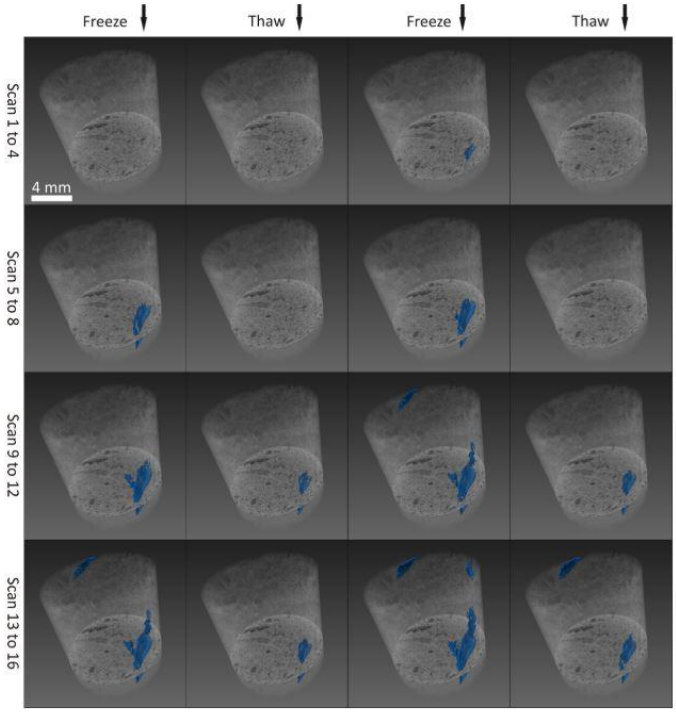

FIGURE 2-14: FRACTURE PROPAGATION IN THE TEST MATERIAL WITH AN INCREASING NUMBER OF FREEZE-THAW CYCLES. IT CAN BE NOTED THAT IN THE FIFTH CYCLE (SCAN 10), THERE IS AN IRREVERSIBLE DEFORMATION IN THE TEST MATERIAL SUCH THAT THE FRACTURE DOES NOT CLOSE-UP UNDER THAWING (DE KOCK ET AL., 2015).

The results of this study bring to fore the theory of ice-crystallization, which lays emphasis on the nucleation and growth of ice crystal in pore spaces, wherein the direction of movement is towards the interior of a material. Ice crystallization has generally been attributed to the to fracture propagation within porous materials. In regards to this, De Kock et al. (2015) state:

> When temperature is raised, the crystallization pressure will be released and indeed, the fracture closes as is observed. During the next freezing stage, the

pressure build-up reopens the fracture to close again upon thawing until fatigue results in the residual strain after multiple cycles (De Kock et al., 2015, p. 2873).

2.8 SUPERSATURATED REGIME

Depending upon the state of the porous material, the walls of its pores may act to effectively confine entrained water to different phases i.e. liquid, gaseous or solid. When water is absorbed into a porous material, its potential energy is lowered once it redistributes itself in the pore spaces (Hall, 1977). In a typical saturated state, the pore spaces in a porous material are filled with water and moisture flow can only occur "under the action of external forces" (Hall, 1977, p. 121). Attaining supersaturation of a brick sample is a slow process and may necessitate the application of a hydraulic potential such as an air pressure difference. This is because for this to happen, liquid water entering the brick sample must purge out the air entrapped in all the pore spaces, including the dead-end pores. The state of supersaturation occurs when water absorbed into a porous solid completely replaces "the air occupying the pores" (Hall, 1977, p. 117).

Typically, vacuum saturation is a process that is adopted to saturate a brick sample, and this helps in determining the "open volume fraction porosity" (p. 10). It is indicated by the following relationship (Hall & Hoff, 2009):

$$\text{Water absorption} = \frac{(w_s - w_d)}{w_d}$$

Where:

w_s is the saturated mass of the brick masonry

w_d is the dry mass of the brick masonry

2.9 FROST DILATOMETRY

Dilatometry is referred to as the measurement of a specimen's dimensions that has undergone permanent expansion after being subjected to freeze-thaw cycles. Frost dilatometry is therefore the methodology used to infer the onset of freeze-thaw damage in porous materials like clay brick masonry. The technique is increasingly seen as a means to assess the key material metric i.e. the

critical degree of saturation, S_{crit}, that would provide an indication of the "material level response" to exposure conditions of freeze-thaw cycles and high moisture contents (Straube et al., 2010, p.4). Based on 'limit state design', experimental objectives typically involve the measurement of strains of brick specimens, which arise after being subjected to freeze-thaw cycles at a certain moisture content. Consequently, specimens that have undergone expansion strains higher than a threshold value (such as 100 microstrains) would have thus endured frost damage. Research based on the frost dilatometry methodology has been undertaken by Mensinga (2009) and Williams (2015), who investigated the critical degree of saturation, S_{crit}, of a diverse sample of brick specimens.

Mensinga (2009) tested three groups of bricks, each belonging to three different chronological epochs i.e. contemporary, 1950s and 1870s. The contemporary brick was manufactured by 'Canada Brick' in the 1990s, while the 'Upper Canada College' and 'Montreal' bricks belong to 1950s and 1880s (Mensinga, 2009). The typical process of experimentation entailed cutting the whole brick specimens into 10mm slices, whereby they were initially dried; their length measurements were taken; they were then vacuum saturated to 100% moisture content; they were dried to target moisture contents; wrapped in a vapor impermeable material; they were subjected to six freeze thaw cycles (alternating between 20°C and -15°C) and finally their strain measurements were performed. In addition to this, their capillary water uptake (A-value) was also determined via the "water uptake test" (Mensinga, 2009, p. 39). WUFI was used to model the time taken for moisture to redistribute in the test specimens at different moisture contents (% degree of saturation), whereby this duration for certain specimens was as high as five days. The results of the study showed that for certain brick specimens, beyond the S_{crit} point, the expansion strains were large in magnitude and as Mensinga (2009) put it, "the tendency for frost dilation to increase as a function of saturation is far from linear for the Upper Canada College and Old Montreal set of brick" (p. 88). The main finding was that for the bricks belonging to the older epochs had a S_{crit} values as low as 25% moisture content (% vacuum saturation), whereas the contemporary bricks had a S_{crit} of 87% moisture content (% vacuum saturation). Similarly, the former brick masonry had higher A-values and porosity, which would have also corresponded to a lower strength. Therefore, this could explain the existence of a S_{crit} value at the lower echelons of moisture contents required for frost damage initiation (see Figure 2-15).

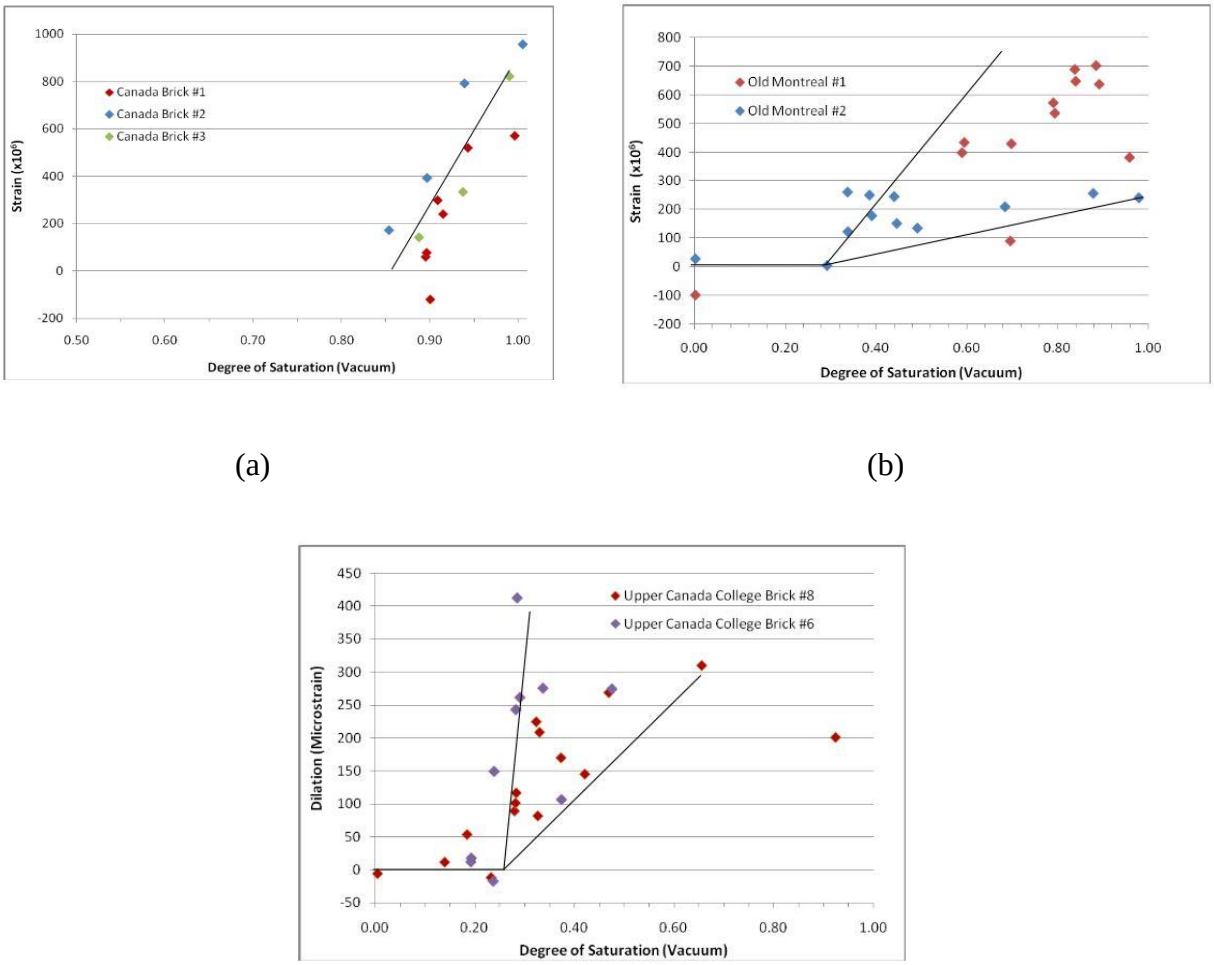

(a) (b)

(c)

FIGURE 2-15: (A) THE STRAINS VS MOISTURE CONTENT (% VACUUM SATURATION) OF BRICK TYPE 'CANADA BRICK' SHOWING THE ONSET OF FROST DECAY. (B) THE STRAINS VS MOISTURE CONTENT (% VACUUM SATURATION) OF BRICK TYPE 'OLD MONTREAL' SHOWING THE ONSET OF FROST DECAY. (C) THE STRAINS VS MOISTURE CONTENT (% VACUUM SATURATION) OF BRICK TYPE 'UPPER CANADA COLLEGE BRICK' SHOWING THE ONSET OF FROST DECAY (MENSINGA, 2009)

Williams (2015) also investigated the S_{crit} of century old brick specimens via the frost dilatometry methodology. The study involved testing brick slices (2d frost dilatometry) as well as half-brick samples (3d frost dilatometry). 2-d refers to measuring the expansion of the thin specimens along two directions, whilst 3-d measurements were done on half brick samples along with all three axes. The experimental approach was similar to that of Mensinga (2009), although there were evidently some differences in the freeze-thaw temperatures, cycles and equipment used. The strains measurements of the brick slices were taken along the x and y axes, thereby the trends of frost

decay for these axes were plotted and the S_{crit} point determined. The results from the frost dilatometry testing indicated that the critical degree of saturation obtained through 2-d measurements varied between brick samples (between 70 – 80%), despite the bricks having the same physical characteristics. On the other hand, 3-d measurements showed that bricks expanded erratically under different moisture contents and freeze-thaw cycles (see Figure 2-16). The study highlighted the following important aspects of studying the durability of bricks against freeze-thaw deterioration (B. Williams & Richman, 2017):

1) 2-d measurements of brick specimens through the frost dilatometry approach may not provide an accurate depiction of the critical degree of saturation of bricks that are in-situ.
2) 3-d frost dilatometry is a more accurate way of assessing the critical degree of saturation of bricks, wherein this can be more precisely correlated to the field values.

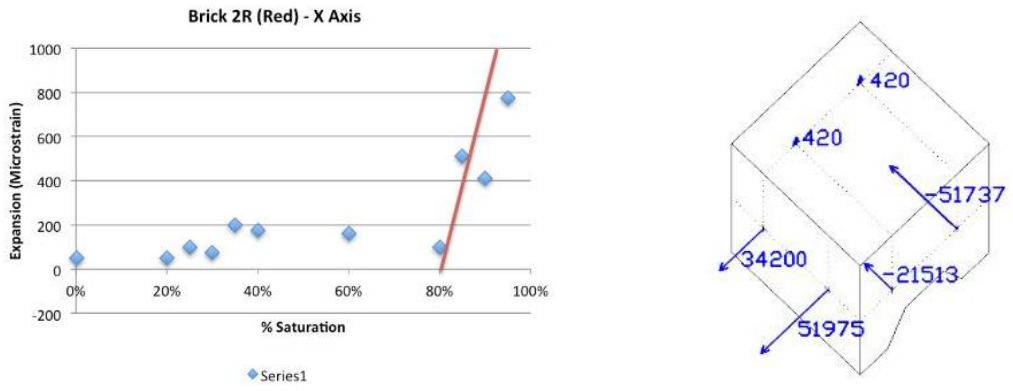

(a) (b)

FIGURE 2-16: (A) THE STRAINS VS MOISTUTRE CONTENT (% VACUUM SATURATION) GRAPH FOR A BRICK SPECIMEN (ALONG THE X AXIS). (B) THE EXPANSION AND SHRINKAGE STRAINS SEEN AT THE X AND Y AXES FOR THE HALF BRICK SAMPLE (WILLIAMS, 2015)

It is important to note that in earlier studies, frost dilatometry testing of a small sample size of bricks has been seen to produce great variability in results pertaining to the S_{crit} metric. In this regards, Van Straaten, Trainor and Schumacher (2016) investigated an alternative approach known as bulk sampling on the repeatability of S_{crit} measurements. The need for this has arisen as it has been observed that "…high strain variance has been found for highly saturated samples (*of brick masonry*) in some cases after freeze-thaw cycling" (p. 182). Therefore, the process for bulk sampling entails "removal of a large number of samples with the goal of randomly capturing the range of units" (Van Straaten et al., 2016, p. 178). The methodology of the study involved initially

conducting A-value tests of 47 bricks obtained from a building project in Ottawa. This essentially provided a glimpse on test specimens' properties, and their ability to absorb water through capillary uptake. In order to improve the technique of measurement of the dimensions of brick specimens, Van Straaten et al. (2016) tested limestone sample slices to account for "mechanical wear effects" (p. 183). For this purpose, they recommended that measurements prior to the freeze-thaw cycling need to be repeated until the difference between two successive readings is just 0.001mm and measurements after the freeze-thaw cycles are done only once. The study also tested a batch consisting of 12 limestone slices each at 80%, 90% and 100% moisture content (% vacuum saturation). The main findings were that the slices at a moisture content above the critical degree of saturation showed "significant variation" (p. 184), which has been attributed largely to the heterogenous internal microstructure of the test specimens (Van Straaten et al., 2016). The study recommended opting for "mean strain" (p. 184) in order to enhance the repeatability of measurements in frost dilatometry testing (Van Straaten et al., 2016).

2.10 GAPS IN THE LITERATURE REVIEWED

Following are the gaps in the literature reviewed:

1) Research on this subject area has focused on test specimens that were typically brick slices

2) Williams (2015) had tested half brick samples along the x and y and measured the strains at moisture contents, which corresponded to the S_{crit} of slices. The study however did not consider strains on the z-axis and the S_{crit} on that axis.

3) Study did not look at trends of frost decay of the half-brick samples, which would have been manifested by the evolution of microstrains from lower to higher moisture contents

4) Van Straaten (2014) looked at how the frost dilatometry methodology could be improved for testing brick slices but not half-brick samples.

5) Literature on how the physical properties of porous materials influence their strength and resistance to damage has generally focused on test specimens that are larger sized samples or whole bricks

6) Deterioration of clay brick masonry may be a culmination of the complex interaction of pores, which is perhaps underestimated in existing research that has pivoted solely on slices.

3 SCOPE

3.1 APPROACH

The approach for this dissertation starts with an overview of freeze-thaw deterioration in brick masonry, whereby a literature review on the subject reveals seminal work done in the field. The focus of the discussion included studies on the physical and mineralogical properties that govern the initiation of damage. Additionally, moisture storage and transport in porous materials have been examined in order to provide a fundamental understanding on how it would potentially impact the assessment of the risk of freeze-thaw deterioration of bricks This important aspect of brick masonry durability also inevitably influence their microstructure, thereby having an immense bearing on the moisture storage, uptake and transport internally. Standards governing freeze-thaw deterioration have also been studied, wherein the apparent drawbacks to assessing this type of failure have been identified. As a continuation of work undertaken by Mensinga (2009) and Williams (2015), this research project adopts the 'frost dilatometry' methodological approach to testing samples of historic brick masonry for the onset of freeze-thaw damage. The testing approach adopted in this research project has been adjusted to mimic (as much as possible) experimental procedures pertaining to frost dilatometry testing.

4 METHODOLOGY

Eight brick samples were selected to be part of the study, such that they were in a rather intact state. It is important to mention that these samples did not contain any glaringly large fissures or deformities that would have otherwise rendered them inappropriate for testing. The main aspects of the testing involved the cutting of samples; drying; vacuum saturation; preparation of the specimens for freeze-thaw testing and length measures before and after the freeze-thaw cycling. The methodology follows closely the procedures of frost dilatometry experimentation outlined in Mensinga (2009), Straaten (2014) and Williams (2015) (see Figure 4-1).

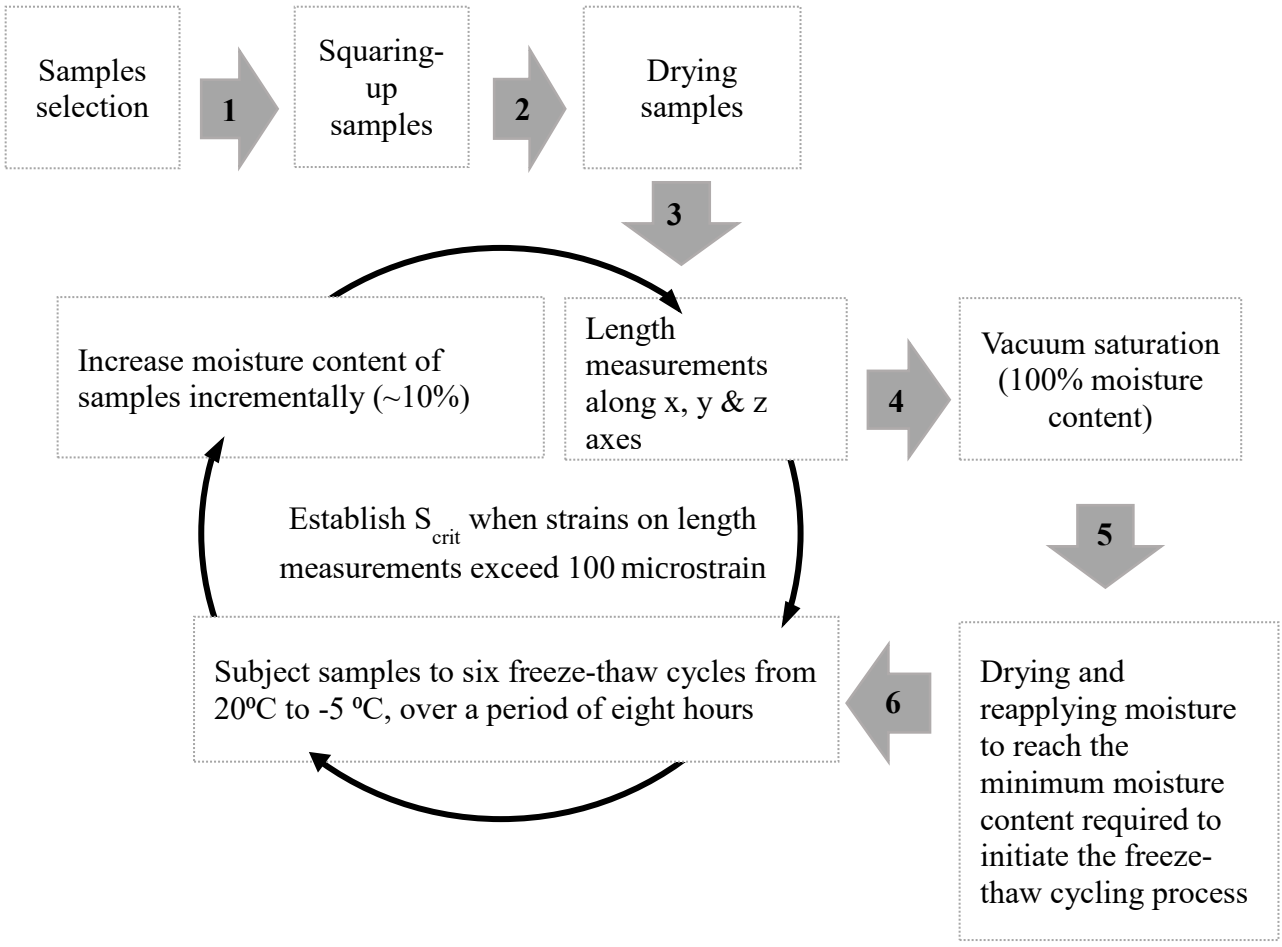

FIGURE 4-1: A SCHEMATIC SHOWING THE GENERAL SEQUENCE OF PROCEDURES FOLLOWED FOR THE FROST DILATOMETRY EXPERIMENTATION PROCESS

4.1 CUTTING OF SAMPLES

In order to be able to take accurate measurements of dimensions along the x, y and z axes, an attempt was made to square-up the samples with a diamond bladed masonry saw (DeWalt Industrial Tool – Heavy Duty Industrial Saw) (see Figure 4-2). However, it would be stressed here that the saw may not have cut the samples with high precision, leaving some surfaces and edges to remain jagged. Similarly, some samples did have residual mortar adhered to the surfaces. These were not entirely scraped off for the ensuing testing process due to the risk this could result in the sample dimensions to be considerably altered (and not conform to typical 'half-brick' dimensions). For the purpose of this study, such irregularities have been ignored but may warrant careful attention in similar research work on brick masonry.

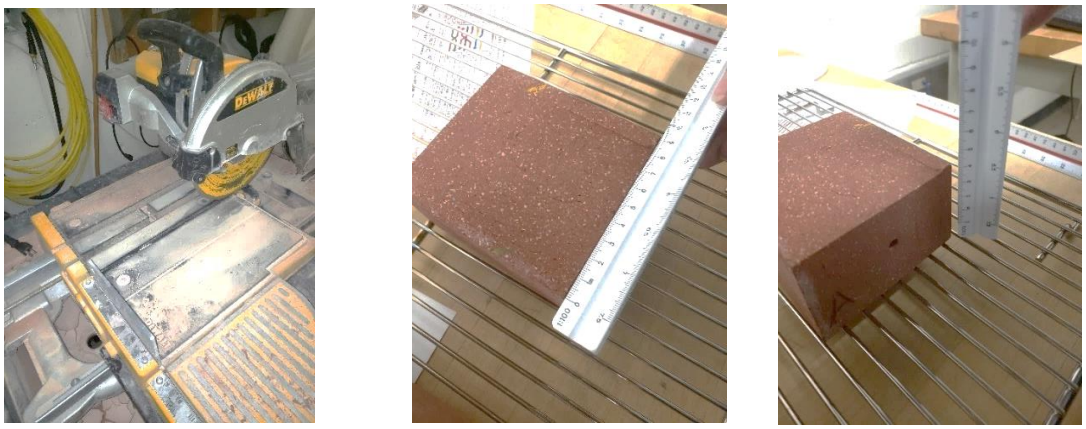

(a) (b) (i) (b) (ii)

FIGURE 4-2: (A) A DIAMOND EDGE SAW-BLADE WAS USED IN CUTTING THE BRICK SAMPLES. (B) (I) & (II) IN THIS CASE, AN ATTEMPT HAS BEEN TO PERFECTLY SQUARE UP HALF-BRICK SAMPLES FOR ACCURATE MEASUREMENTS ALONG THE X, Y AND Z AXES.

4.2 DRYING

In general accordance to ASTM C67/67M-19, the brick samples were dried at a temperature of 105°C in the laboratory oven (Fisher Scientific – Laboratory Instrument). The drying time was kept at 24 hours, whereby the bricks were weighed on a mass scale (OHAUS) every two hours to monitor changes in mass. Once it was established that there was no change in mass higher than 0.2% of the mass recorded earlier, the brick samples were taken out of the oven and set aside to

cool. They were kept inside a desiccator at room temperature to prevent them from absorbing moisture from the environment (see Figure 4-3).

(a)

(b)

(c)

FIGURE 4-3: (A) THE BRICK SAMPLES WERE DRIED IN THE LABORATORY OVEN AT 105ºC FOR 24 HOURS. (B) THE SAMPLES WERE WEIGHED ON THE WEIGHING SCALE. (C) THE BRICK SAMPLES WERE SET ASIDE TO COOL IN A DESICCATING VESSEL.

4.3 MEASUREMENTS OF SPECIMENS' DIMENSIONS

An electronic micrometer (Mitutoyo Digimatic Micrometer) and an inch micrometer (Mitutoyo) were used to take measurements of dimensions along different axes of the brick samples. The electronic micrometer measured lengths from 75mm (3") to 100mm (4"), whilst the inch micrometer was used to measure lengths from 50mm (2") to 75mm (3"). The former was used to measure the longer length dimensions of the brick samples, particularly along the x and y axes (see Figure 4-4). On the other hand, the thickness of the brick sample, which is denoted as the z-axes was measured using an inch micrometer. In contrast to Mensinga (2009) and Williams (2015), length measurements in this study were done without the need for drilling pin targets in the brick samples. The approach adopted a jig-based setup, which is an improved practice of "measurement repeatability" (p. 85) recommended by Van Straaten (2014).

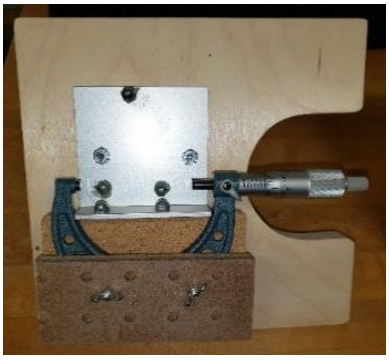

(a)

(b)

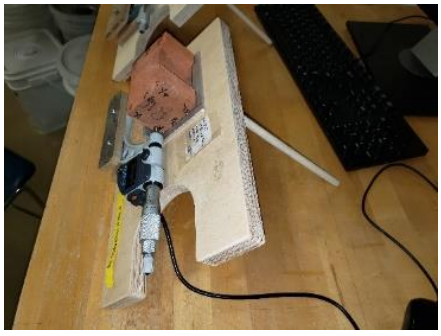

(c)

FIGURE 4-4: (A) TO (C) MICROMETER JIGS FOR THE INCH AND ELECTRONIC MICROMETER, WHEREBY THEY ARE ELEVATED FROM THE HORIZONTAL TO ENABLE PERFECTLY ALIGNED MEASUREMENTS

For accurate measurements, micrometer jigs that were inclined to the horizontal were developed (see Figure 4-5). This way, the brick samples could sit perfectly aligned on the resting platform next to the spindle, thereby ensuring a degree of precision in measurements. The spindle was positioned to take measurements at the same point along the different axes, whereby the sample was rotated in 180° after each measurement. It is noteworthy that care was taken to ensure that the spindle did not wear away any brick surface during the measurements.

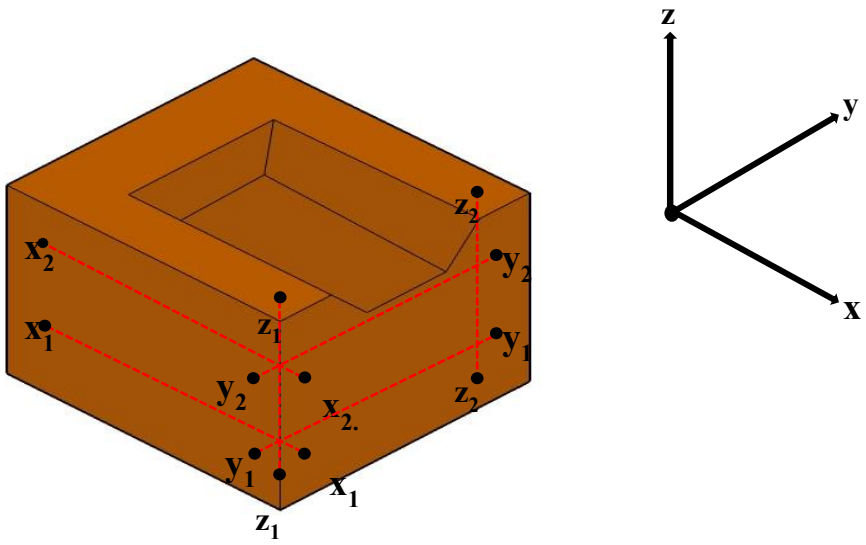

FIGURE 4-5: THE SET OF MEASUREMENTS FROM 1 TO 4 TAKEN ALONG THE X, Y AND Z-AXES CORRESPONDING TO OPPOSITE SURFACES OF THE BRICK SAMPLE

The 'x-axis' measurements are the longitudinal dimensions parallel to the width of the brick sample. Similarly, the 'y-axis' denotes the dimensions parallel to the depth of the brick sample. Finally, the 'z-axis' are the dimensions of the brick sample along its height (see Figure 4-5) (Williams, 2015).

Based on the length measurements taken, the strains were calculated as follows (Mensinga, 2009):

$$\varepsilon = \frac{l_6 - l_0}{l_0} \times 10^6$$

ε is the expansion (microstrains)

l_6 is the specimen length after 6 freeze thaw cycles

l_0 is the length of the specimen at the dry state

4.4 DETERMINATION OF THE SATURATED MASS OF BRICK SAMPLES VIA THE VACUUM SATURATION APPROACH

Both Mensinga (2009) and (Williams, 2015) had compared the saturated masses of brick samples via the boil and the vacuum saturation methods. They found that the vacuum saturation method produced a greater difference in saturated mass for certain types of bricks when compared to the boil method. Similarly, there was also less variability in low porosity bricks via the former method, making it generally a more reliable approach to saturate brick samples. Therefore, this study had adopted a vacuum saturation approach to saturating the brick samples, owing primarily due to the effectiveness and time-based convenience of the process.

The sequence of procedures required for the vacuum saturation of the brick samples had been adapted from Mensinga (2009). The experimental setup involved a desiccator, vacuum pump (Edwards-28) and a distilled water reservoir connected with tubing and valves. The valves connected to the desiccator had been adjusted to openings currently on the desiccator lid, such that unlike in Mensinga (2009), there was no intermediate 'atmosphere' valve connecting the vacuum pump to the desiccator. The 'atmosphere' valve in the experimental setup for this study was independently connected to the desiccator, and had no connection to the vacuum pump

Once the brick samples were placed on the leveling supports present at the bottom of the desiccator vessel, the lid was shut tight and the vacuum pump was switched on. The pressure drop in the desiccator had been adjusted to 0.01atm (or -29.6inHg) as outlined in Mensinga (2009). It is pertinent to mention here that Williams (2015) maintained a pressure of about -1atm (-27.75inHg), however the experimental setup was slightly different to the one adopted for this study. Once the desired magnitude of pressure was reached in the desiccator, the valve connecting it to the pump was shut off, wherein the pump was now exposed to the atmosphere. The valve connecting the reservoir to the desiccator was switched on, thereby allowing the distilled water to flow into the desiccator. The valve was kept open until all the brick sample are fully submerged. Once submerged, the valve was shut off and the valve connecting the atmosphere to the desiccator was opened. This raised the pressure inside the desiccator back to the ~1atm (0inHg). As per Mensinga (2009), the brick samples were left to soak in the water for an hour.

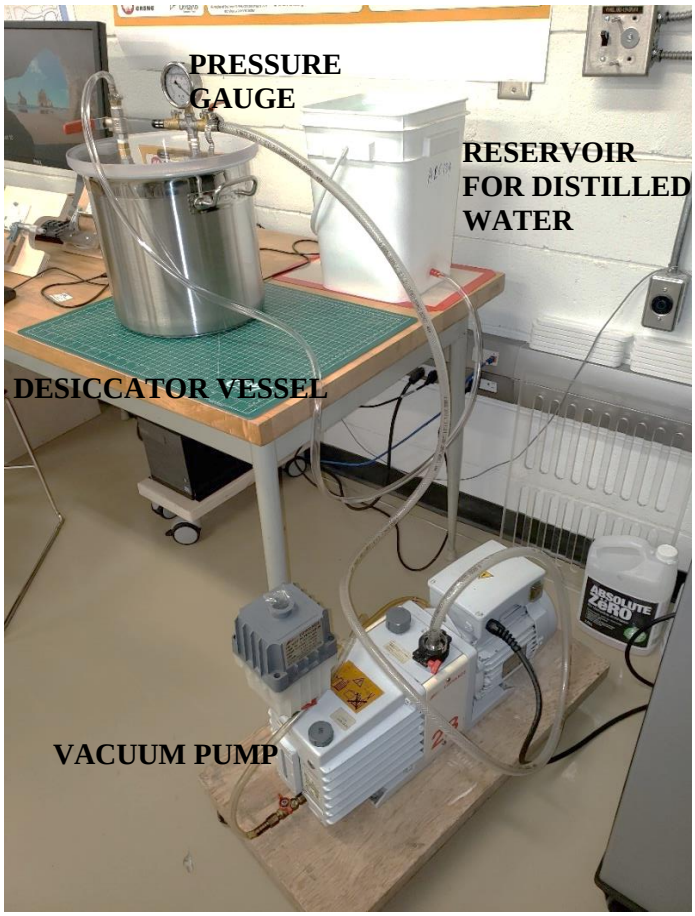

FIGURE 4-6: THE EXPERIMENTAL SETUP FOR VACUUM SATURATION OF THE BRICK SAMPLES CONSISTED OF A VACUUM PUMP, WATER RESERVOIR, AND A DESICCATOR VESSEL. THE PRESSURE INSIDE THE DESICCATOR VESSEL WAS MONITORED VIA THE GAUGE THAT WAS ATTACHED TO ITS LID.

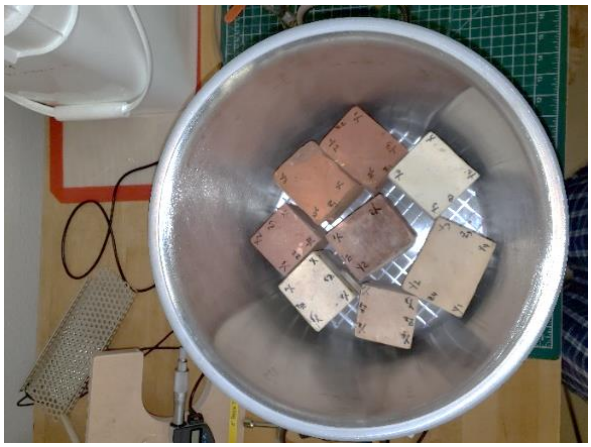

FIGURE 4-7: THE TEST SAMPLES WERE PLACED ON A LEVELLING RACK INSIDE THE DESICATOR VESSEL. THEY WERE ARRANGED IN AN ORDER TO ENSURE THAT ALL OF THEM COULD BE VACUUM SATURATED AT THE SAME TIME.

FIGURE 4-8: THE BRICK SAMPLES WERE SUBJECTED TO A VACUUM INSIDE THE VESSEL, WHEREBY THE GAUGE HERE INDICATED THE PRESSURE INSIDE TO BE -1ATM (~30 INHG).

FIGURE 4-9: ONCE THE RIGHT LEVEL OF VACUUM PRESSURE WAS REACHED (I.E. 0ATM OR -30INHG), THE VALVE CONNECTING THE RESERVOIR TO THE DESICCATOR VESSEL WAS OPEN ALLOWING IT BE FILLED WITH DISTILLED WATER

4.5 PREPARATION OF BRICK SPECIMENS FOR FREEZE-THAW TESTING

The saturated brick samples were removed from the desiccator vessel and the excess moisture was wiped off using a clean paper towel. They were weighed on the mass scale and the new saturated mass was recorded. Similarly, the difference between the saturated and the dry mass of the brick samples was also calculated. This value indicated the amount of moisture required to fill most of the pore space. Based on the S_{crit} of the slices, a minimum moisture content that is about 20% less, was determined for each brick sample. Therefore, the mass of the brick sample at that minimum moisture content was calculated and was set as the 'target mass' for the ensuing drying process. The brick samples were then placed in the oven where they dried at different rates. The samples are weighed at about 20-minute intervals to monitor the mass loss chronologically. Once the mass of the brick sample has reached the 'target mass', the brick samples are removed from the oven. If the brick sample's mass is not very close to the 'target mass', the sample was placed on the mass scale and distilled water was carefully reapplied using a dropper. The typical technique of application entailed distributing moisture in the sample by rubbing it on the surface, such that it was evenly absorbed into the specimen. Once there was deposition of moisture on the surface of the brick sample, it was absorbed further into the sample through capillary action (Mensinga, 2009).

FIGURE 4-10: A DROPPER WAS USED TO APPLY DISTILLED WATER ON THE BRICK SAMPLE, ALL THE WHILE METICULOUSLY MONITORING THE CHANGE IN MASS

FIGURE 4-11: THE TECHNIQUE OF REAPPLYING MOISTURE SUCH THAT IT IS EVENLY DISTRIBUTED IN THE BRICK SPECIMEN

Once the bricks reached their target mass, either through drying or by the reapplication of additional moisture on the surface, they were tightly wrapped in cling film. The film was basically a vapor impermeable material, which restricted the egress of moisture in the form of water vapor out of the brick sample (see Figure 4-12). According to Straube et al. (2010), careful attention needs to be put in reducing "the air space between the surface of the specimen and the sealant material" (p. 5). The brick samples were then left for about 18 hours to let the moisture redistribute in the brick samples. Depending upon the A-value of the considered samples, the time required to allow all of the moisture to redistribute within the material could be as long as 72 hours (Straube et al., 2010). After a period of about 48 hours, length measurements of the brick samples were taken again. The brick sample was carefully removed from the cling film and re-weighed. Any differences in the dimensions and mass were hence recorded. The brick samples were then re-wrapped in the cling film, to prevent further loss of moisture from the specimen.

FIGURE 4-12: THE BRICK SAMPLES HAVE BEEN TIGHTLY WRAPPED IN TWO LAYERS OF CLING FILM

The cling-film wrapped brick samples were then place in a waterproof Ziplock bag, and the air inside was removed using a modified ‘vacuum cleaner’ (see Figure 4-13). This was done with the purpose to remove air pockets inside the Ziplock bag that would have otherwise had an insulating effect resulting in a non-uniform distribution of temperature in the sample upon immersion in the refrigerant bath.

FIGURE 4-13: AIR WAS REMOVED FROM INSIDE THE ZIPLOCK BAG USING A MODIFIED ‘VACUUM CLEANER’.

(a)

(b)

(c)

FIGURE 4-14: (A) TO (C) THE SAMPLES WERE PLACED INSIDE ZIPLOCK BAGS AND IMMERSED IN THE BATH

The samples in the Ziplock bag were carefully placed inside the refrigerant bath, wherein the machine (PolyScience) was programmed via the controller to run six freeze-thaw cycles from 20°C to -15°C. It is noteworthy that the refrigerant in the machine was in a circulating motion due to the machine pump that was constantly running, thereby helping to evenly distribution of temperature required for the cycles (see Figure 4-15).

FIGURE 4-15: THE PROGRAM FOR THE FREEZE-THAW CYCLES IS BEING RUN AS SEEN ON THE CONTROLLER'S SCREEN.

4.6 THE TIME REQUIRED TO COOL/THAW

Before the samples were subjected to the freeze-thaw cycles part of the frost dilatometry experimentation process, it was necessary to determine the total time taken for a half-brick sample to thaw and cool to the thawing temperature. This follows the approach taken by Van Straaten (2014), who recommended drilling a hole along the longest axis in the center of the half brick sample and inserting in a thermistor probe (HOBOware datalogger). The probe and the opening were then sealed with tape. Another thermistor probe was placed inside the bath to monitor the actual temperature inside the refrigerant bath in the freeze-thaw machine. The brick sample, which was sealed tight in a Ziplock bag, was placed inside the freeze-thaw machine (Julabo ME) containing glycol as the refrigerant, and the temperature was dropped from 20°C to -15°C.

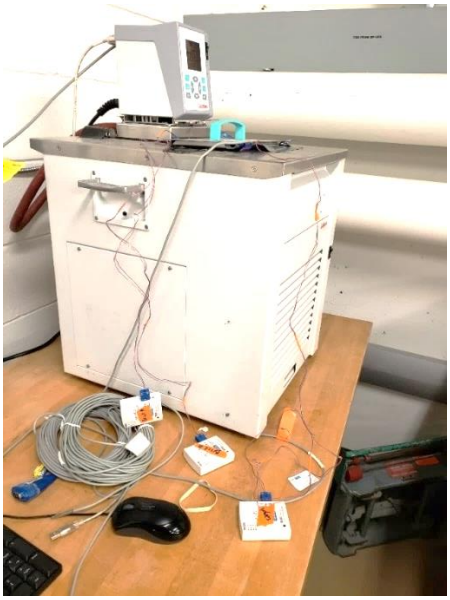

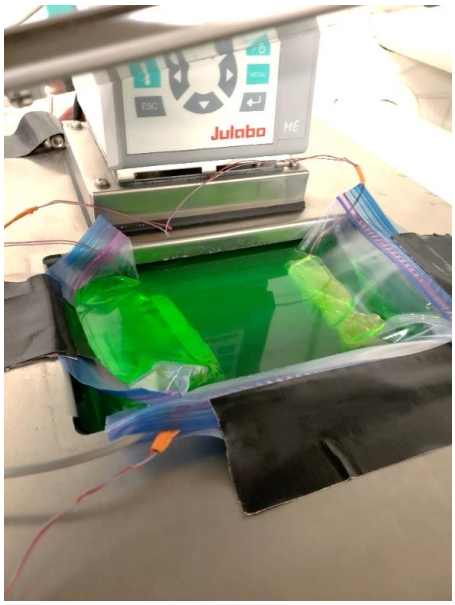

(a) (b)

FIGURE 4-16: (A) TO (B) TO MONITOR THE TEMPERATURE VARIATION INSIDE THE BRICK, THERMISTOR PROBES WERE INSERTED IN THE CENTER OF THE BRICK SAMPLES. THE SAMPLE WAS THEN SEALED TIGHT IN A ZIPLOCK BAG AND IMMERSED IN THE GLYCOL BATH. SIMILARLY, A THERMISTOR PROBE WAS ALSO INSERTED IN THE BATH TO MONITOR THE TEMPERATURE VARIATION

4.7 FREEZE-THAW CYCLING OF THE BRICK SAMPLES

Once the brick samples attained the required moisture content, freeze-thaw cycling was performed in an "automatic freeze-thaw chamber" (Williams, 2015, p. 68). Williams (2015) kept brick samples in a horizontally inclined position in a refrigerator, where they were subjected to freeze-thaw cycles by way of convective currents that helped cool/thaw the inside temperature. Similarly, nine freeze-thaw cycles from 30°C to -30°C were done and each cycle was 12 hours long. On other hand, Mensinga (2009) immersed the brick samples in "a programmable temperature controlled refrigerating circulator manufactured by VWR, filled with a half-ethylene-glycol, half water mixture" (p. 83). In this study, an approach similar to that in Mensinga (2009) and Van Straaten (2014) have been adopted. The brick samples had been placed in a refrigerating circulator, whereby the refrigerant is half-propylene and half-water. Furthermore, the thawing and cooling temperatures had been set to be 20°C to -15°C respectively each, whereby the rate at which this occurred was 17.5°C per hour, similar what was adopted by Van Straaten (2014) and Mensinga (2009). Upon reaching the cooling temperature, the refrigerant bath remained at that temperature

for a further two hours so that there was a uniform distribution of temperature in the core of the brick sample.

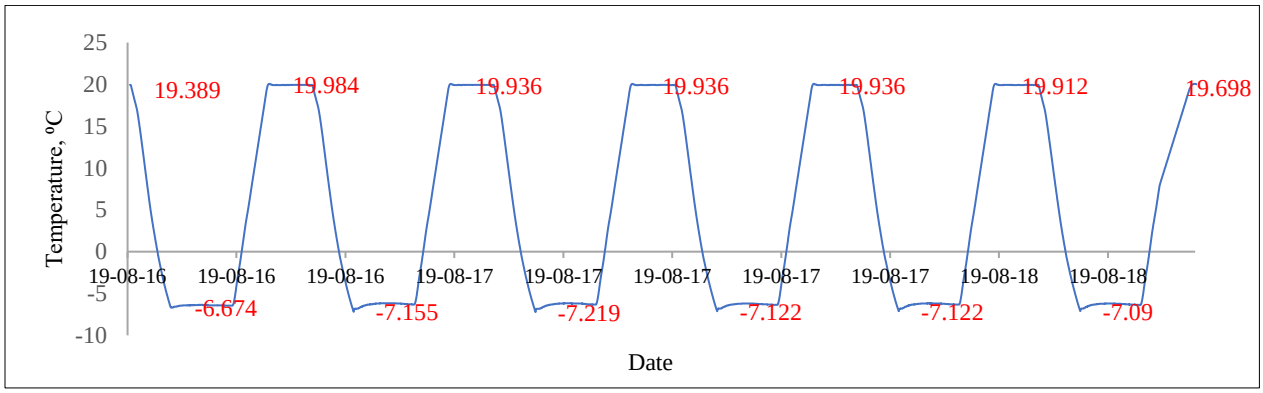

FIGURE 4-17: SIX FREEZE THAW CYCLES ALTERNATING BETWEEN APPROXIMATELY 20ºC TO -7.2ºC FROM THE 16TH OF AUGUST TO 18TH OF AUGUST. MEASUREMENTS WERE TAKEN BY THE TEMPERATURE DATALOGGER.

Figure 4-17 shows the temperature measurements performed by the Hobo temperature datalogger between the 16th and 18th of August, whereby the minimum temperature that the freeze-thaw machine could drop to was only about -7.2ºC.

4.8 INCREASING MOISTURE OF BRICK SAMPLES TO HIGHER MOISTURE CONTENTS

The brick samples were subjected to freeze-thaw cycles with moisture contents between the ranges ~58% - 100%. For most of the brick samples, distilled water was applied via the technique discussed above till about the third set of freeze-thaw cycles. At certain moisture contents (say at about ~77% generally at the end of the third set of freeze-thaw cycles), some of the brick samples had reached a ‘capillary saturation’ state such that application of distilled water on the surface would not further increase the moisture content of the sample. Therefore, in order to attain a higher moisture content (say ~87%), brick samples must be subjected to a hydraulic potential to force the entry of water into the inaccessible pores. The bricks samples were thus vacuum saturated raising the moisture content (to 100%) and then dried slowly to attain the target moisture content specific to the brick sample considered. Like the approach described earlier, the samples were kept on the weighing scale and the changes in masses of the samples were meticulously monitored to reach the target values.

4.9 THE BRICK SAMPLES

4.9.1 NOMENCLATURE AND LOCATION

TABLE 3: EIGHT BRICK SAMPLES BELONGING TO DIFFERENT LOCATIONS WERE TESTED

Sr. #	Brick sample nomenclature	Image	Location
1	295C-F2		Location A
2	309-EF2		Location A
3	60		Location A
4	305-EB4		Location B
5	295A-EB3		Location B

Sr. #	Brick sample nomenclature	Image	Location
6	297-EB2		Location B
7	295A-F4		Location B
8	349-ER1		Location B

4.9.2 GENERAL OBSERVATIONS ABOUT THE BRICK SAMPLES

There were some differences in the outward appearance of the brick samples, such that some of the brick samples were seen to have pits and cracks on their exterior surfaces. This non-uniform composition contributed to a rough texture on the surface. Similarly, there were brick samples that had smooth surfaces, which was a result of the way they were sliced by the diamond edged saw machine. In this case, any adhered mortar or flaws on the upper surfaces would have been removed by slicing that part off. It is assumed that the type of brick sample surface would have an impact on the way moisture would have been absorbed into the interior. Also noteworthy was the appearance of flakes in brick sample type 297-EB2 and a visibly large crack across a face of sample type 60, after the fifth set of freeze-thaw cycles, indicating the impact of frost damage on the physical integrity of the samples.

(a) Sample type 60 (b) Sample type 297-EB2

FIGURE 4-18: (A) – (B) THE BRICK SAMPLES HAVE VISIBLE CRACKS AND PITS ON THEIR SURFACES. AS EVIDENT, THERE IS ALSO THE PRESENCE OF AN AIR POCKET IN EACH SAMPLE.

(a) Sample type 60 (b) Sample type 297-EB2

FIGURE 4-19: (A) – (B) A CRACK IS SEEN ON SAMPLE TYPE 60, WHEREAS FLAKING ON THE SURFACE OF SAMPLE TYPE 297-EB2 AFTER THE FIFTH SET OF FREEZE THAW CYCLES

5 TEST RESULTS OF THE BRICK SLICES

TABLE 4: RESULTS FOR THE PROPERTIES OF THE BRICK SLICES TESTED IN THE STUDY

Sample Notation	Dry density (kg/m^3)	A-value (kg/m2s1/2)	Permeability (ng/sPam)	Wref (%MCw)	Wcap (%MCw)	Vac Sat (%MCw)	Scrit (%Vac Sat)	Scrit M (%MCw)
295C-F2	1548	0.518	26.4	0.04%	23.1%	25.3%	78.4%	19.8%
309-EF2	1558	0.302	21.8	0.14%	23.3%	24.3%	79.0%	19.2%
60	1692	0.546	22.1	0.08%	19.5%	21.4%	73.4%	15.7%
305-EB4	1618	0.101	37.4	9.58%	23.2%	31.0%	84.4%	26.2%
295A-EB3	1627	0.165	17.8	0.64%	24.2%	25.0%	85.5%	21.4%
297-EB2	1799	0.257	18.5	0.40%	25.2%	26.3%	77.1%	20.2%
295A-F4	1596	0.127	18.3	0.83%	19.9%	22.1%	88.1%	19.5%
349-ER1	1667	0.197	10.8	0.16%	16.6%	16.9%	87.3%	14.8%

5.1.1 A-VALUE AND S_{CRIT} OF SLICES

Based on the test results for the slices, the range of A-values was between 0.101 $kg/m^2s^{1/2}$ and 0.546 $kg/m^2s^{1/2}$, whereby brick sample type 60 had the highest A-value at 0.546 $kg/m^2s^{1/2}$. Similarly, brick sample type 305-EB4 had the lowest A-value at 0.101 $kg/m^2s^{1/2}$. Brick sample type 295A-F4 had the highest S_{crit} value at 88.1%. However, brick sample type 60 had the lowest S_{crit} value at 73.4%.

6 RESULTS FROM FROST DILATOMETRY TESTING OF HALF-BRICK SAMPLES

6.1 THE TIME REQUIRED TO COOL

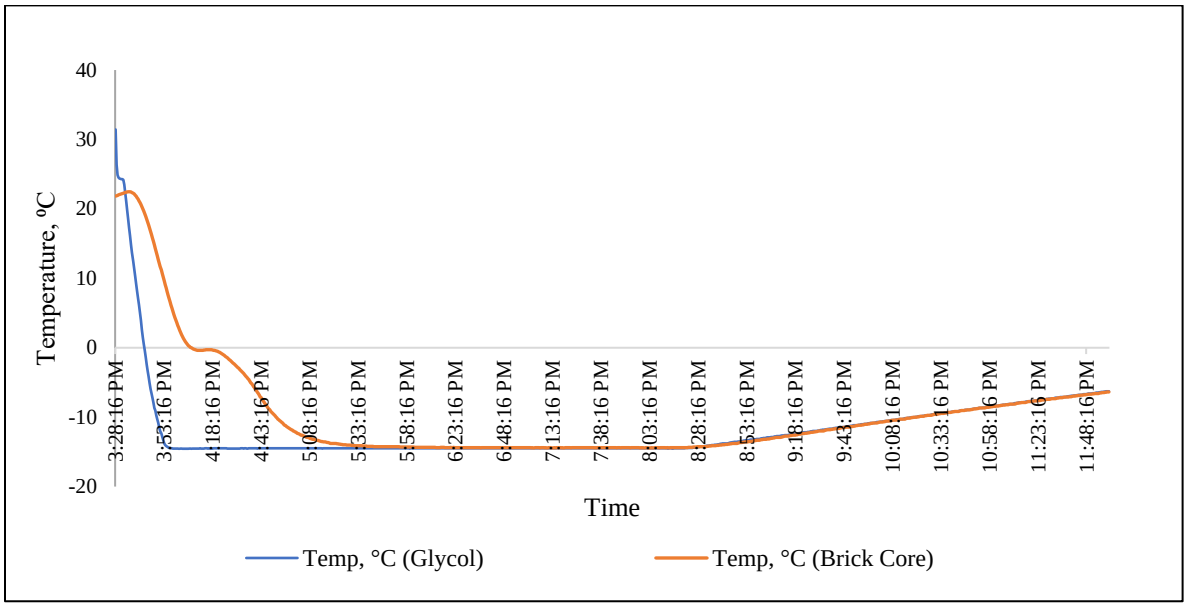

FIGURE 6-1: THE CORE OF THE BRICK TAKES ABOUT TWO HOURS TO REACH THE SAME TEMPERATURE AS THE BATH (FOR COOLING AT -15ºC)

As seen in Figure 6-1, the temperature of the glycol was initially 30ºC before it dropped to about -15ºC in about 25 minutes. On the other hand, owing to its latent heat capacity, the brick core dropped to -15ºC in approximately two hours. Therefore, the time lag between glycol and the brick core in reaching the minimum setpoint temperature was two hours. In each freeze-thaw cycle, the setpoint was left at the cooling and thawing temperatures for 2 hours, so that there was a uniform distribution of temperature to the brick core.

6.2 DRY MASS OF SAMPLES

There is great variation of dry mass among the different brick samples, such that the range of the masses is from 574g to 868g. Brick sample type 295A-EB3 has the highest dry mass, at 868g, while type 295A-F4 has the lowest mass at 574g (see Table 5).

TABLE 5: DRY MASSES OF BRICK SAMPLES THAT WERE SUBJECTED TO 105ºC IN AN OVEN OVERNIGHT

Sample Notation	Dry Mass (g)
295C-F2	760.500
309-EF2	766.000
60	701.000
295A-EB3	868.000
305-EB4	695.500
297-EB2	633.500
295A-F4	574.000
349-ER1	624.000

6.3 MASS OF SAMPLES AFTER VACUUM SATURATION

The results of vacuum saturation, which is expressed as the moisture content, as a percentage of weight of the brick sample show the typical range to be between 17.0% to 24.9%. Brick sample type 297-EB2 has the highest moisture content as a % of the dry mass, at 26.0%. Similarly, brick sample type 349-ER1 has the lowest moisture content as a % of the dry mass, at 17.0% (see Table 6).

TABLE 6: MASS OF THE SAMPLES AFTER BEING VACUUM SATURATED IN DISTILLED WATER

Brick Sample Notation	Saturated mass of bricks samples (g)	Mass of moisture at 100% saturation (g)	Vac Sat (% MCw)
295C-F2	949.5	189.00	24.9%
309-EF2	943.0	177.00	23.1%
60	846.0	145.00	20.7%
295A-EB3	1084.0	216.00	24.9%
305-EB4	866.5	171.00	24.6%
297-EB2	798.5	165.00	26.0%
295A-F4	694.5	120.50	21.0%
349-ER1	730.0	106.00	17.0%

6.4 TARGET MOISTURE CONTENT AND MASSES OF BRICK SAMPLES FOR SUCCESSIVE FREEZE-THAW CYCLES

The initial moisture content of the test specimens was about 20% less than the S_{crit} values of the slices of the same sample. The range of initial moisture contents varied between 53.4% to 68.1%. At the start of the first set of freeze-thaw cycles, brick sample type 295A-F4 had the highest moisture content, at 68.1%. On the other hand, brick sample type 60 had the lowest moisture content at 53.4%. The brick sample types, whose moisture contents ranged at the lower spectrum of the range (60, 297-EB2, 295C-F2 and 309-EF2), were subjected to five sets of freeze thaw

cycles to attain a final moisture content above 90%. Brick sample types 295A-F4, 349-ER1, 305-EB4 and 295A-EB3 had a moisture content above 90%, at the fourth set of freeze-thaw cycles. The samples were not subjected to freeze-thaw cycles at a moisture content of 100% (see Table 7 Table 8).

6.4.1 MOISTURE CONTENT

TABLE 7: BASED ON THE SLICES SCRIT, TARGET MOISTURE CONTENTS AT 10% INCREMENTS FOR SUCCESSIVE FREEZE-THAW TEST CYCLES HAS BEEN DETERMINED

Brick Sample Notation	Target Moisture Contents (MC) of brick samples (% Vacuum Saturation) at sets of freeze-thaw cycles				
	Initial MC at the 1st set of freeze-thaw cycles	MC at 2nd set of freeze-thaw cycles	MC at 3rd set of freeze-thaw cycles	MC at 4th set of freeze-thaw cycles	MC at 5th set of freeze-thaw cycles
295C-F2	58.4	68.4	78.4	88.4	98.4
309-EF2	59.0	69.0	79.0	89.0	99.0
60	53.4	63.4	73.4	83.4	93.4
295A-EB3	64.4	74.4	84.4	94.4	
305-EB4	65.5	75.5	85.5	95.5	
297-EB2	57.1	67.1	77.1	87.1	97.1
295A-F4	68.1	78.1	88.1	98.1	
349-ER1	67.3	77.3	87.3	97.3	

6.4.2 MASS

TABLE 8: THE TARGET MASSES OF BRICK SAMPLES CORRESPONDING TO THE RESPECTIVE MOISTURE CONTENTS

Brick Sample Notation	Target Mass of Brick Samples (g) at sets of freeze-thaw cycles				
	Initial MC at the 1st set of freeze-thaw cycles	MC at 2nd set of freeze-thaw cycles	MC at 3rd set of freeze-thaw cycles	MC at 4th set of freeze-thaw cycles	MC at 5th set of freeze-thaw cycles
295C-F2	870.85	889.75	908.65	927.55	946.45
309-EF2	870.36	888.06	905.76	923.46	941.16
60	778.39	792.89	807.39	821.89	836.39
295A-EB3	1007.16	1028.76	1050.36	1071.96	
305-EB4	807.57	824.67	841.77	858.87	
297-EB2	727.75	744.25	760.75	777.25	793.75
295A-F4	656.10	668.15	680.20	692.25	

Brick Sample Notation	Target Mass of Brick Samples (g) at sets of freeze-thaw cycles				
	Initial MC at the 1st set of freeze-thaw cycles	MC at 2nd set of freeze-thaw cycles	MC at 3rd set of freeze-thaw cycles	MC at 4th set of freeze-thaw cycles	MC at 5th set of freeze-thaw cycles
349-ER1	695.32	705.92	716.52	727.12	

6.5 ACTUAL MOISTURE CONTENT AND MASS OF BRICK SAMPLES BEFORE AND AFTER WRAPPING WITH CLING FILM

A meticulous attempt was made in raising the moisture content of the brick samples to be as near as possible to the target moisture content, which has been discussed in section 6.4 above. It was, however, observed that the actual moisture contents of the brick samples were different before wrapping with cling film at the start of the freeze-thaw cycles (known as 'BW' in Table 9) and after the six freeze-thaw cycles (known as 'AF' in Table 9). The largest reduction between BW and AF was about 4.2% of its dry mass, whereby it occurred for brick sample type 295A-EB3 after the fourth set of freeze-thaw cycles. The same sample consistently had differences in moisture content above 1%, after each set of freeze-thaw cycles. The lowest reduction between BW and AF was about 0.2%, and it occurred in brick sample type 305-EB4 after the third set of freeze-thaw cycles (see Table 11).

6.5.1 MOISTURE CONTENT

TABLE 9: ACTUAL MOISTURE CONTENT (% VACUUM SATURATION) BEFORE AND AFTER WRAPPING WITH CLING FILM

Brick Sample Notation	The actual moisture contents of brick samples (% vacuum saturation) at sets of freeze-thaw cycles									
	Initial MC at the 1st set of freeze-thaw cycles		MC at 2nd set of freeze-thaw cycles		MC at 3rd set of freeze-thaw cycles		MC at 4th set of freeze-thaw cycles		MC at 5th set of freeze-thaw cycles	
	BW	AF	BW	AF	BW	AF	BW	AF	BW	AF
295C-F2	57.9	57.1	68.0	67.5	78.0	75.7	87.7	87.2	97.2	96.7
309-EF2	58.8	56.5	69.2	68.6	79.1	75.7	88.7	88.4	98.4	97.4
60	53.1	49.7	63.8	63.4	73.8	72.8	83.5	82.8	92.8	92.4
295A-EB3	64.6	63.2	74.5	74.3	84.7	84.5	98.4	94.2		
305-EB4	65.5	62.6	75.7	74.6	85.7	85.1	95.8	94.8		
297-EB2	56.7	54.5	67.6	67.3	77.9	77.0	87.6	86.7	96.7	95.1

Brick Sample Notation	The actual moisture contents of brick samples (% vacuum saturation) at sets of freeze-thaw cycles									
	Initial MC at the 1st set of freeze-thaw cycles		MC at 2nd set of freeze-thaw cycles		MC at 3rd set of freeze-thaw cycles		MC at 4th set of freeze-thaw cycles		MC at 5th set of freeze-thaw cycles	
	BW	AF	BW	AF	BW	AF	BW	AF	BW	AF
295A-F4	68.0	65.6	78.8	78.0	88.0	85.5	98.1	97.1		
349-ER1	67.0	75.5	77.8	76.9	87.3	85.4	96.8	95.7		
BW and AF stand for 'MC before wrapping with film' and 'MC after six freeze-thaw cycles' respectively										

6.5.2 MASS

TABLE 10: ACTUAL MASS OF BRICK SAMPLES (G) BEFORE AND AFTER WRAPPING WITH CLING FILM

Brick Sample Notation	The actual mass of brick samples (g) at sets of freeze-thaw cycles									
	Initial MC at the 1st set of freeze-thaw cycles		MC at 2nd set of freeze-thaw cycles		MC at 3rd set of freeze-thaw cycles		MC at 4th set of freeze-thaw cycles		MC at 5th set of freeze-thaw cycles	
	BW	AF	BW	AF	BW	AF	BW	AF	BW	AF
295C-F2	870	868.5	889	888	908	903.5	921	920	936.	936.0
309-EF2	870	866	888.5	887.5	906	900	915	914.5	933.	932.0
60	778	773	793.5	793	808	806.5	822.5	821.5	835.	834.0
295A-EB3	1007.5	1004.5	1029	1028.5	1051	1050.5	1048.5	1047.5		
305-EB4	807.5	802.5	825	823	842	841	842.5	841		
297-EB2	727	723.5	745	744.5	762	760.5	778.00	776.5	782.	780.0
295A-F4	656	653	669	668	680	677	676.50	675.5		
349-ER1	695	704	706.5	705.5	716.	714.5	714.00	713		
BW and AF stand for 'MC before wrapping with film' and 'MC after six freeze-thaw cycles' respectively.										

6.5.3 DIFFERENCE BETWEEN TARGET AND ACTUAL MOISTURE CONTENTS (%)

TABLE 11: DIFFERENCES IN MOISTURE CONTENT (%) OF BRICK SAMPLES BEFORE WRAPPING IN CLING FILM AFTER SIX FREEZE-THAW CYCLES

Brick sample notation	1st set of freeze thaw cycles	2nd set of freeze thaw cycles	3rd set of freeze thaw cycles	4th set of freeze thaw cycles	5th set of freeze thaw cycles
	BW- AF, Δ (%)	BW- AF, Δ (%)	BW- AF, Δ (%)	BW- AF, Δ (%)	BW- AF, Δ (%)
295C-F2	0.8	0.5	2.3	0.5	0.5
309-EF2	2.3	1	3.4	0.3	1
60	2.3	0.6	3.4	0.7	0.4
295A-EB3	3.4	0.4	1	4.2	
305-EB4	1.4	0.2	0.2	1	
297-EB2	2.9	1.1	0.6	0.9	1.6
295A-F4	2.2	0.3	0.9	1	
349-ER1	2.4	0.8	2.5	1.1	

BW and AF stand for 'MC before wrapping with film' and 'MC after six freeze-thaw cycles' respectively

6.6 LENGTH AND MASS CHANGES AT DIFFERENT MOISTURE CONTENTS

Length measurements of the different brick samples were taken at the dry state and after each set of freeze-thaw cycles (see Appendix B – Length measurements of specimens). An average of the dimensions across certain axes was taken, and this was denoted as x-avg, y-avg and z-avg. It is noteworthy that the brick samples, in some situations, were not completely squared up, thereby length measurements across certain axis points due to surface irregularities were not taken. For example, in the case of brick sample type 295C-F2, length measurement of the x-axis was only taken along the x1-x1 and x2-x2 points; for the y-axis, measurements were taken along y1-y1, y2-y2 and y3-y3 and finally for the x-axis, it was only z1-z1. The averages of the dimensions measured were hence considered as x-avg, y-avg and z-avg.

6.7 STRAIN CALCULATIONS (REMAINING GRAPHS ARE IN APPENDIX A)

Following the frost dilatometry testing, strain measurements along the x, y and z-axes were measured and have hence been depicted in subsequent graphs. In case the S_{crit} point can be discerned from the datapoints, a trendline has been included to the indicate the incidence of frost damage. Based on the approach adopted by Williams (2015a) and Mensinga (2009), a trend line which would intercept the y-axis at 100 microstrains would indicate the moisture content corresponding to the S_{crit} point (Appendix A – Strains vs Moisture Content (% Saturation)for the 'strains vs moisture content' graphs pertaining to points along the x, y and z-axes).

6.7.1 STRAIN VS MOISTURE CONTENT GRAPHS FOR THE BRICK SAMPLE TYPE 295C-F2

6.7.1.1 AVERAGE STRAINS

For the determination of S_{crit}, no discernible trend has been observed in the average strain measurements along the x and y axes for the brick sample type '295C-F2'(see Figure 6-2 and Figure 6-3). No expansions strains are observed, whereby there exist large contraction strains (negative microstrains) seen to decrease consistently after each set of freeze-thaw cycles at the test moisture contents. There is, thus, a non-uniform decrease in the magnitude of the negative microstrains. On the other hand, for the z-axis, a trend can be seen whereby at increasing moisture contents (between 57.9% to 97.2), the microstrains are increasing from negative to positive. In this case, the S_{crit} point can be determined; the intersection between the trend line and extrapolation of the y-axis at 100 microstrains results it to be at about 88% moisture content (% of vacuum saturation) (see Figure 6-4).

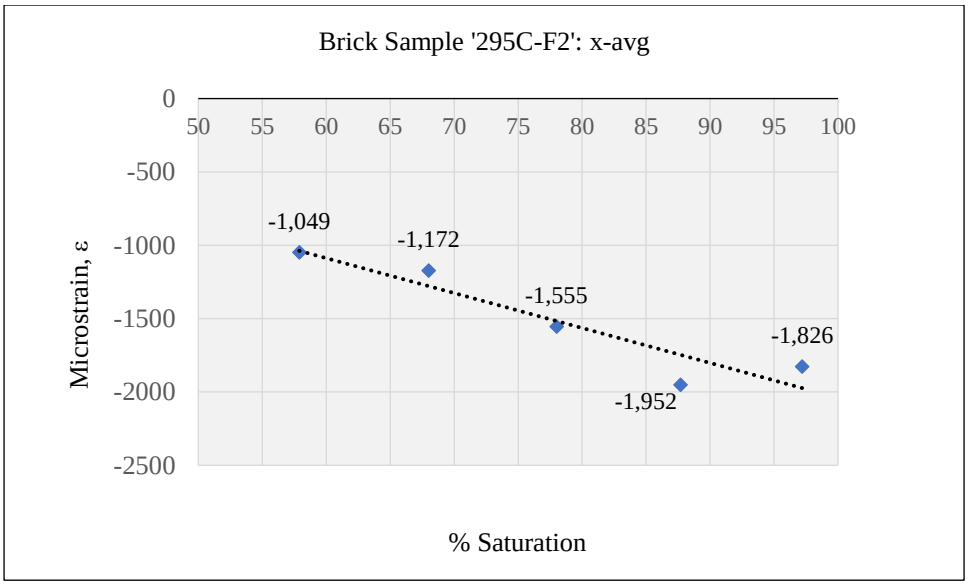

FIGURE 6-2: AVERAGE STRAINS IN THE X-AXIS

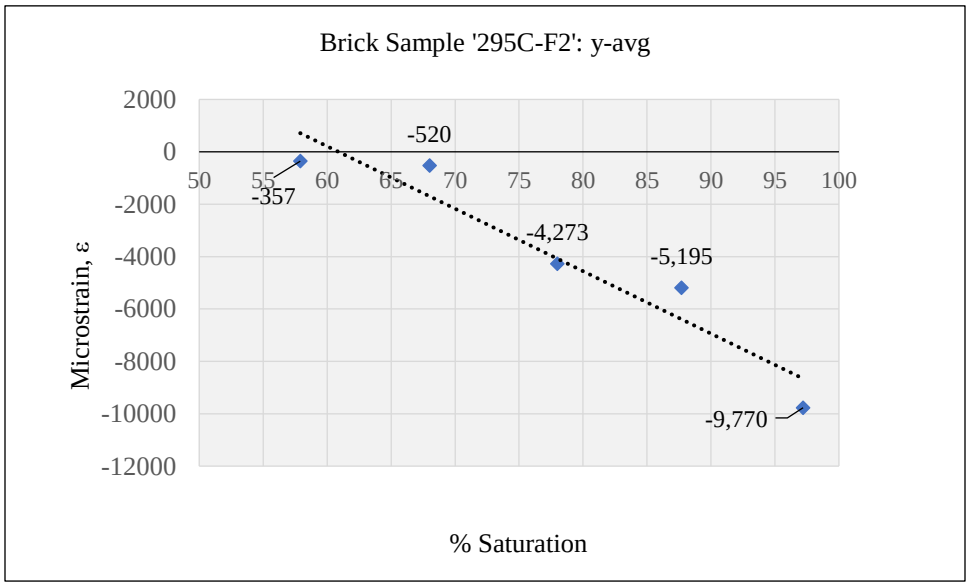

FIGURE 6-3: AVERAGE STRAINS IN THE Y-AXIS

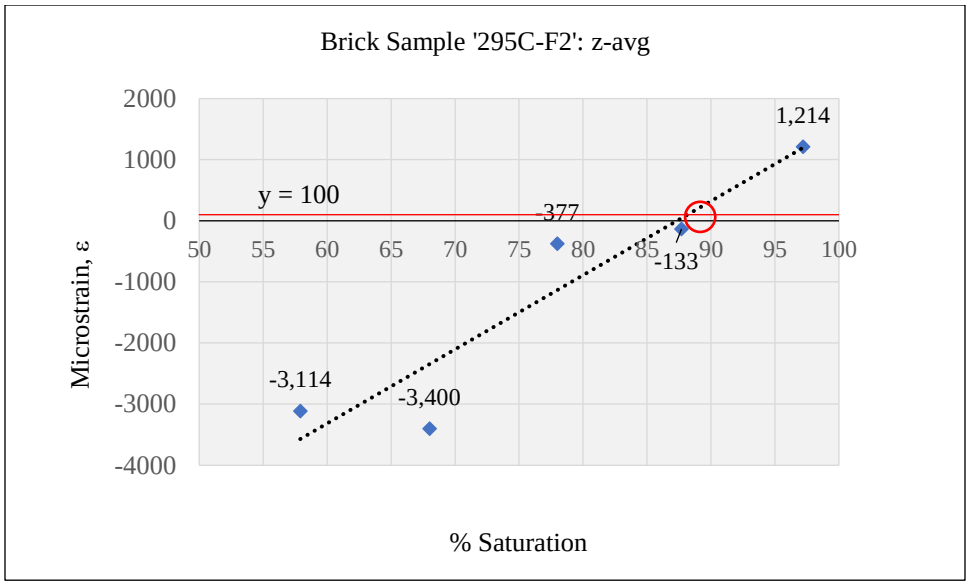

FIGURE 6-4: AVERAGE STRAINS IN THE Z-AXIS

6.7.1.2 STRAINS ALONG THE Y AXIS POINTS

Strain calculations based on the length measurements along the y1-y1 and y2-y2 axes revealed a trend of increasing microstrains as the moisture content increased (at each successive set of freeze-thaw cycles) (see Figure 6-5 and Figure 6-6). However, the S_{crit} points that can be discerned from the graphs, are at about 97.5% and 67.5% moisture content (% vacuum saturation) for the y1-y1 and y2-y2 axes respectively.

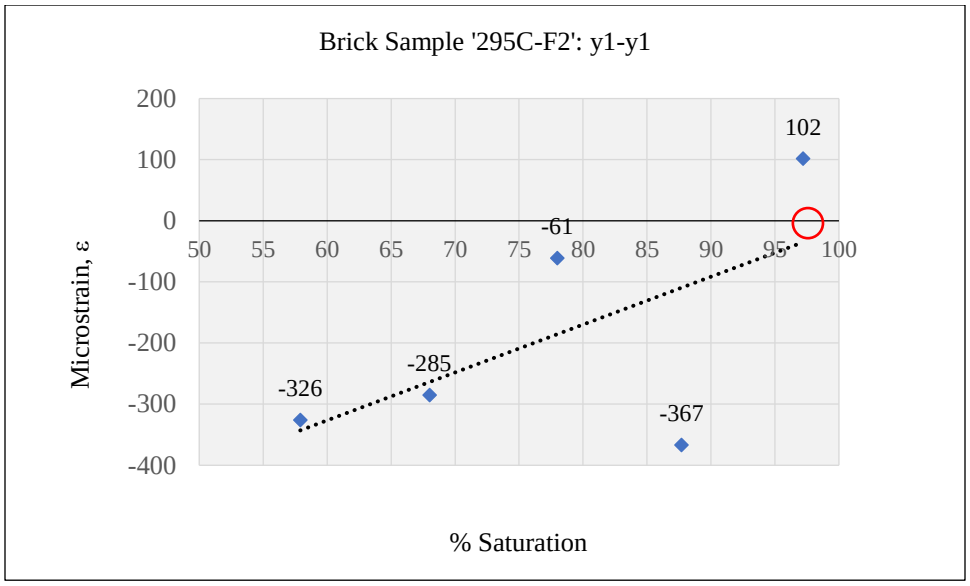

FIGURE 6-5: STRAINS ALONG THE Y1-Y1 AXIS

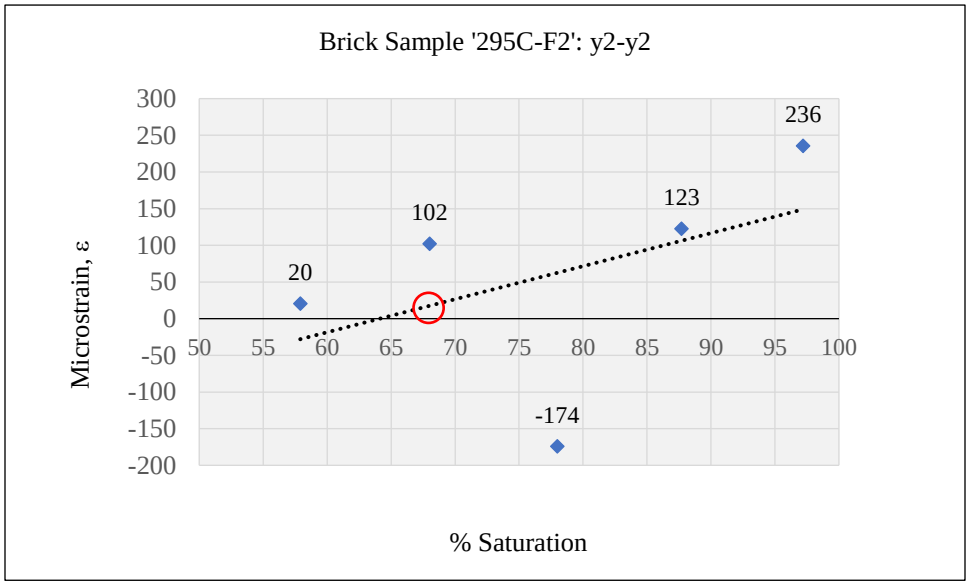

FIGURE 6-6: STRAINS ALONG THE Y2-Y2 AXIS

6.7.2 STRAIN VS MOISTURE CONTENT GRAPHS FOR THE BRICK SAMPLE TYPE 309-EF2

6.7.2.1 AVERAGE STRAINS

As seen from Figure 6-7 to Figure 6-8, for brick sample type 309-EF2, the microstrains are non-uniform, with expansion as well as shrinkage occurring along all three axes. For the average strains along the x-axis, the microstrains at the initial moisture content is seen to be 114 microstrains. Similarly, for the z-axis, the microstrains for brick sample type 309-EF2 is 3501. Thus, in this case, the S_{crit} point could not be clearly ascertained

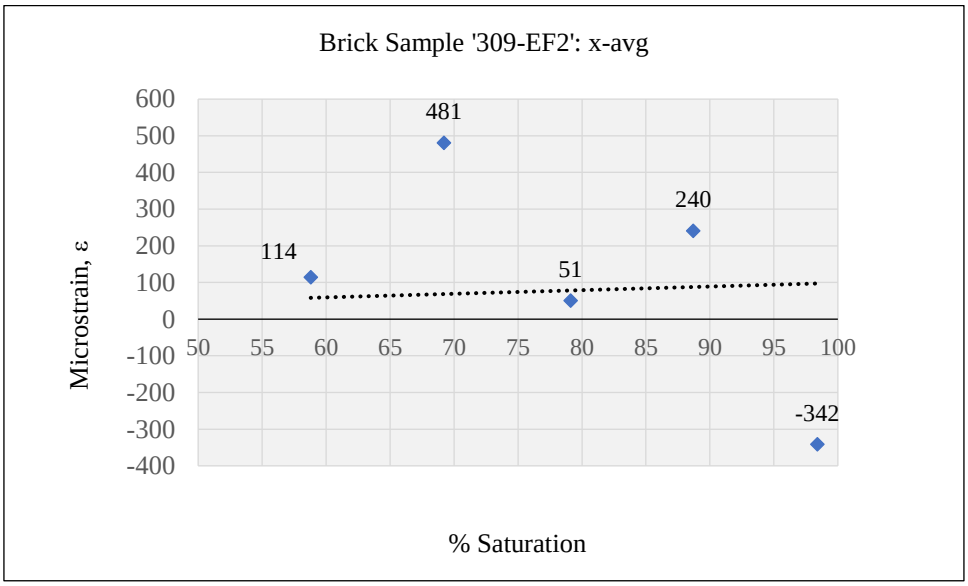

FIGURE 6-7: AVERAGE STRAINS ALONG THE X-AXIS

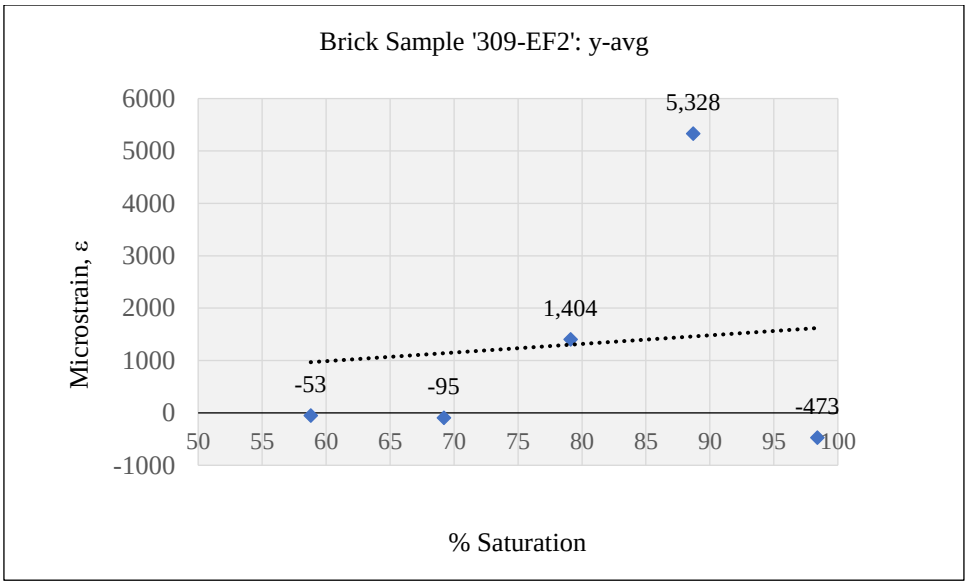

FIGURE 6-8: AVERAGE STRAINS ALONG THE Y-AXIS

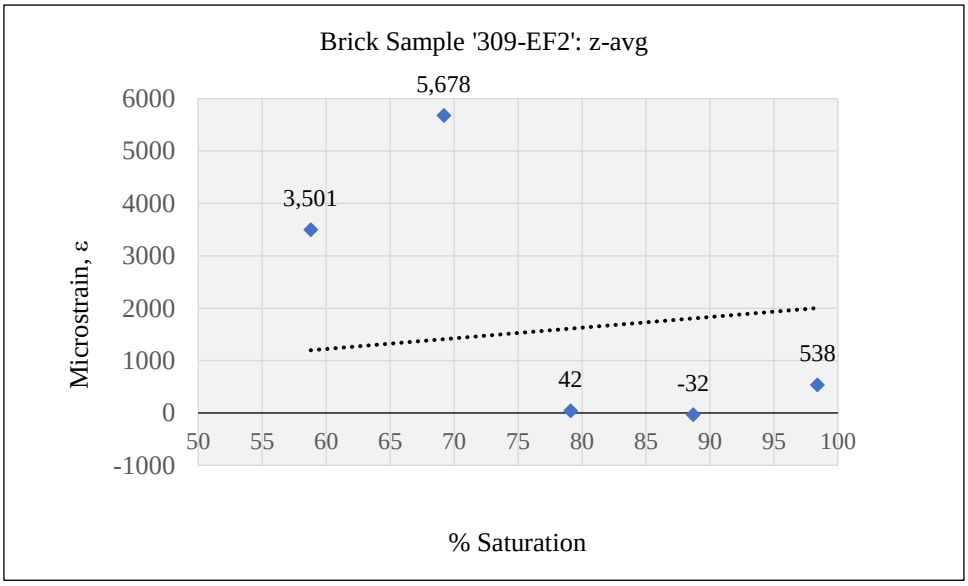

FIGURE 6-9: AVERAGE STRAINS ALONG THE Z-AXIS

6.7.3 STRAIN VS MOISTURE CONTENT GRAPHS FOR THE BRICK SAMPLE TYPE 60

6.7.3.1 AVERAGE STRAINS

As seen from Figure 6-10, Figure 6-11 and Figure 6-12, for brick sample type 60, the microstrains are non-uniform, with expansion as well as shrinkage occurring along all three axes. For the average strains along x-axis, the initial microstrains is -269, which is seen to decrease consistently with increasing moisture contents (% vacuum saturation). Similarly, for the average strains along the y and z axes, the initial microstrains are 549 and 462 microstrains respectively. Thus, in this case, the S_{crit} point could not be clearly ascertained.

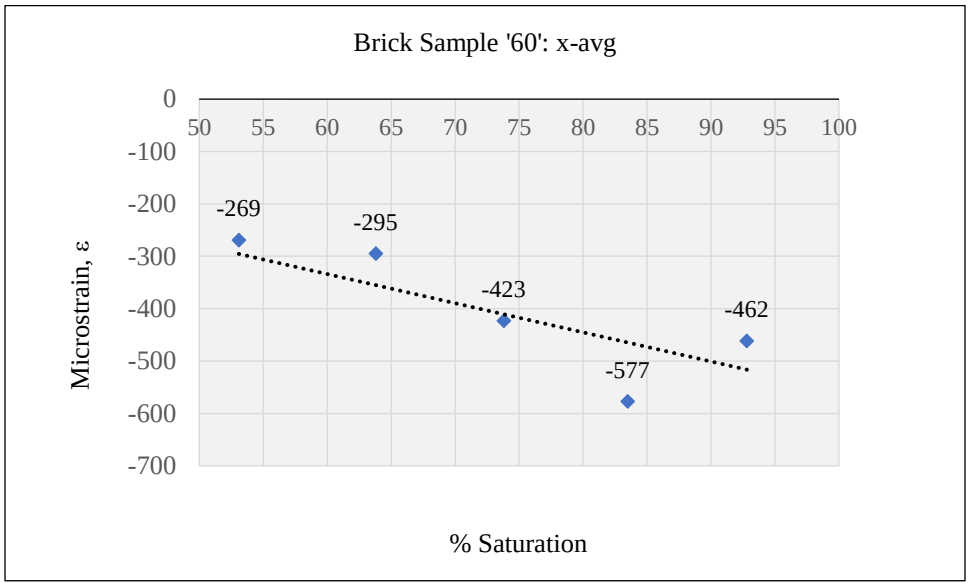

FIGURE 6-10: AVERAGE STRAINS ALONG THE X-AXIS

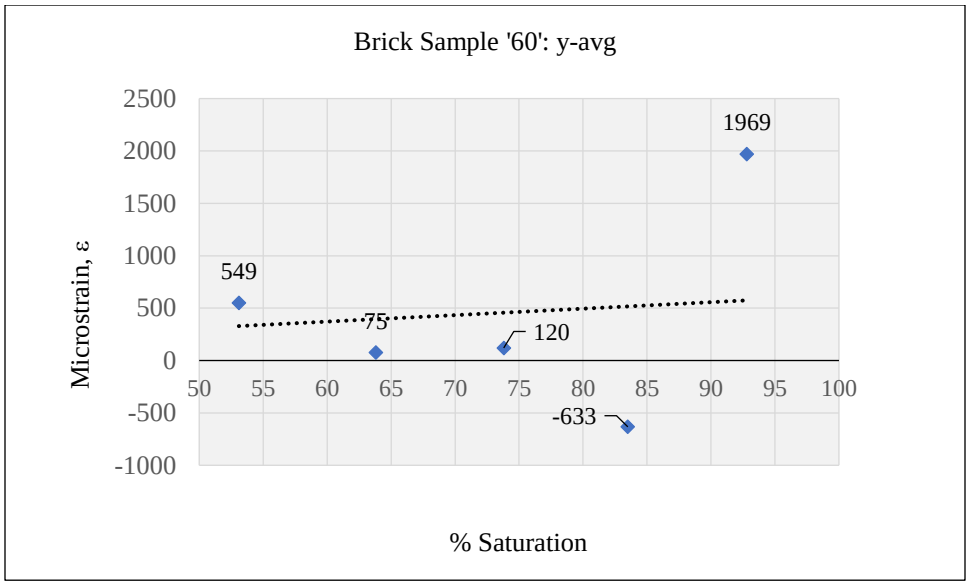

FIGURE 6-11: AVERAGE STRAINS ALONG THE Y-AXIS

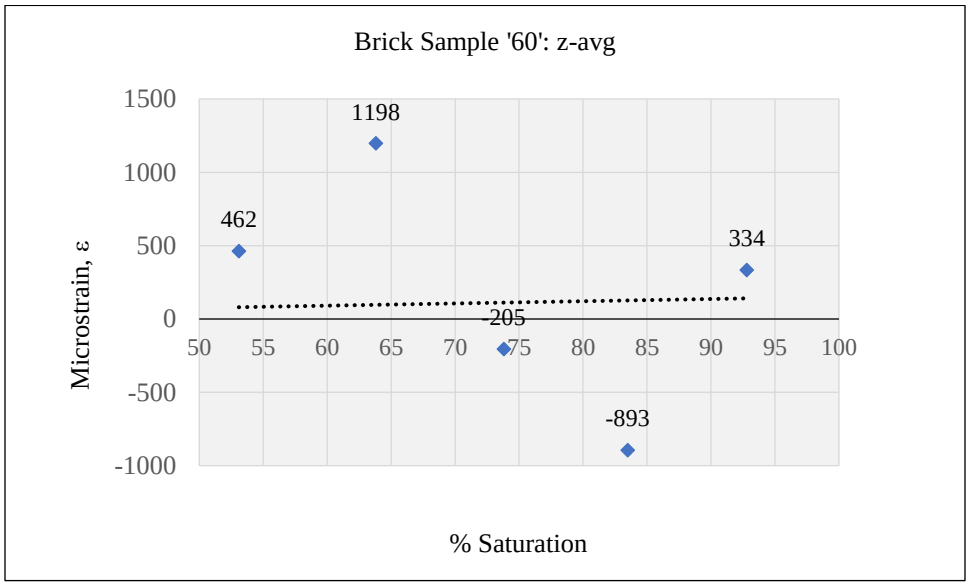

FIGURE 6-12: AVERAGE STRAINS ALONG THE Z-AXIS

6.7.3.2 STRAINS ALONG X, Y AND Z-AXES

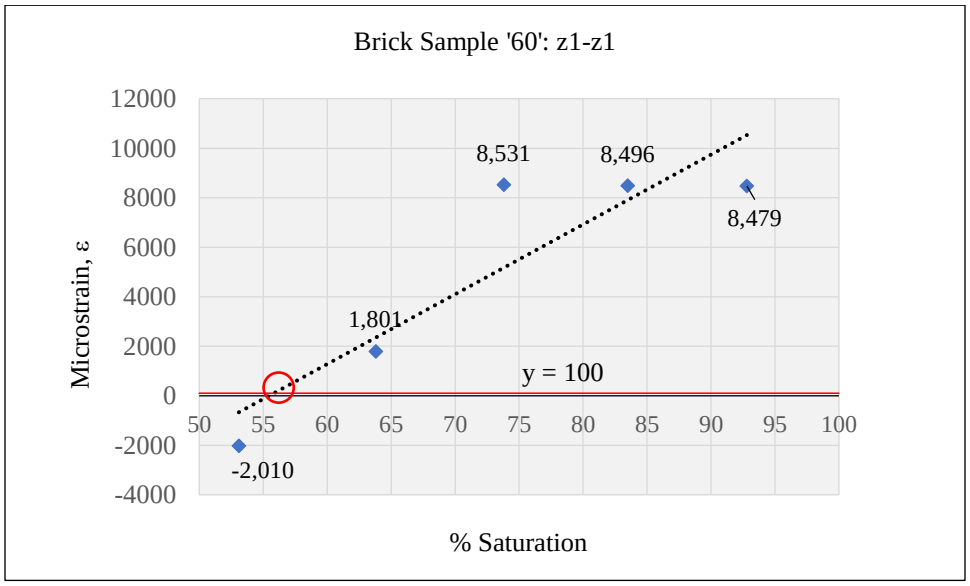

FIGURE 6-13: STRAINS ALONG THE Z1-Z1 AXIS

In Figure 6-13, a trend has been observed whereby the microstrains ar0e seen to be increasing at moisture content increments (53.1% to 92.8%). Based on the intersection between trend line and the y-axis extrapolated at 100 microstrains, the moisture content at which S_{crit} occurs is about 56% (% vacuum saturation).

6.7.4 STRAIN VS MOISTURE CONTENT GRAPHS FOR THE BRICK SAMPLE TYPE 295A-EB3

6.7.4.1 AVERAGE STRAINS

As seen from Figure 6-14 and Figure 6-16, for brick sample type 295A-EB3, the microstrains are non-uniform, with expansion as well as shrinkage occurring along all three axes. For the average strains along x-axis, the initial microstrains is 430; along the y-axis, the initial microstrains is 884, while for the z-axis, the initial microstrains is 1209. The datapoints do not delineate any consistent trends that could have indicated the onset of frost damage. Thus, in this case, the S_{crit} point could not be clearly ascertained.

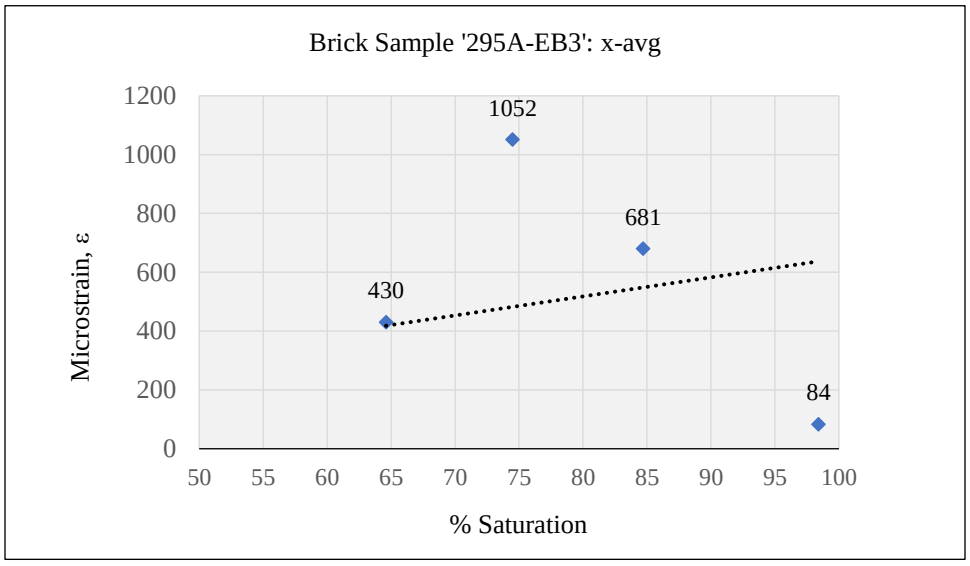

FIGURE 6-14: AVERAGE STRAINS ALONG THE X-AXIS

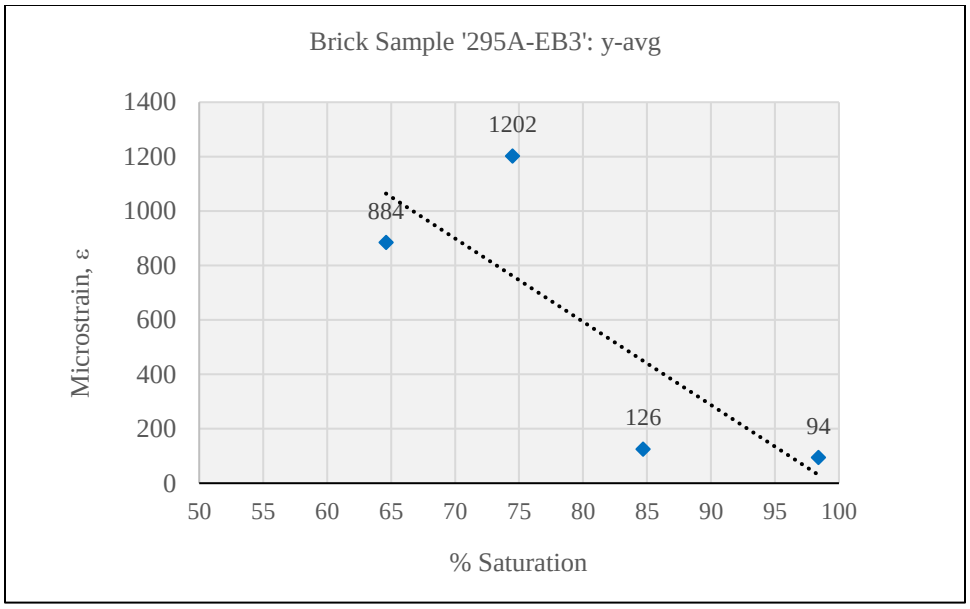

FIGURE 6-15: AVERAGE STRAINS ALONG THE Y-AXIS

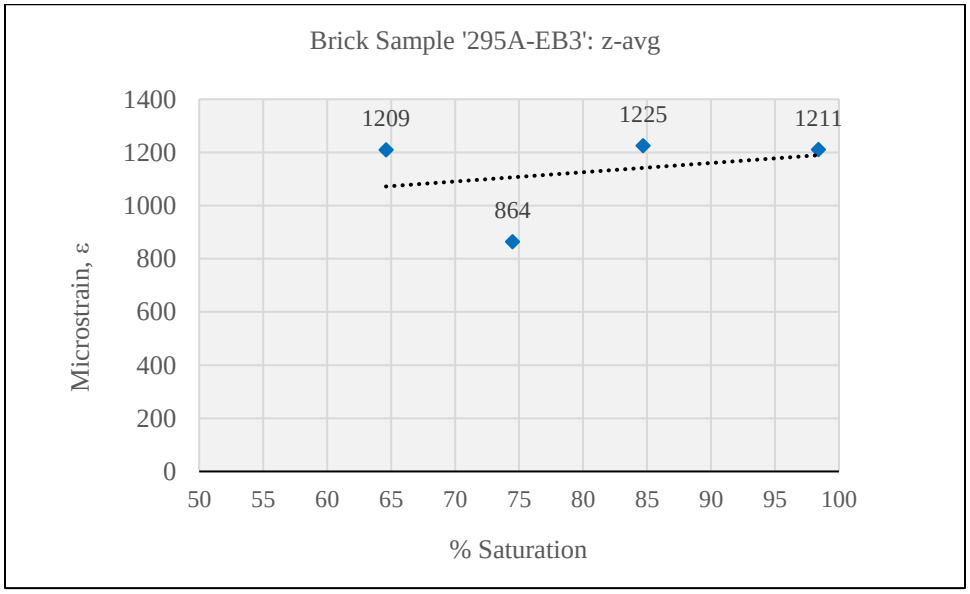

FIGURE 6-16: AVERAGE STRAINS ALONG THE Z-AXIS

6.7.5 STRAIN VS MOISTURE CONTENT GRAPHS FOR THE BRICK SAMPLE TYPE 305-EB4

6.7.5.1 AVERAGE STRAINS

As seen from Figure 6-17 to Figure 6-19, for the brick sample type 295A-EB3, the microstrains are non-uniform, with expansion as well as shrinkage occurring along all three axes. For the average strains along x-axis, the initial microstrains is -913 (negative microstrains); along the y-axis, the initial microstrains is 560, while for the z-axis, the initial microstrains is -1772 (negative microstrains). In Figure 6-17Figure 6-18, the datapoints do not delineate any consistent trends that could have indicated the onset of frost damage. Thus, in this case, the S_{crit} point could not be clearly ascertained. However, for the average strains on the z-axis, a trend delineating increasing microstrains at the test moisture contents (65.5% to 95.8%) is observed (see Figure 6-19). Therefore, based on the intersection of the trend line and the extrapolation of y-axis at 100 microstrains, the S_{crit} point is the moisture content at about 81% (% vacuum saturation).

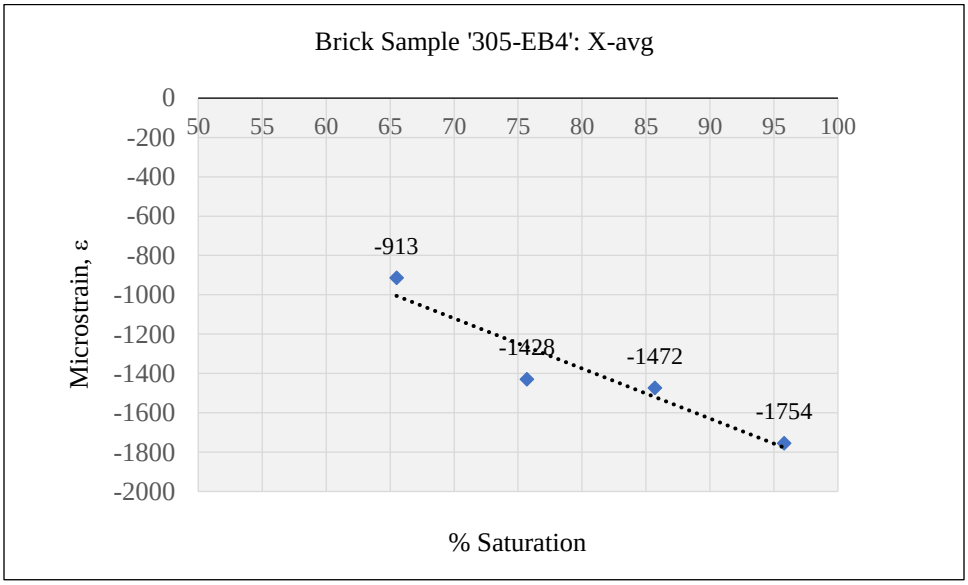

FIGURE 6-17: AVERAGE STRAINS ALONG THE X-AXIS

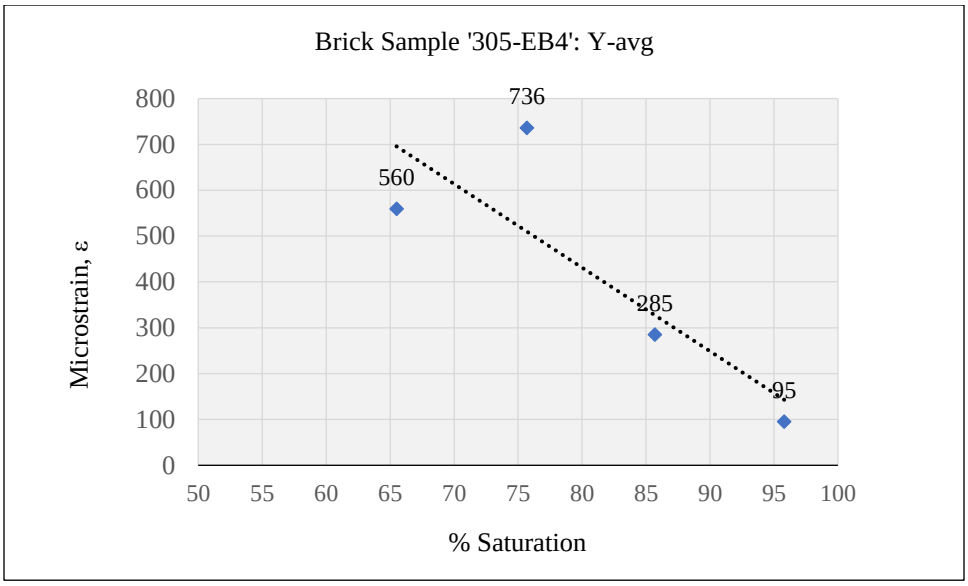

FIGURE 6-18: AVERAGE STRAINS ALONG THE Y-AXIS

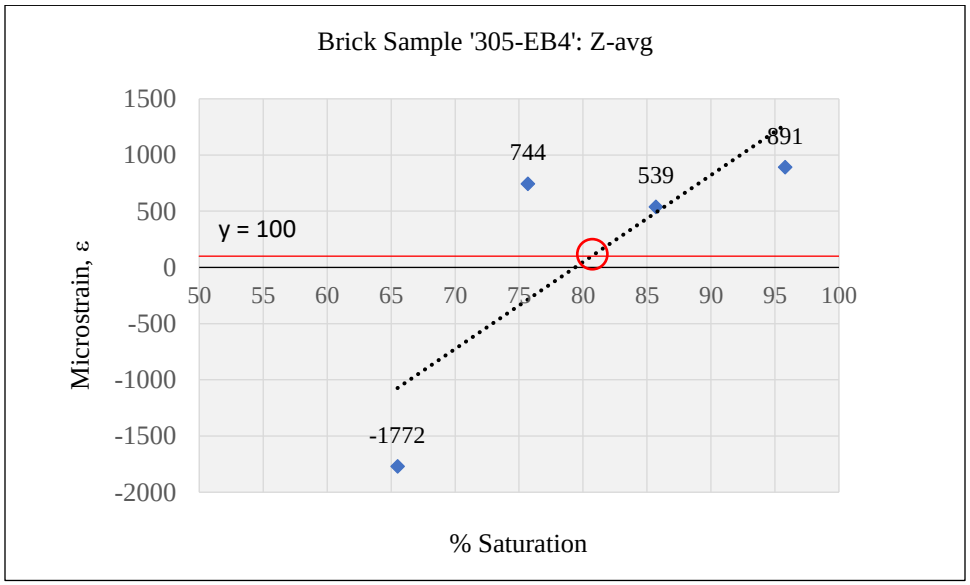

FIGURE 6-19: AVERAGE STRAINS ALONG THE Z-AXIS

6.7.6 STRAIN VS MOISTURE CONTENT GRAPHS FOR THE BRICK SAMPLE TYPE 297-EB2

6.7.6.1 AVERAGE STRAINS

As seen from Figure 6-20 Figure 6-22, for brick sample type 297-EB2, the microstrains are non-uniform, with expansion as well as shrinkage occurring along all three axes. For the average strains along x-axis, the initial microstrains is -857 (negative microstrains); along the y-axis, the initial microstrains is 729, while for the z-axis, the initial microstrains is -1216 (negative microstrains). In Figure 6-20Figure 6-21, the datapoints do not delineate any consistent trends that could have indicated the onset of frost damage. Thus, in this case, the S_{crit} point could not be clearly ascertained. However, for the average strains on the z-axis, a trend delineating increasing microstrains at the test moisture contents (56.7% to 96.7%) is observed (see Figure 6-22). Therefore, based on the intersection of the trend line and the extrapolation of y-axis at 100 microstrains, the S_{crit} point is the moisture content at about 77.5% (% vacuum saturation).

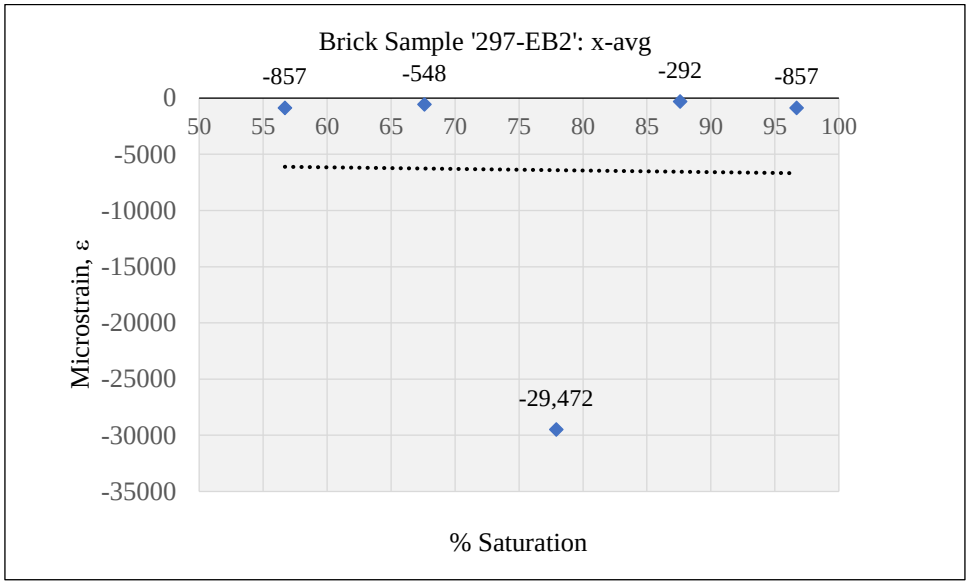

FIGURE 6-20: AVERAGE STRAINS ALONG THE X-AXIS

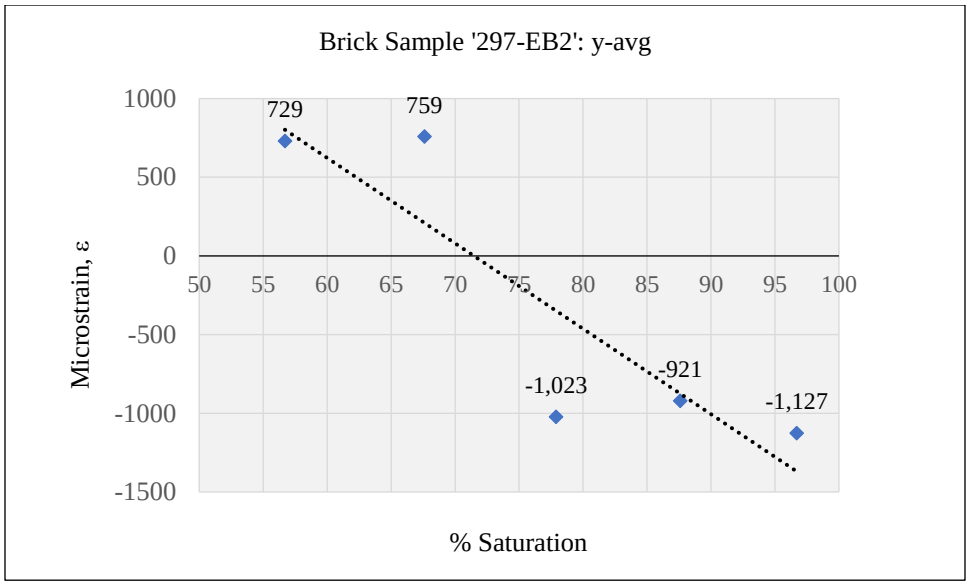

FIGURE 6-21: AVERAGE STRAINS ALONG THE Y-AXIS

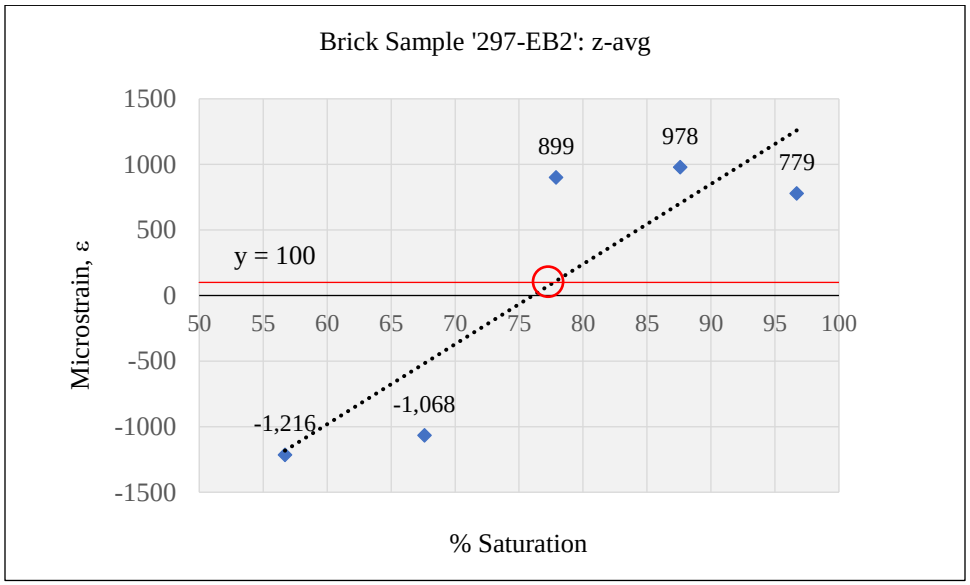

FIGURE 6-22: AVERAGE STRAINS ALONG THE Z-AXIS

6.7.7 STRAIN VS MOISTURE CONTENT GRAPHS FOR THE BRICK SAMPLE TYPE 295A-F4

6.7.7.1 AVERAGE STRAINS

As seen from Figure 6-23 to Figure 6-25, for brick sample type 295A-F4, the microstrains are non-uniform, with expansion as well as shrinkage occurring along all three axes. For the average strains along x-axis, the initial microstrains is 1759; along the y-axis, the initial microstrains is 1025, while for the z-axis, the initial microstrains is -1738 (negative microstrains). In Figure 6-23Figure 6-24, the datapoints do not delineate any consistent trends that could have indicated the onset of frost damage. Thus, in this case, the S_{crit} point could not be clearly ascertained. However, for the average strains on the z-axis, a trend delineating increasing microstrains at the test moisture contents (68% to 98.1%) is observed (see Figure 6-25). Therefore, based on the intersection of the trend line and the extrapolation of y-axis at 100 microstrains, the S_{crit} point is the moisture content at about 90% (% vacuum saturation).

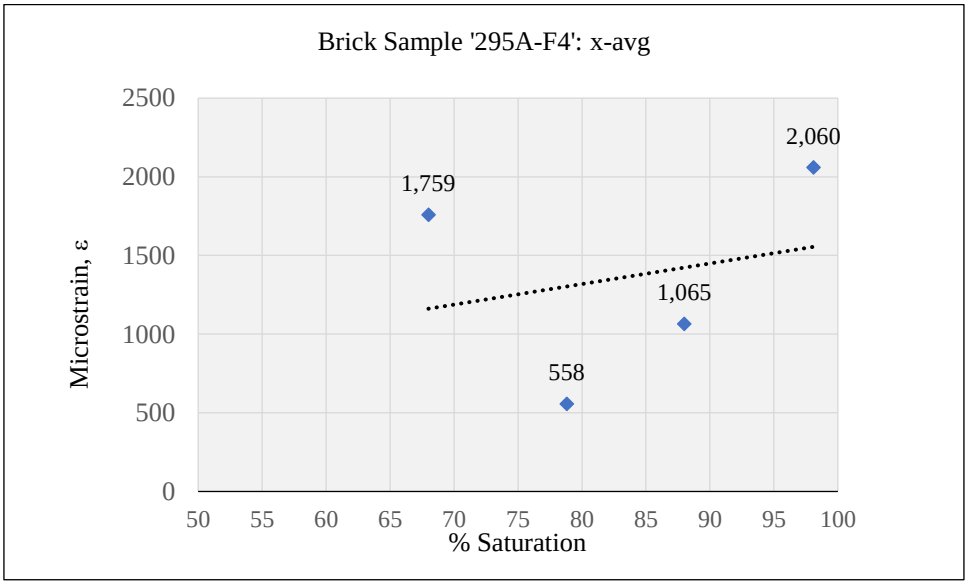

FIGURE 6-23: AVERAGE STRAINS ALONG THE X-AXIS

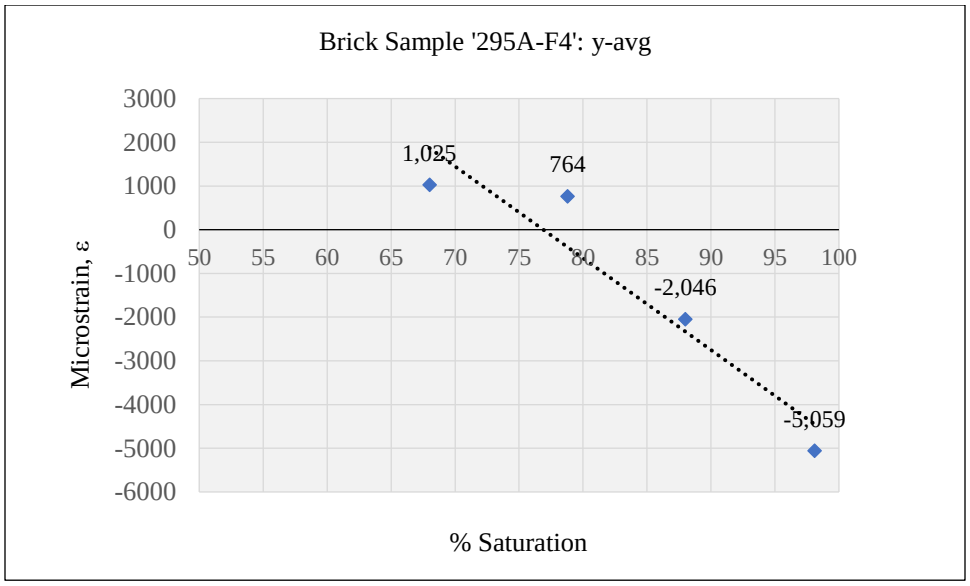

FIGURE 6-24: AVERAGE STRAINS ALONG THE Y-AXIS

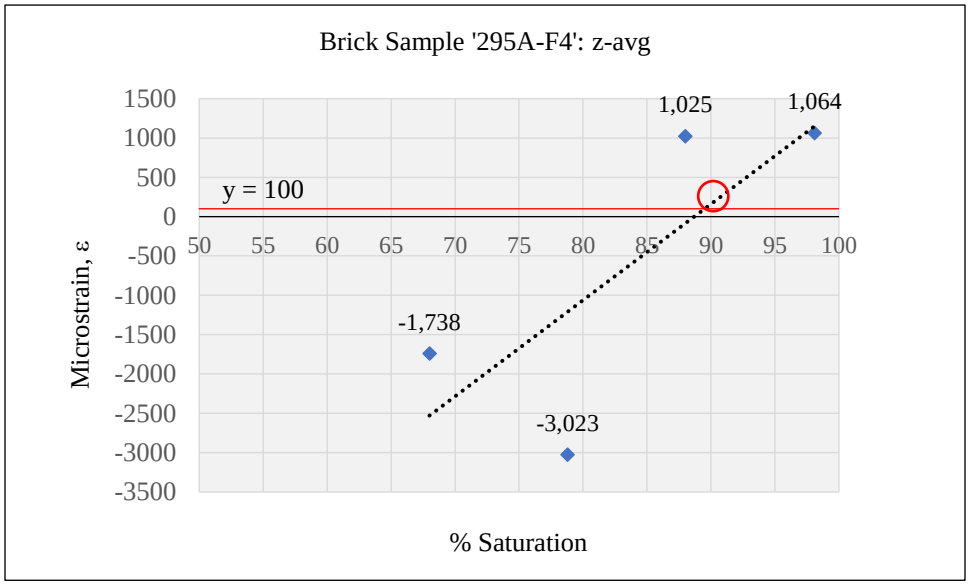

FIGURE 6-25: AVERAGE STRAINS ALONG THE Z-AXIS

6.7.8 STRAIN VS MOISTURE CONTENT GRAPHS FOR THE BRICK SAMPLE TYPE 349-ER1

6.7.8.1 AVERAGE STRAINS

As seen from Figure 6-26 to Figure 6-28, for brick sample type 349-ER1, the microstrains are non-uniform, with expansion as well as shrinkage occurring along all three axes. For the average strains along x-axis, the initial microstrains is -4401 (negative microstrains); along the y-axis, the initial microstrains is 1001, while for the z-axis, the initial microstrains is 542. The average strains for the x-axis are negative at all the test moisture contents. The datapoints do not delineate any consistent trends that could have indicated the onset of frost damage. Thus, in this case, the S_{crit} point could not be clearly ascertained.

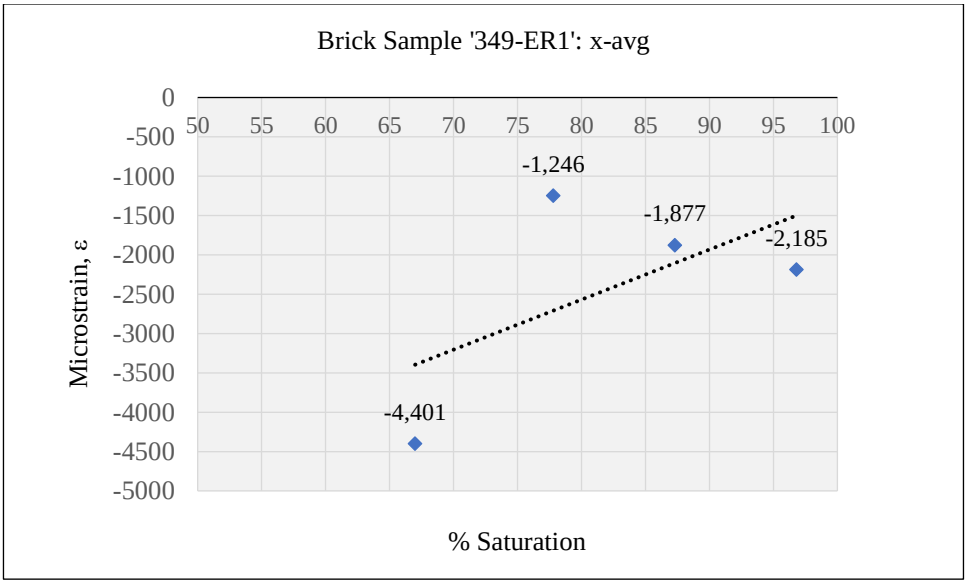

FIGURE 6-26: AVERAGE STRAINS ALONG THE X-AXIS

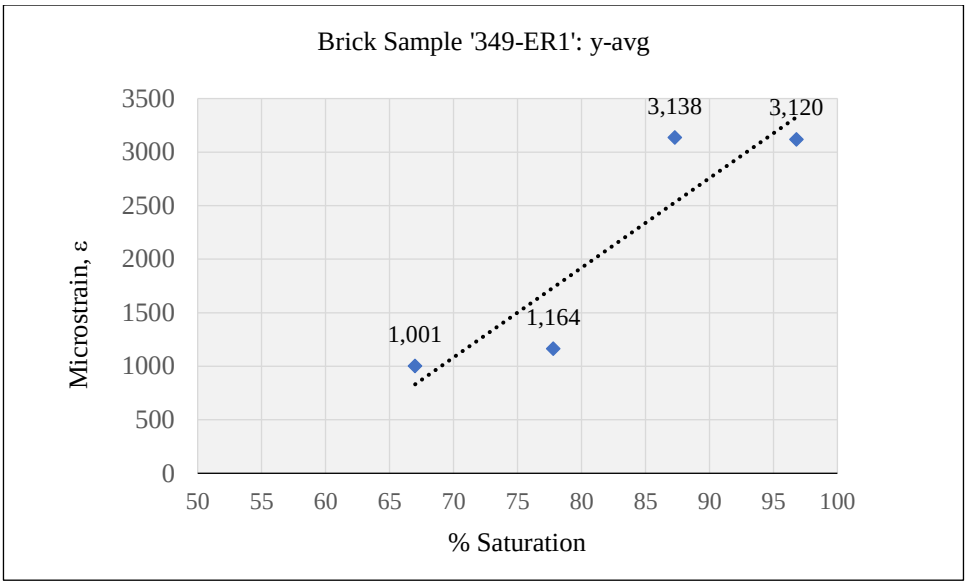

FIGURE 6-27: AVERAGE STRAINS ALONG THE Y-AXIS

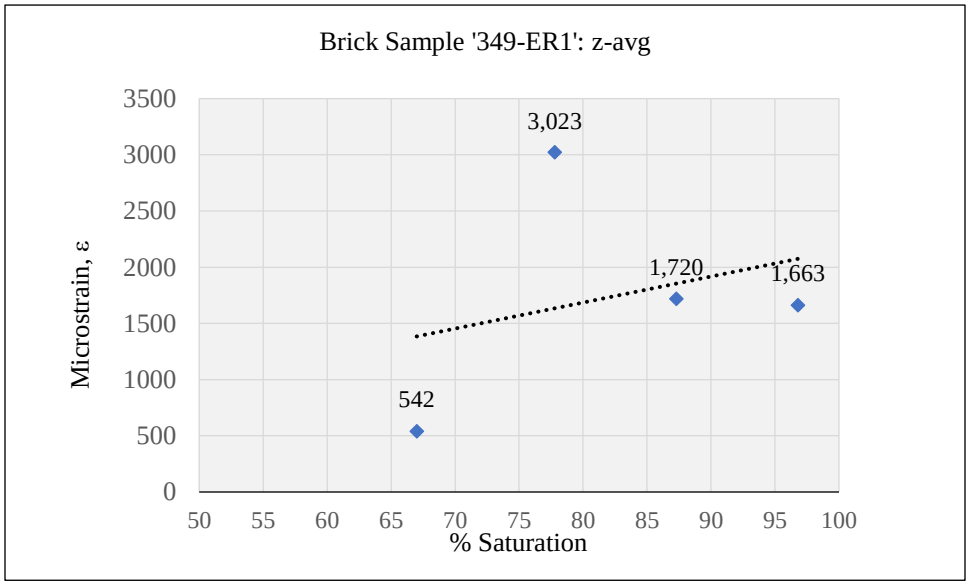

FIGURE 6-28: AVERAGE STRAINS ALONG THE Z-AXIS

6.7.8.2 STRAINS ALONG THE X, Y AND Z-AXES

In Figure 6-29, a trend has been observed whereby the microstrains are seen to be increasing at moisture content increments (67% to 96.8%). Based on the intersection between the trend line and the y-axis extrapolated at 100 microstrains, the moisture content at which S_{crit} occurs is about 92% (% vacuum saturation).

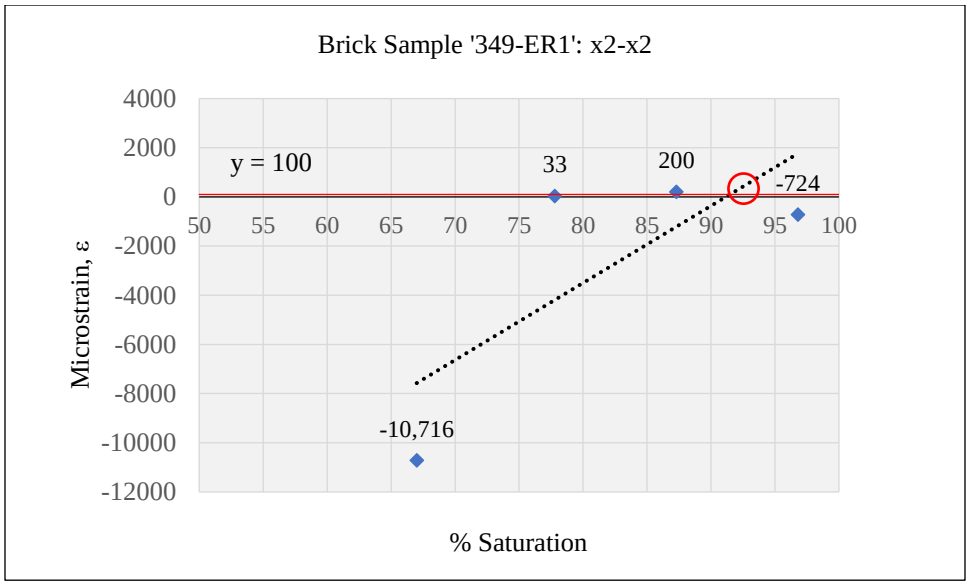

FIGURE 6-29: STRAINS ALONG THE X2-X2 AXIS

6.8 A SUMMARY OF THE S_{CRIT} OF HALF-BRICK SAMPLES

As seen from Table 12, all the brick samples tested showed some trend of frost decay, except for brick sample types 309-EF2 and 295A-EB3, where the points of critical degree of saturation was not evident in the graph. Following are observations on the results:

1) For brick sample type 60, the S_{crit} is seen to occur at 56% moisture content (% vacuum saturation) along the z1-z1 axis. This value is significantly lower in magnitude compared to the S_{crit} of the slice, which is at 73.4% moisture content. It is also noteworthy that sample type 60 has the highest A-value (among all the brick samples) at 0.5466 kg/m^{2}s$^{1/2}$, thereby corresponding to the lowest S_{crit} among the samples tested.
2) For sample type 295C-F2, the S_{crit} is seen to occur at the 88%, 97.5% and 67.5% moisture content (%vacuum saturation) at the z-avg, y1-y1 and y2-y2 axes respectively. The former two S_{crit} values are about respectively 10% and 20% higher than the S_{crit} of the slice, which is 78.4% moisture content.
3) For brick sample type 297-EB2, the S_{crit} is seen to occur at 77.5% moisture content (%vacuum saturation) at the z-avg axis. It is interesting to observe that this value is similar in magnitude (only 0.2% lower) to the S_{crit} of the slices, which is at 77.7% moisture content.

4) For brick sample type 349-ER1, the S_{crit} is seen to occur at 92% moisture content (%vacuum saturation) at the x2-x2 axis. On the other hand, it is interesting to observe that this value is only about 4.7% higher than the S_{crit} for slices, which is at 87.3% moisture content.
5) For brick sample type 295A-F4, the S_{crit} is seen to occur at 90% moisture content (%vacuum saturation) at the z-avg axis. It is interesting to observe that this value is only about 1.9% higher than the S_{crit} of slice, which is at 88.1% moisture content. As the sample with the second lowest A-value at 0.127 $kg/m^2s^{1/2}$, it also has the highest S_{crit} value amongst all the slices tested.
6) For brick sample type 305-EB4, the S_{crit} is seen to occur at 81% moisture content at the z-avg axis. It is interesting to observe that it is about 3.4% lower than the S_{crit} of the slice.

TABLE 12: A SUMMARY OF THE SCRIT FROM FROST DILATOMETRY TESTING OF HALF BRICK SAMPLES AND RESULTS

Brick nomenclature	Frost dilatometry testing of half brick samples				Results	
	S_{crit} discerned? (Yes/No)	S_{crit} (%vacuum saturation) and the axis at which it occurs		Vacuum saturation (%MC of dry mass)	S_{crit} (%vacuum saturation) of brick slices	A-value ($kg/m^2s^{1/2}$)
60	Yes	56%	z1-z1	20.7%	73.40%	0.546
295C-F2	Yes	88%	z-avg	24.9%	78.40%	0.518
		97.5%	y1-y1			
		67.5%	y2-y2			
309-EF2	No	Not Applicable		23.1%	79.00%	0.302
297-EB2	Yes	77.5%	z-avg	26.0%	77.10%	0.257
349-ER1	Yes	92%	x2-x2	17.0%	87.30%	0.197
295A-EB3	No	Not Applicable		24.9%	85.50%	0.165
295A-F4	Yes	90%	z-avg	21.0%	88.10%	0.127
305-EB4	Yes	81%	z-avg	24.6%	84.40%	0.101

7 DISCUSSION

As per the experimental hypothesis, it was expected that there would be zero microstrains at lower moisture contents (say about 20% below the slice S_{crit}) and subsequently a gradual increase in microstrains to 100 microstrains, whereby ideally the S_{crit} point could be clearly identified. It is evident from the results of the frost dilatometry testing of half-brick samples that the strains observed were non-uniform, whereby there were also incidences of large initial strains as well as shrinkage occurring along different axes evaluated (see Figure 6-2Figure 6-29 and Appendix A – Strains vs Moisture Content (% Saturation)). The results of this study were inconsistent with what had been seen in earlier work, especially in relation to the general trend of frost decay observed for brick slices that were tested in Mensinga (2009) and Williams (2015). The plausible reasons are discussed in the subsequent subsections.

7.1 TRENDS OF FROST DECAY

There were, however, also instances in this study, where trends could be observed, and the onset of frost damage could be inferred. Based on the scatter of the datapoints, a trend line was drawn in specific cases, whereby the S_{crit} could be discerned at the point where this line intersected an extrapolation of the y-axis at 100 microstrains. It is noteworthy that the S_{crit} could only be identified at certain axes, and only when the strains appeared to be increasing at the test moisture contents. There were instances where the strain at the preceding moisture content was shrinkage (negative microstrains), however the strain at the next moisture content was large expansion microstrains. Therefore, this result could help identify the S_{crit} point despite its non-conformance to typically observed trends in the slices' strains vs moisture content graphs (see Figure 6-4 as an example). There were also results for certain samples, which had large initial expansion or shrinkage strains. In this case, it was observed that there was a consistent occurrence of strains of similar magnitude at almost all test moisture contents, thereby rendering the results unreliable in the analysis of the S_{crit} point, as they could indicate frost damage would have initiated at lower moisture contents (see Figure 6-26 as an example).

It was observed that the S_{crit} points identified for some of the half-brick samples were closer in magnitude to the S_{crit} of the slices, especially for samples that had a comparatively lower A-value. This reinforces the understanding that the capillary uptake ability of the brick influences the way

moisture distribution occurs in its pore network, thereby impacting the point at which frost damage can initiate its internal microstructure. Bricks that have a lower A-value also tend to have a less extensive porosity and have S_{crit} values usually positioned at the higher end spectrum of moisture contents. Despite the sample size being small in this study, the identification of S_{crit} values has possibly been clearer in the cases where the brick sample type had a lower A-value (see Figure 7-1).

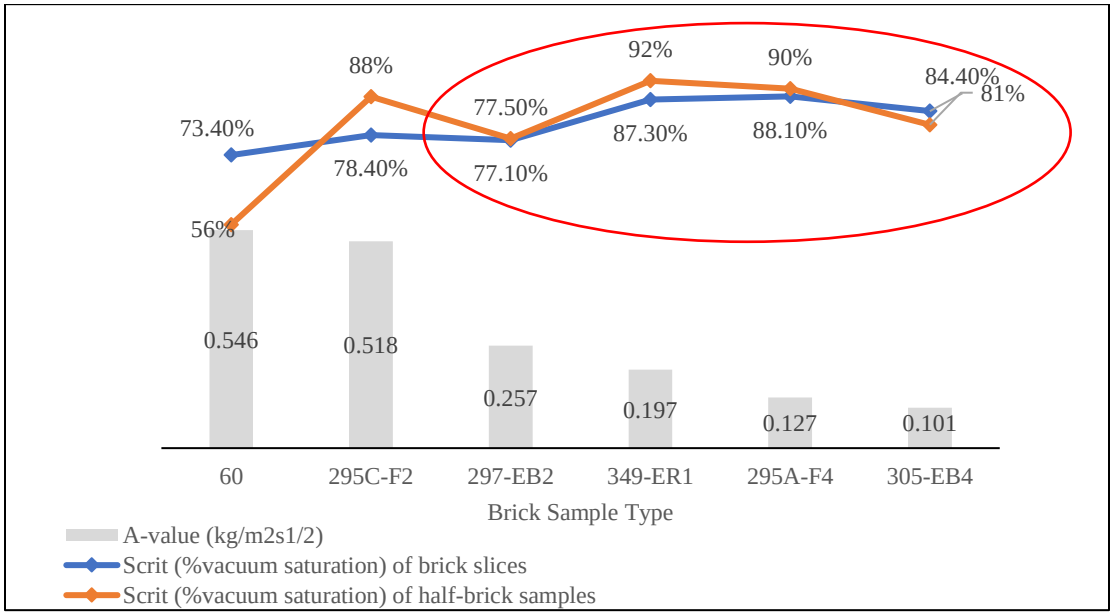

FIGURE 7-1: THE VARIATION OF S_{CRIT} (% VACUUM SATURATION) OF HALF BRICK SAMPLES AGAINST THE S_{CRIT} OF SLICES (% VACUUM SATURATION) IN THE BACKDROP OF THE SPECIMEN A-VALUE ($KG/M^2S^{1/2}$)

The non-uniform scattering of datapoints that has manifested in large microstrains (either in expansion or shrinkage) could be plausibly attributed to an irregular distribution of moisture in the brick samples. As the dimensions of the half-brick samples in the x, y and z axes were comparable to the slices, the former would have had a relatively more sophisticated network of pore spaces and capillaries held therein. Similarly, the interaction of pores with one another in a larger sized sample may have resulted in strains of a larger magnitude in the axes considered.

The z-axis S_{crit} points for half-brick sample types 60 and 295C-F2 had a greater variation to their slices S_{crit} compared to other test specimens. Due to the former's larger A-value and associated higher porosity, it may be possible that they would constitute a more non-uniform distribution of pore spaces.

It was observed from most of the results (about 83%) where the S_{crit} point could be discerned that it was evidently occurring along the z-axis, which had the shortest dimension compared to the x and y axes of the brick samples. It is also possible that when moisture was applied to the brick samples and left to distribute over a span of 18 hours, it may not have been completely redistributed in the sample as bricks with a low A-value may take a longer time for moisture redistribution to occur (Mensinga, 2009). This would potentially have confined the moisture on the surface extremities, particularly near the faces of the brick samples, thereby resulting in the irregular strains seen in the results of certain axes (such as the x and y axis). For example, in case of sample type 349-ER1, where the S_{crit} point was discernible on the x-axis, its x dimensions were like what would be that for z-axes. It is however important to mention that an average of measurements along the different axes had also been taken to reduce a risk of uncertainty.

Comparing the study's results to three-dimensional frost dilatometry results in Williams (2015), it is evident that the samples in the latter study also experienced large expansion and shrinkage strains. However, those samples were only tested at moisture contents like their S_{crit} values, which had earlier been determined through frost dilatometry testing of slices. On the other hand, it is important to mention in Mensinga (2009)'s study, there were brick samples that had S_{crit} values as low as 25% moisture content (% vacuum saturation). It, however, important to mention that this S_{crit} value was for brick slices and it is not clear which axis it pertained to.

The incidence of excessive strains could potentially have arisen due to material fatigue as a result of continuous freeze-thaw loading. Cracks within the internal microstructure of the brick masonry have propagated in a manner that expansion and shrinkage could be observed at all the axes.

7.2 NEGATIVE STRAINS

The incidence of negative strains is remarkably shedding light on the occurrence of shrinkage happening predominantly along the x and y axes of most of the brick samples. However, it has been observed that, for the z-axis, there have been strains that are increasing at the test moisture contents. Therefore, expansion strains were observed to be following almost a linear relationship with the increasing test moisture contents. The behavior of clay brick masonry can be analogized to a sponge, which also constitutes an extensive network of pore spaces. The only difference between the sponge and a clay brick obviously lies in the type of material they constitute.

Therefore, if a sponge is stretched along say, the z-axis, it would be observed that the faces of material parallel to the z-axis (i.e. along the x and y axes) would move inwards. As the expansive strains along the z-axis would increase at ascending increments of moisture content, there would be a corresponding growth in the magnitude of the shrinkage strains along the x and y axes. In this case, the sponge like the clay brick samples of this study, would be experiencing tensile stresses in the z direction. Applying the laws of mechanics, there would be development of compressive forces along the x and y axes to bring the sample into equilibrium. Therefore, in the context of the freeze-thaw cycles that the brick samples have been subjected to, the expansive strains seen at the z-axis is a result of the loading experienced, which is essentially the exposure conditions (moisture content and freeze-thaw cycles). With the overall volume of the test sample being constant, there would be an internal redistribution of material being experienced by the sample, which would be manifested as dimensional changes along the x, y and z axes.

It is interesting to observe that the trends in frost decay were more pronounced on the z-axis, such that expansive strains (or indeed increased dimensions) are occurring here. This axis, which is also considered as the 'height' of the brick sample could in hindsight have been the stronger axis of the sample. On the other hand, the x and y axes would have been the weaker axes for the test samples. It is noteworthy that the bricks have been sourced from buildings, which are assumed to date back to the 1800s, whereby construction practices typical of that era included adoption of load-bearing brick masonry on the facade. In the past, load bearing bricks were manufactured by hand and possibly did not undergo the mechanical extrusion process that is done today. A simple brick manufacturing technique may have included a process like that of annealing of steel, whereby the material is hardened along one axis by striking it at intervals. with a manufacturing tool. This is usually done to steel as it increases its tensile strength; wherein, like load bearing bricks, steel experiences expansive strains along the stronger axis upon loading.

However, the behaviour of the test samples in this study may not entirely be a true depiction of the strains experienced by brick masonry present insitu (in a load bearing façade). In the study, the test samples experienced omni-directional freezing but, the freezing front only approaches from the brick face exposed to the exterior. Therefore, it would be important to understand if the expansive strains or shrinkage strains, as seen in study, occur in practice.

7.3 COOLING TEMPERATURES OF -6.5°C VERSUS -15°C

The results of this study would have been impacted by exposure conditions, such that it is noteworthy that the refrigerant bath temperature did not drop below the cooling setpoint temperature of -15C. Instead, it remained stuck at -6.5C, which is not in accordance to the frost dilatometry approach adopted in other studies. This could have implications on the brick samples, such that certain pore spaces may not have completely frozen over, possibly leading to the irregular expansion and shrinkage seen in the results. Due to inadequate cooling of the specimen, there may not have been significant expansive strains developing in the brick samples, leading to the domination of shrinkage along certain axes.

7.4 CHANGES IN EXPERIMENTAL PROCEDURES

In retrospect, the experimental procedures pertaining to the frost dilatometry testing could be adjusted to include the following changes in approach:

1) When cutting the samples, care should have been exercised not to remove the outer surface bearing the peculiar textural characteristics of the brick masonry to be tested as that would have potentially acted as an effective barrier to moisture flow inwards. Therefore, a sample whose surfaces are clearly squared up may have different uptake abilities compared to its exterior surface, which has a visibly more uneven and rough texture. It is presumed the ability to absorb moisture more readily may inevitably impact the strains experienced by the sample when subjected to freeze thaw cycles. In this study, the great skew in results could presumably be connected to the squaring up of samples and could have been avoided if the exterior surfaces were kept intact. It is, however, important to mention here that samples were squared on most of the faces where mortar was attached on them.
2) There was also a risk of human error involved in the testing primarily because frost dilatometry testing was performed for the first time. It is understood that the technique could possibly have been perfected if it had been done a couple of times beforehand. There was also the issue of using the inch micrometer for measuring the z-axis (it was used as it measured dimensions below 3”), while the electronic micrometer was utilized for measuring dimensions along the x and y axis. This potentially introduced errors in calculation and could have been avoided had only one instrument (preferably the electronic micrometer) was used

for the measurements. Finally, there was also the possibility that the spindle of the micrometers would have grinded some of the brick surfaces, thereby impacting the length measurements taken.

3) Brick sample types 295C-F2, 295A-EB3, 305-EB4 and 60 had mortar attached on their exterior surfaces of their faces. Compared to brick masonry, mortar has different water uptake properties, in that its porosity and water uptake coefficient differ significantly. Similarly, its behavior, particularly under freeze-thaw conditions would have impacted the resultant strains.

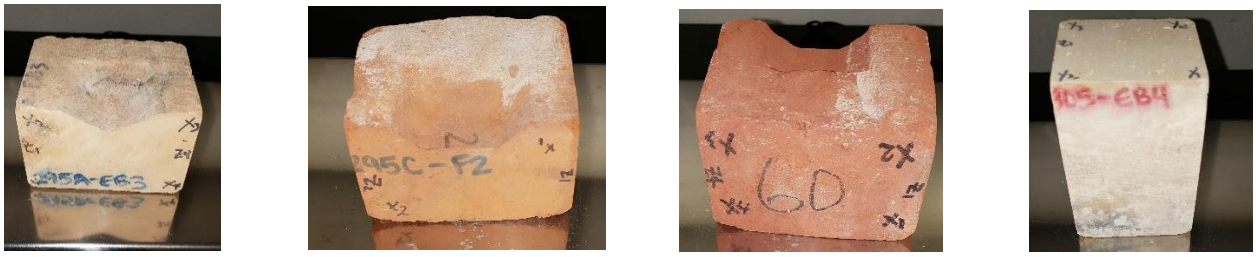

(a) (b) (c) (d)

FIGURE 7-2: (A) TO (D) INDICATES BRICK SAMPLE TYPES 295-EB3, 295C-F2, 60 AND 305-EB4. MORTAR IS SEEN TO BE ADHERED TO THE FACES OF THE TEST BRICK SAMPLES

4) The surfaces of some of the brick samples have played a seemingly active role in the uptake of moisture into the sample. Conversely, other samples have not readily absorbed moisture when water was applied on them to raise the internal moisture content. For moisture to be readily absorbed by the brick sample, a concave depression could have been formed on one of the faces of the brick samples. This would allow for the easy percolation of moisture into the sample.

FIGURE 7-3: THE SURFACE OF THIS BRICK SAMPLE IS READILY ABSORBING MOISTURE

5) The current approach to drying was based on the ASTM C67/67M-19 stipulation on keeping the specimen in the oven overnight for about 24 hours. However, in retrospect, specimens could be dried for more than one day, possibly 48 hours.
6) The brick sample could have been measured along only one axis point, rather than a set of axis points, which are x1-x1, x2-x2, x3-x3 and so as forth delineated in Figure 4-5. It is possible that along different axis points, there would be an incidence of varying material homogeneity. If an average of all the axis points are considered, the strain results may generalize trends of frost damage for that axes as it is not reflective of the variation in the internal microstructure along different axis points. For example, it is possible that along x1-x1 point, there exists an air pocket whereby x2-x2 may be relatively more homogenous. However, an average of these axis points may ignore the aspect of material heterogeneity contributing to the strains experienced.
7) For saturating brick samples under vacuum pressure, the bricks in the study were left to soak for an hour once water flowed into the desiccator vessel (from the water reservoir) and the atmosphere valve was opened. This was based on the approach by Mensinga (2009), however given the size of the samples in the study, this time could potentially have been longer. In the setup that Williams (2015) had devised for vacuum suturing the brick samples, the samples were subjected to a vacuum for half an hour. It is pertinent to mention that due to the differences in setup for vacuum saturation in this study compared to that in Williams (2015), the vacuum was not kept for the same amount of time. However, in retrospect, this could have possibly been more effective in removal of air from all the pore spaces in the brick samples.
8) At higher moisture contents, it was observed that the typical technique to apply moisture to raise the moisture contents was turning out to be unfeasible. This was also manifested as a loss of moisture mass after moisture was applied to the target MC and left to distribute in the sample. Alternatively, to increase the moisture contents above the point whereby capillary suction could no longer take place, the brick samples could have been vacuum saturated to 100% moisture content and dried down to the respective moisture contents.
9) There was moisture loss observed, manifested as a difference in mass before application of the cling film and after application of cling film (sometimes as large as 4.2%). This was possibly occurring because moisture that had been applied earlier was applied in haste, and

possibly had not percolated efficiently into the sample. Similarly, there may have been moisture loss through evaporation from the sample, particularly if it had accumulated on the sample surfaces. Air pockets that may have resulted from an inefficient wrapping of the cling film at certain parts of the sample could have contributed significantly in this vapor loss through convection. At the pore level, hysteretic effects may possibly have governed this phenomenon, leading to the desorption of moisture internally from the pore spaces. In retrospect, the mass of the sample should have been weighed just before placing inside the freeze-thaw machine. In this way, if there were significant moisture loss observed, the moisture could have been applied on the surface and let to distribute to ensure that it was consistent with the respective test target moisture contents.

10) Both Mensinga (2009) and Williams (2015) had used the WUFI program to determine the time taken for moisture to equilibrate in the slices, and ascertained it to be about 18 hours. Similarly, in this study, the time allocated for moisture to equilibrate in the brick samples was also 18 hours. As discussed earlier, this time may have been short in retrospect, given the dimensions of the brick specimens considered. For one of test specimens (brick slices) in the Mensinga (2009) study, the redistribution time was determined to be about five days. As this was just a slice that required this duration of time, it is hence presumed that a half brick sample of the same brick may have required a time longer than five days. Therefore, an understanding on the physical properties of the brick samples (pertaining to the A-values) would help in the determination of the exact time that a sample of certain dimensions would require to enable complete distribution of the moisture to internal micro-spaces.
11) The determination of A-value of the half-brick samples had not been undertaken; earlier test results of for the brick slices were relied upon as an indictor of this metric for half-brick samples. In retrospect, an evaluation of the variation of the magnitude of this property (from slices to larger sized samples) would have provided an improved understanding on the suction kinetics in play. Additionally, this would help in the assessment of the freeze-thaw damage occurring in the larger sized samples.
12) The bulk density of the brick samples should have been determined through an appropriate testing procedure, whereby this would help provide a better understanding, albeit at a macro level, the distinction in pore characteristics between the brick samples tested.

7.5 THE NEXT TESTING STEPS

Based on the frost dilatometry testing of the eight brick samples in this study, the next testing steps involve the following:

1) Testing a larger sample size i.e. possibly bulk sampling as was done in the Van Straaten et al. (2016) study, would help provide a context for the repeatability of measurements, and minimize the variations in strains seen as per this study's results. Similarly, the acquisition of bricks from one location (like one façade in a building) could also help in the determination of mean values, as similar bricks may perform in an alike manner. Additionally, if bricks were sourced from diverse locations, a common trend in frost decay could possibly have been identified, even if the exact magnitude of the strains may vary from brick to brick. Again, this adds in to the concept of bulk sampling, which would provide a more extensive dataset to analyze from.
2) Williams (2015) had also studied the frost decay trends of contemporary brick sourced from local manufacturers. Testing such bricks under experimental conditions like those enacted in this study, would help provide a context to the frost decay trends observed. For example, if half-brick samples of modern clay brick behave in a similar way to samples tested in this study, it can be inferred that the dimensional size of the sample is a limiting factor in observing meaningful trends in freeze-thaw deterioration. On the other hand, if modern brick samples, along all axes, show trends as seen for brick slices in the Mensinga (2009) and Williams (2015) studies, then there needs to be a re-evaluation of other factors contributing to the unpredictability in the results seen in this study. Therefore, the contemporary bricks would act effectively as 'control' bricks.
3) In this study, results for slices were compared to that of half-brick samples. As the tests for the slices were not part of this study, the next stage of testing would involve working with whole brick samples. This essentially means performing the A-value, bulk density, permeability, W_{ref} and W_{cap} tests on slices as well as half brick samples, which constitute one whole brick sample, as a continuous experimentation process. As different laboratory environments could potentially pose the risk of operator errors and the repeatability of measurements, it may be prudent to do the whole gamut of testing at one place.

7.6 NOISE THRESHOLD

In earlier studies by Mensinga (2009) and Williams (2015), the trends of frost decay included the quintessential trend of frost decay manifested by low strains in the test samples till the critical degree of saturation and then a sudden spike in the magnitude of strains beyond this point. The magnitude of strains that would determine the onset of damage was dictated fundamentally by a dimension change equivalent to 100 microstrains. However, the test specimens in question were brick slices, which are comparatively smaller in volume, thus possessing fewer material deficiencies (like air pockets, cracks or any other internal anomalies) compared to larger sized brick samples. Therefore, this 100 microstrains threshold may be especially applicable to brick slices only. In larger sized samples, the noise threshold may necessitate to be increased to consider the complexity of the material that has been tested. An appropriate limit such as the 100 microstrains threshold can be determined by finding out the magnitude of mean strain experienced by many brick samples sourced from the same location.

7.7 MATERIAL HETEROGENITY

The great variation in strains occurring at the all the axes in all the test samples is understood to be occurring most probably due to material non-homogeneity, which is possibly also manifested by the presence of cracks and fissures internally. Material non-homogeneity arises due to several factors, which are a result of the following:

1) The firing temperatures
2) The manufacturing processes
3) The constituent raw materials
4) The age of the brick
5) The location in the building from where the brick was extracted from

This would contribute to the development of air pockets within the brick sample and influence essentially the way moisture is stored and distributed within the sample. Similarly, the way fractures propagate in the material on exposure to freeze-thaw cycles would also be influenced by this how a brick has formed or weathered over the course of time. Presence of raw materials like crushed aggregate, stone or rock could also be hotspots of localised anomalies in clay brick

masonry. All of this in turns impacts the behaviour of the brick under extreme exposure condition, thereby having implication the predictability of results of a specimen tested through frost dilatometry.

8 CONCLUSIONS AND RECOMENDATIONS

This study investigated the critical degree of saturation, S_{crit}, of half brick samples via the frost dilatometry methodology. It also explored how the existing approach to testing could be adjusted based on test specimens of a larger size. In contrast to brick slices, which have shown discernible S_{crit} points in earlier studies, the results of this study showed an irregularity of strains along the x, y and z axes dimensions. The strain vs moisture content (% vacuum saturation) graphs for certain axes showed expansion or shrinkage strains occurring consistently across all the test moisture contents. This defied the study hypothesis, which was based on the understanding that the trends in frost decay are gradual till a certain point i.e. the S_{crit} point; subsequently, the datapoints corresponding to the strains would congregate into almost a linear relationship at moisture contents above the S_{crit} value. The anomalous relationship between the specimen strains and moisture content, as seen in the study's results, bring to attention the fact that clay brick masonry is a porous material with a behaviour that is inherently variable. It is also unknown how internal cracks or fissures, if they exist in the tested bricks, impacted their freeze-thaw behavior. Moreover, the complex interaction between the pore network and pore spaces, particularly in the way moisture redistribution occurs could also explain instances of expansion and shrinkage strains occurring almost alternately at all test moisture contents. It is important to acknowledge the impact of the firing temperature, the constituent raw materials and the manufacturing process in brick masonry durability. Similarly, the age of brick masonry and its location in a building before it was extracted out are also important points to consider. Material heterogeneity may have contributed to this unpredictability in results, and may in future work, necessitate improved approaches to frost dilatometry testing to consolidate the repeatability of measurements. It is however pertinent to mention here that despite the erratic strains seen in the x and y axes of most of the specimens, S_{crit} points discerned from the z-axis of the half brick samples could correlate closely to the S_{crit} points of the slices. Future work would involve testing whole bricks, and possibly other types of porous materials. Mapping the porosity of test specimens via Mercury Intrusion Porosimetry (MIP) could also provide a glimpse of the pore distribution and pore size of porous materials. A mineralogical analysis of brick samples tested in frost dilatometry would also shed light on the pore characteristics and resistance to freeze-thaw deterioration in such materials. Future work must also entail unidirectional freeze-thaw testing, as that would help provide a better approximation of in-situ conditions.

Based on the evaluation of results from the frost dilatometry testing of the brick samples, following are recommendations for consideration when undertaking experimentation:

1) Brick specimens should have been wet to lower moisture contents (possibly to as low as 20% vacuum saturation) and then subjected to freeze-thaw cycles. This would have helped in discerning the S_{crit} along axes, where it would have potentially been around a lower range of moisture contents.
2) The strains after the first set of freeze thaw cycles (at the initial test moisture content) should have been evaluated to understand if the specimen could be further tested. This study in retrospect could have avoided further testing of specimens that may already have undergone damage
3) The sample size was small to infer any significant correlation between brick property and the S_{crit} points. In retrospect, a sampling plan should have been exercised in the selection of samples to ensure the randomness of the tests.
4) There was a possible contamination of brick sample 349-ER1 by the refrigerant, as when it was removed after the third set of freeze-thaw cycles, some polyethylene glycol was seen inside the Ziplock bag. This could have happened possibly because of the jagged edges of the sample puncturing the Ziplock bag. In retrospect, all the edges of the brick samples could have been rounded-off using sandpaper.
5) At higher moisture contents, it was evident that applying distilled water on the surfaces of the samples did not result in an increased moisture content of the brick samples. Therefore, the bricks were vacuum saturated (to a 100% moisture content) and then dried to the respective moisture contents. It was observed that vacuum saturation of the brick samples did not result in the same mass equivalent to 100% moisture content at the beginning of the freeze thaw tests. The difference was as high as 2% in magnitude lower than the initial masses (at 100% moisture content). This could be attributed to the fact that the brick samples were not completely dry before they were vacuum saturated. Samples should have been completely dried before subjecting them to vacuum saturation.
6) Performing freeze-thaw cycles at 5% moisture content intervals would help in meticulously monitoring the progression of microstrains into the ‘frost damage zone’.

7) The usage of an inch micrometer could potentially pose the risk of human errors in the measurements taken. Ideally, one electronic micrometer should have been used for taking measurements along all axes.
8) In retrospect, the mortar that has been seen to be adhered to the faces of the brick samples should have been completely removed. The presence of this may have contributed to the great variance in strains.

APPENDIX A – STRAINS VS MOISTURE CONTENT (% SATURATION)

A 1 TYPE 295C-F2

A1.1 STRAINS ALONG THE X, Y AND Z-AXES

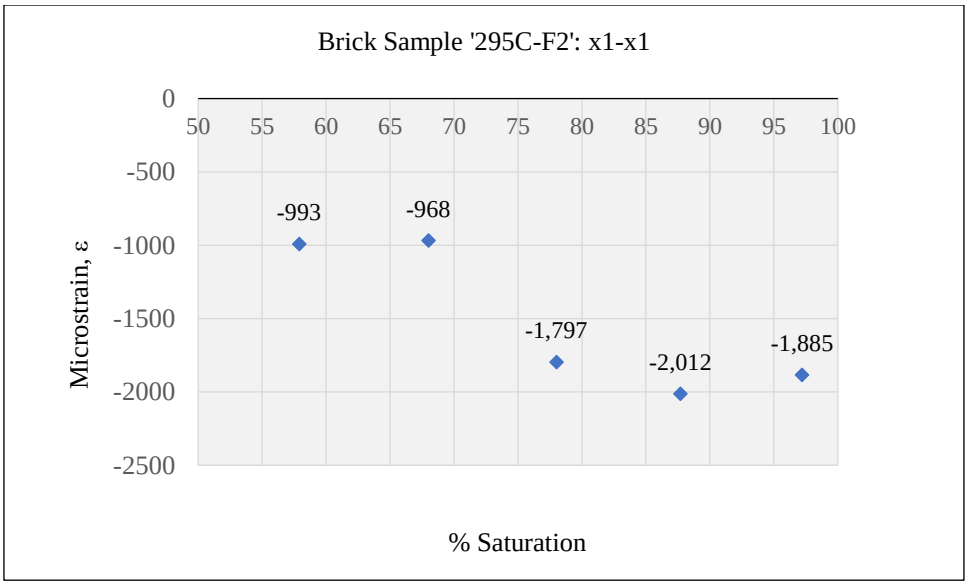

APPENDIX A 1: STRAINS ALONG THE X1-X1 AXIS

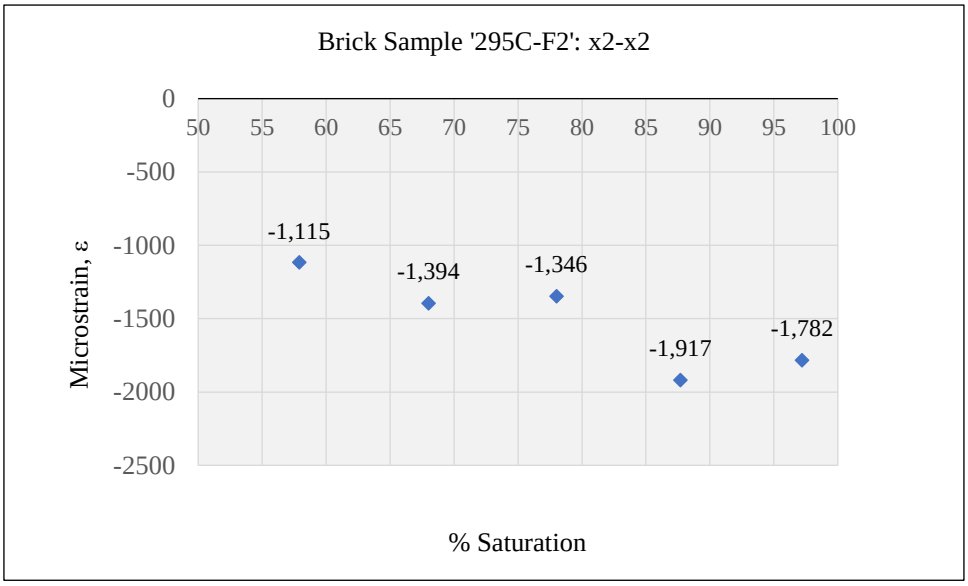

APPENDIX A 2: STRAINS ALONG THE X2-X2 AXIS

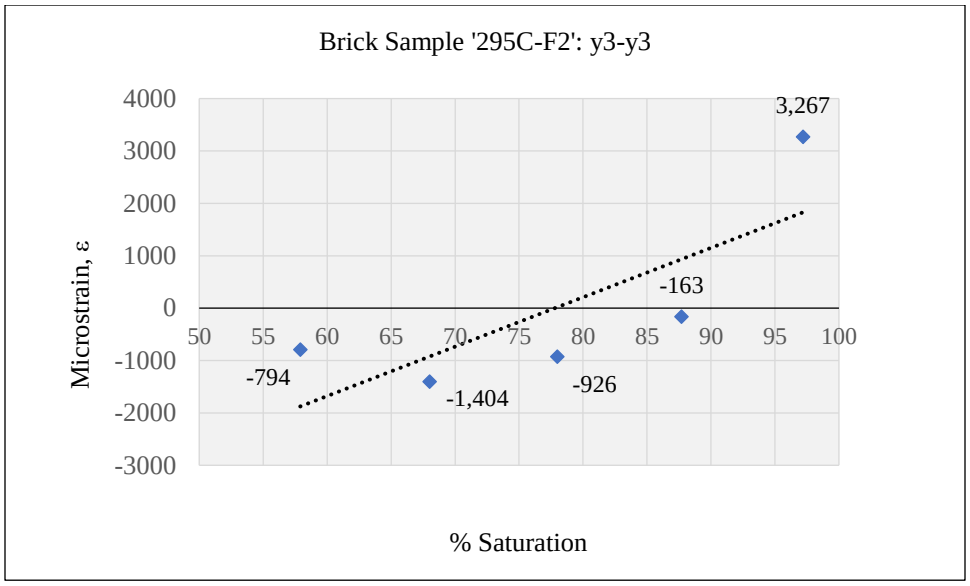

APPENDIX A 3: STRAINS ALONG THE Y3-Y3 AXIS

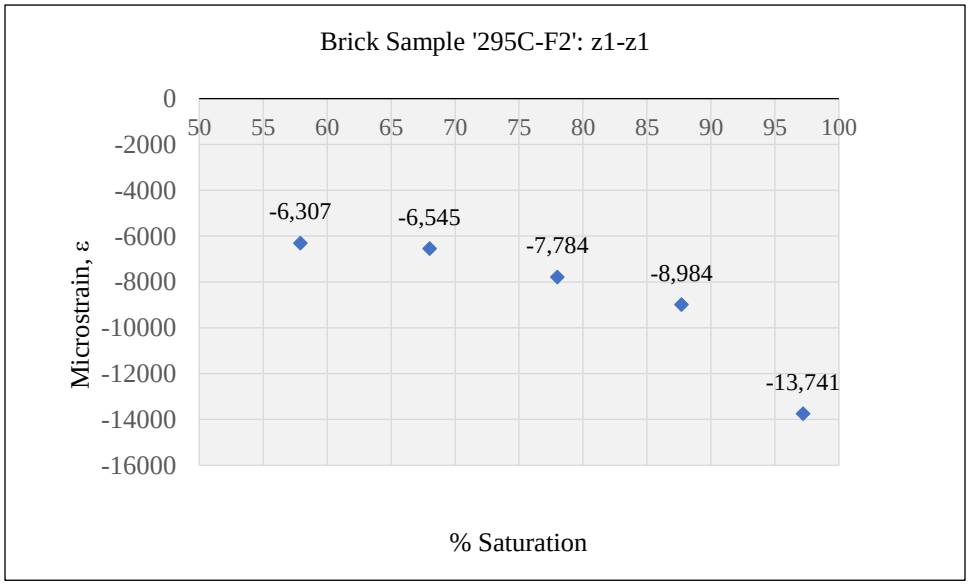

APPENDIX A 4: STRAINS ALONG THE Z1-Z1 AXIS

A 2 TYPE 309-EF2

A2.1 STRAINS ALONG X, Y AND Z-AXES

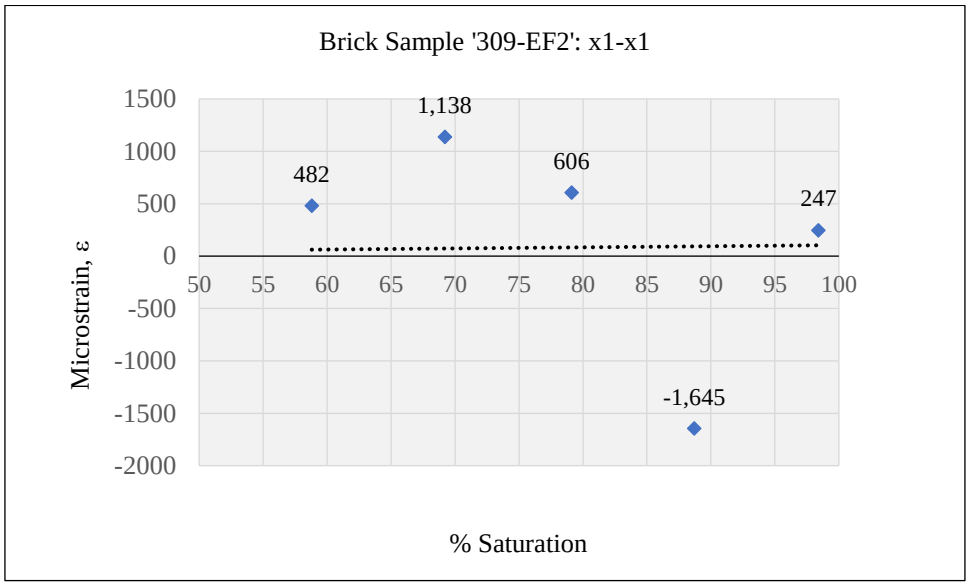

APPENDIX A 5: STRAINS ALONG THE X1-X1 AXIS

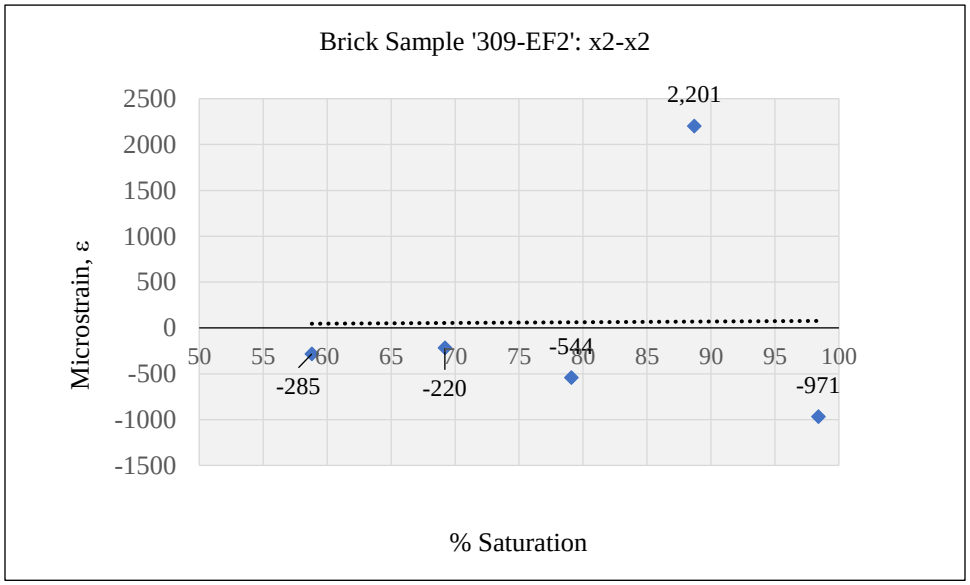

APPENDIX A 6: STRAINS ALONG THE X2-X2 AXIS

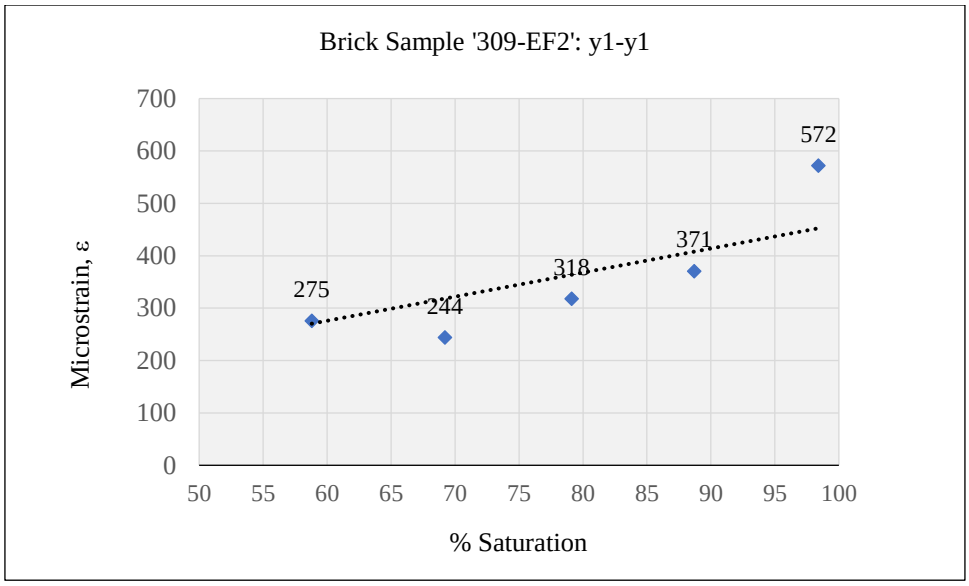

APPENDIX A 7: STRAINS ALONG THE Y1-Y1 AXIS

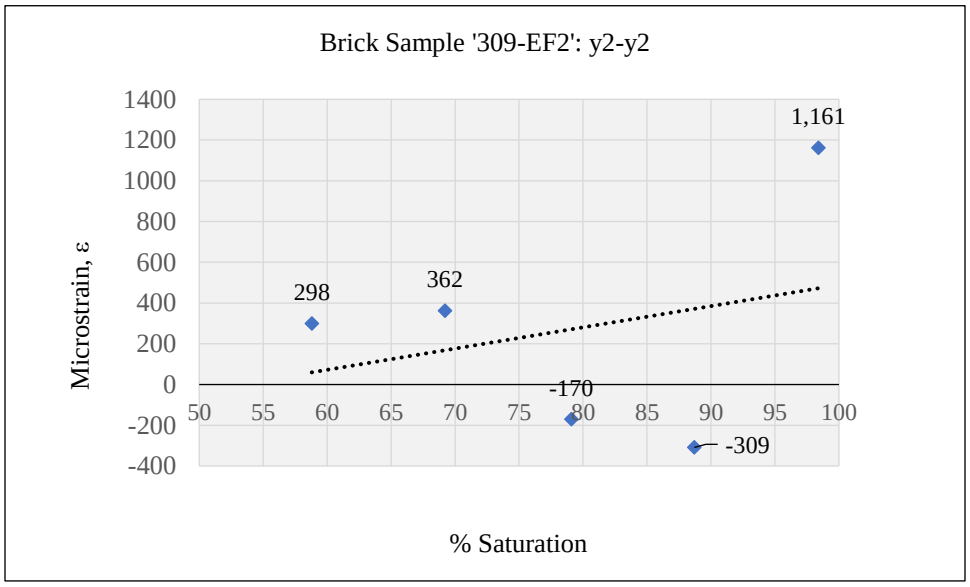

APPENDIX A 8: STRAINS ALONG THE Y2-Y2 AXIS

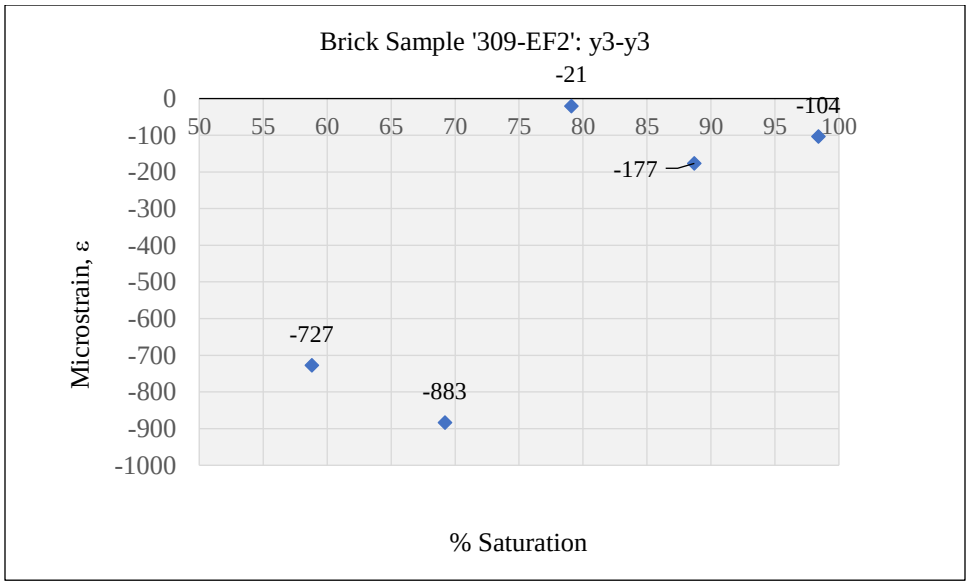

APPENDIX A 9: STRAINS ALONG THE Y3-Y3 AXIS

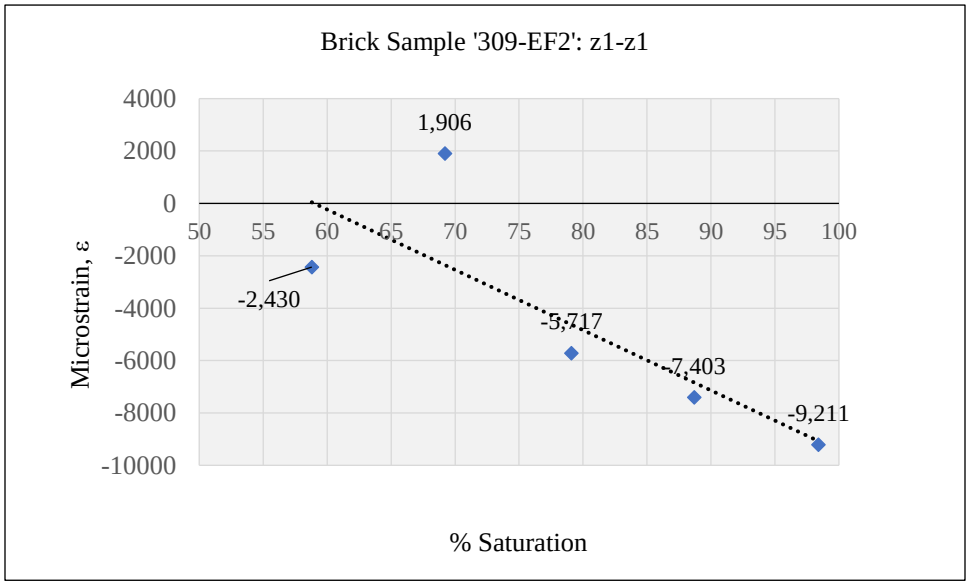

APPENDIX A 10: STRAINS ALONG THE Z1-Z1 AXIS

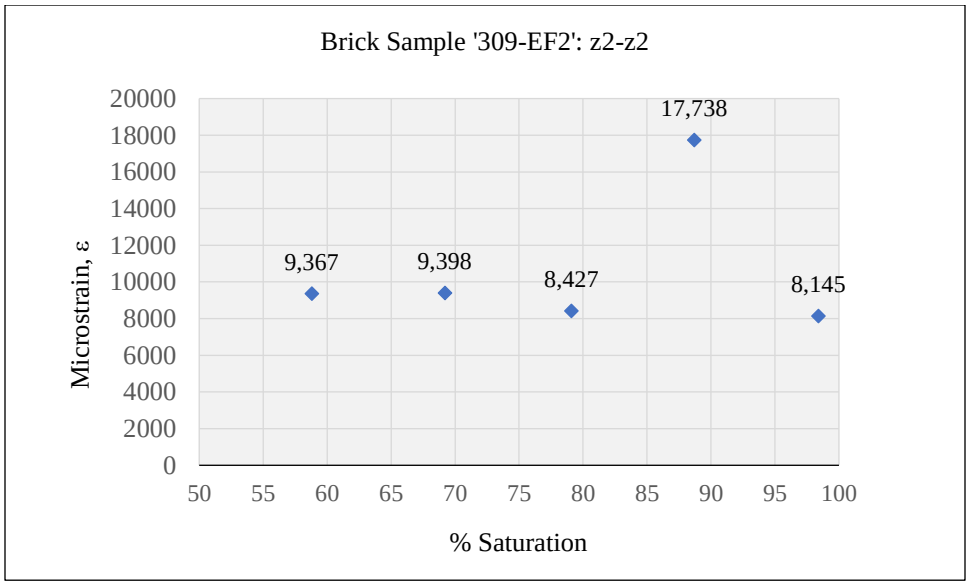

APPENDIX A 11: STRAINS ALONG THE Z2-Z2 AXIS

A 3 TYPE 60

A3.1 STRAINS ALONG X, Y AND Z-AXES

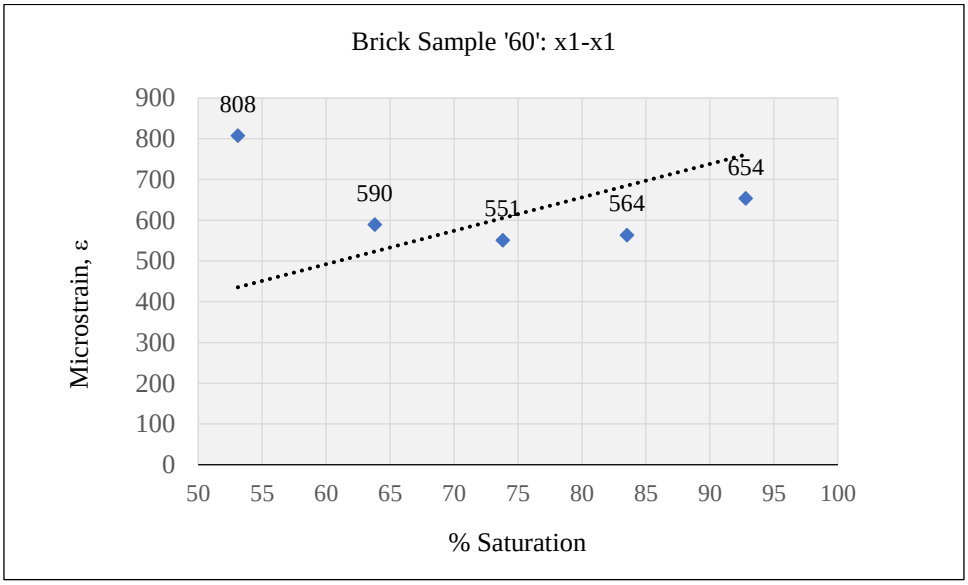

APPENDIX A 12: STRAINS ALONG THE X1-X1 AXIS

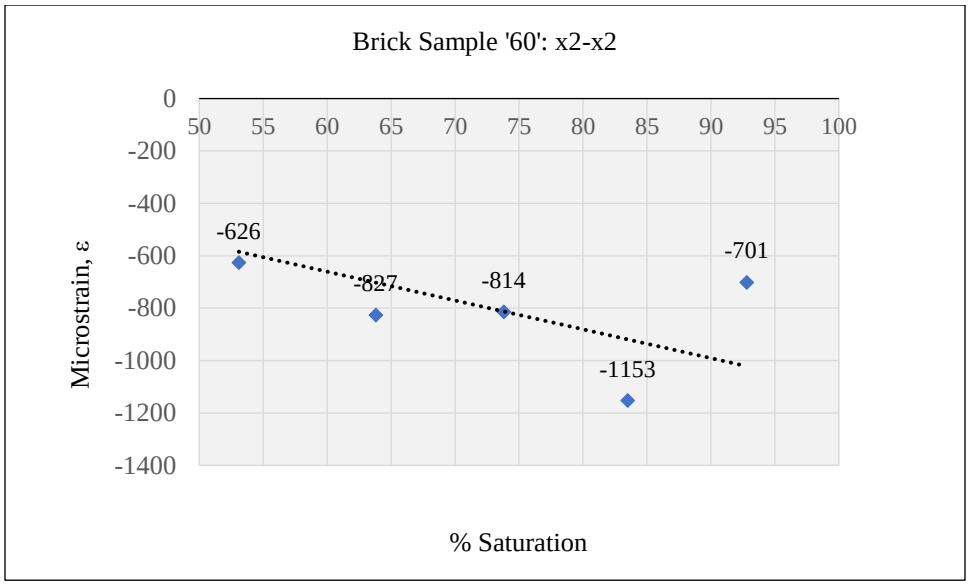

APPENDIX A 13: STRAINS ALONG THE X2-X2 AXIS

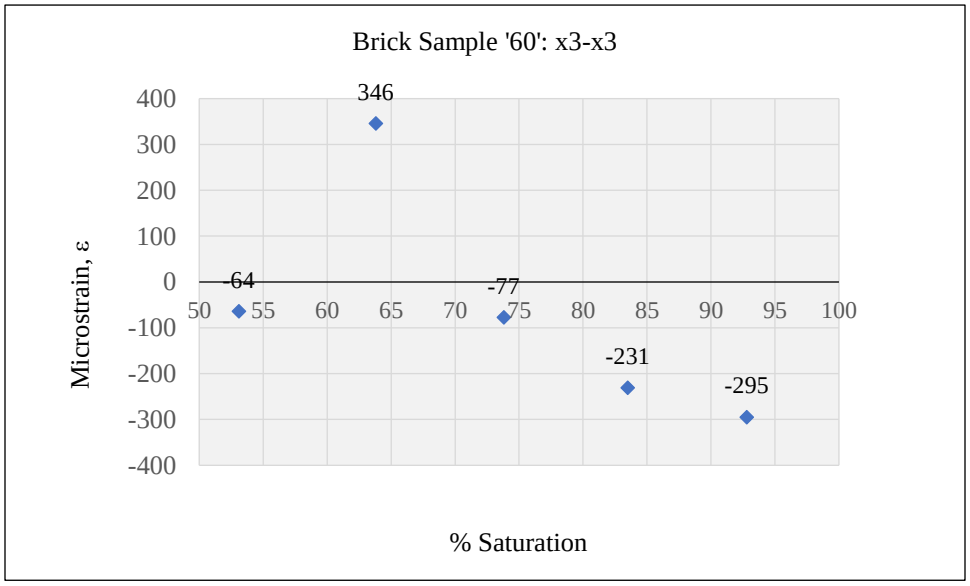

APPENDIX A 14: STRAINS ALONG THE X3-X3 AXIS

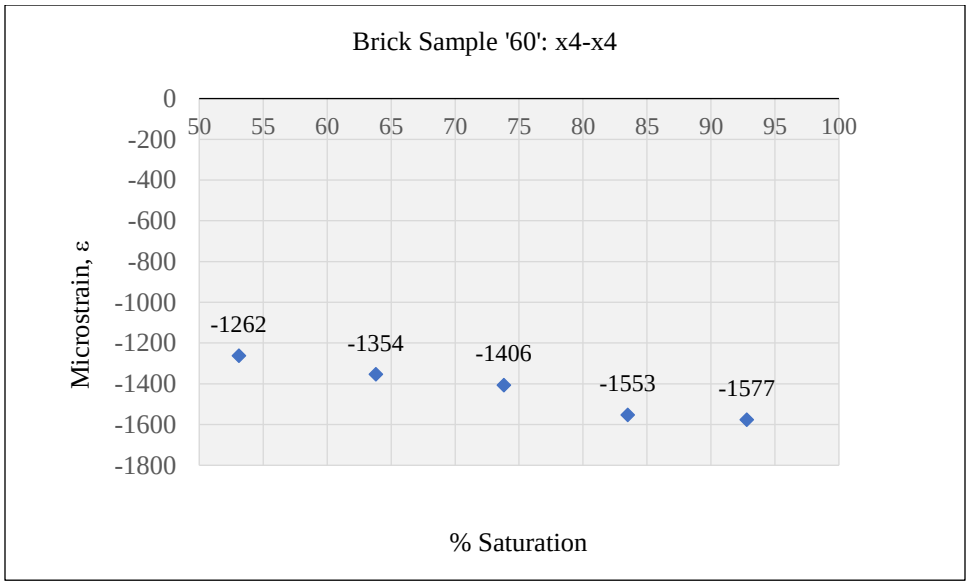

APPENDIX A 15: STRAINS ALONG THE X4-X4 AXIS

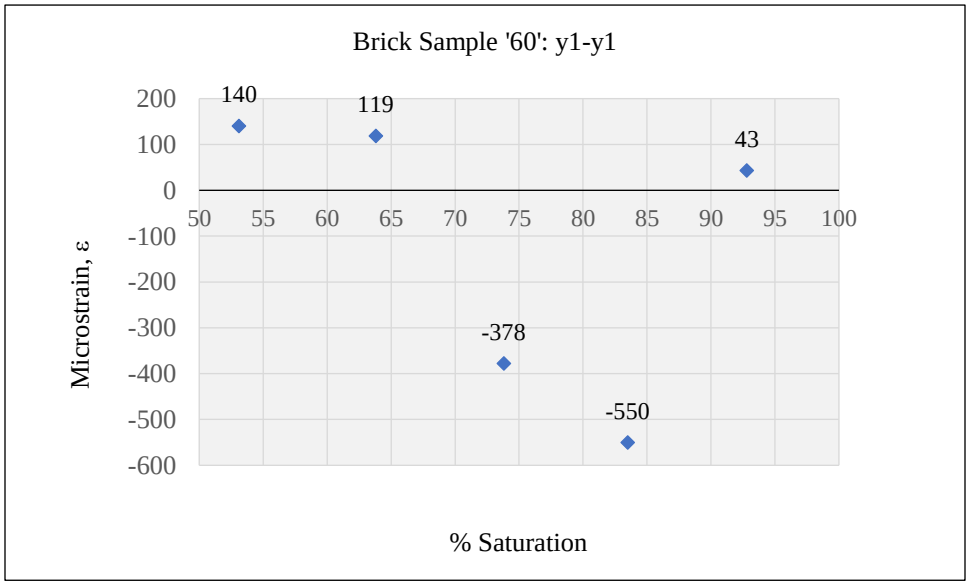

APPENDIX A 16: STRAINS ALONG THE Y1-Y1 AXIS

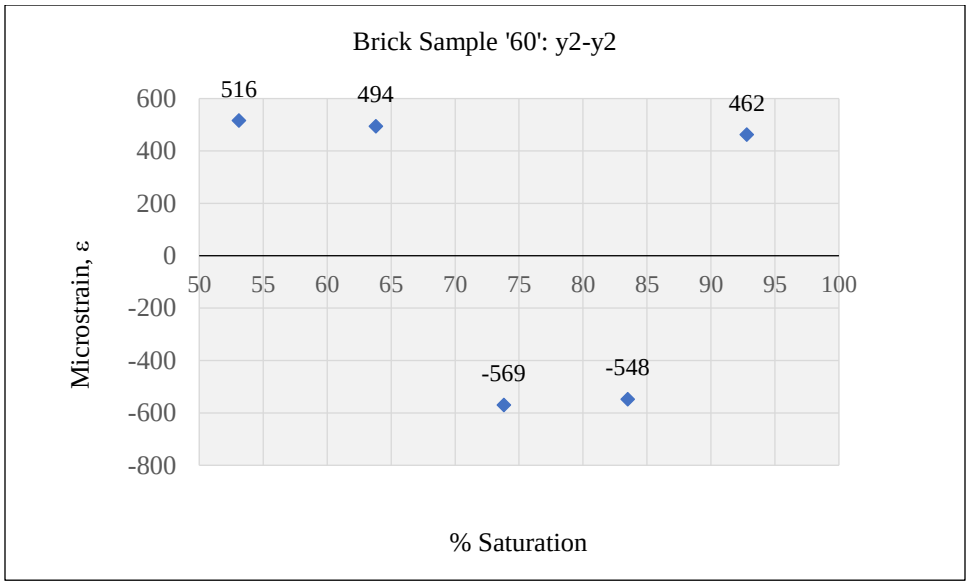

APPENDIX A 17: STRAINS ALONG THE Y2-Y2 AXIS

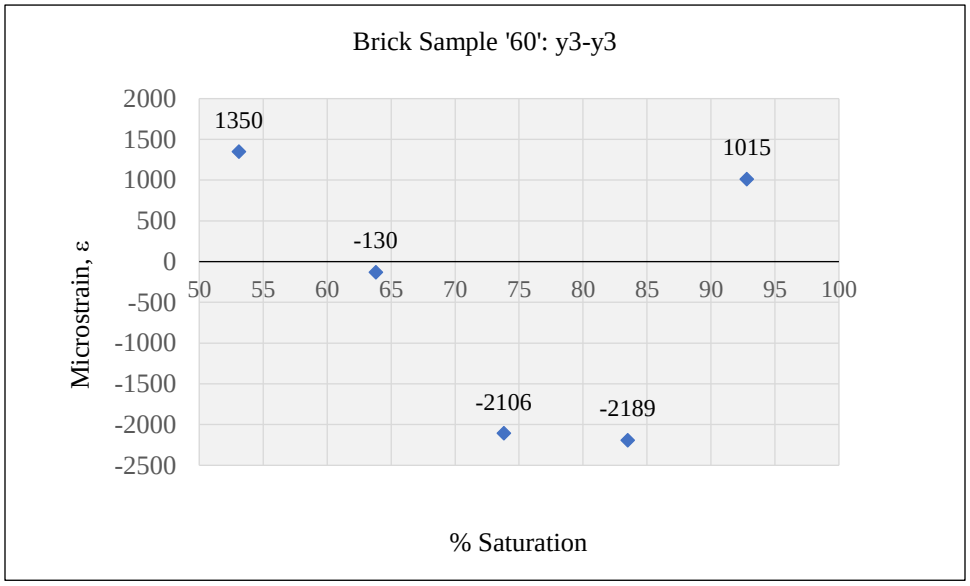

APPENDIX A 18: STRAINS ALONG THE Y3-Y3 AXIS

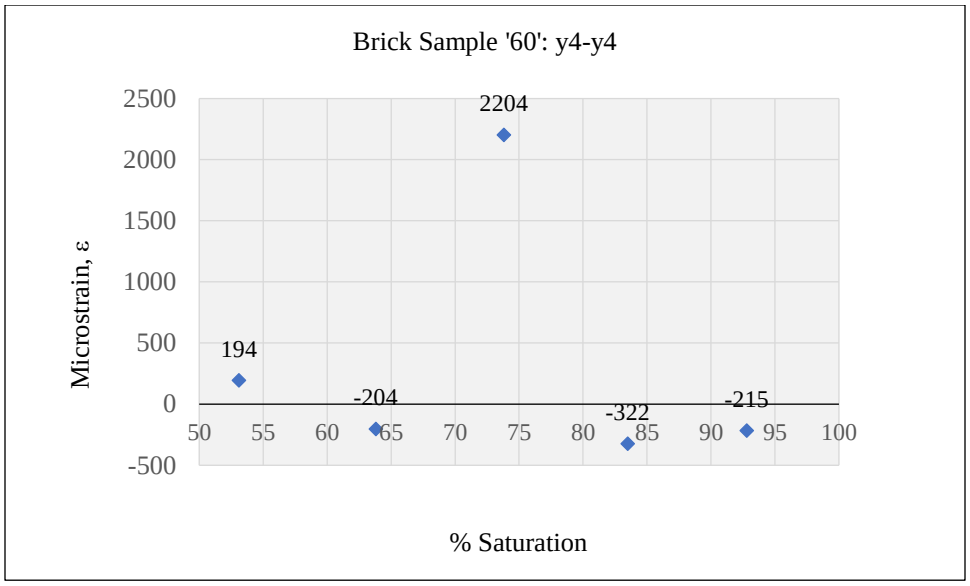

APPENDIX A 19: STRAINS ALONG THE Y4-Y4 AXIS

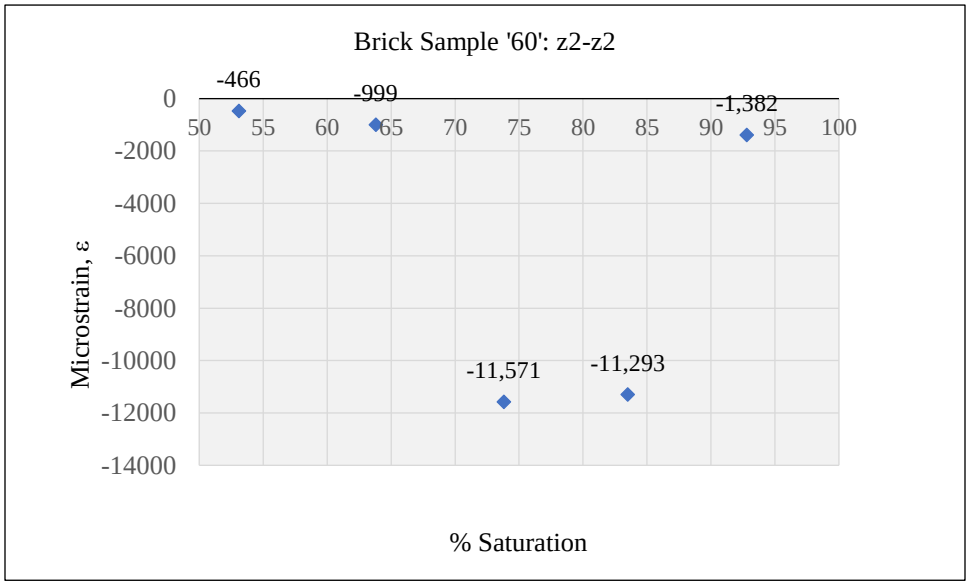

APPENDIX A 20: STRAINS ALONG THE Z2-Z2 AXIS

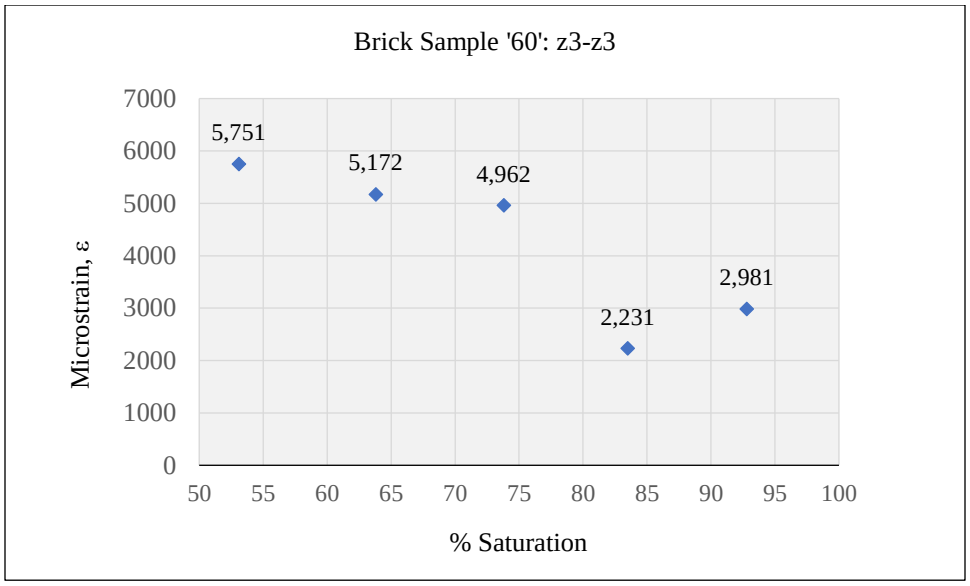

APPENDIX A 21: STRAINS ALONG THE Z3-Z3 AXIS

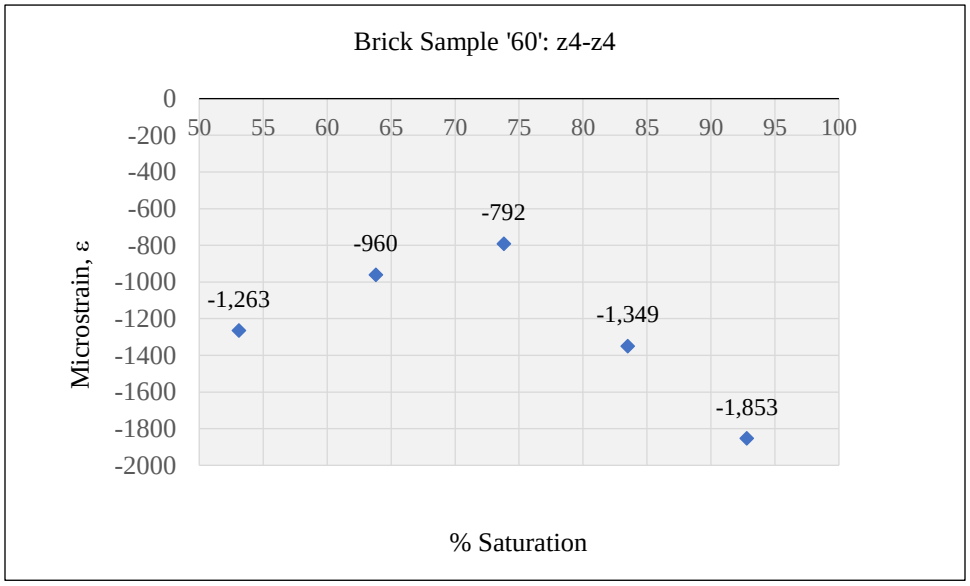

APPENDIX A 22: STRAINS ALONG THE Z4-Z4 AXIS

A 4 TYPE 295A-EB3

A4.1 STRAINS ALONG THE X, Y AND Z- AXIS

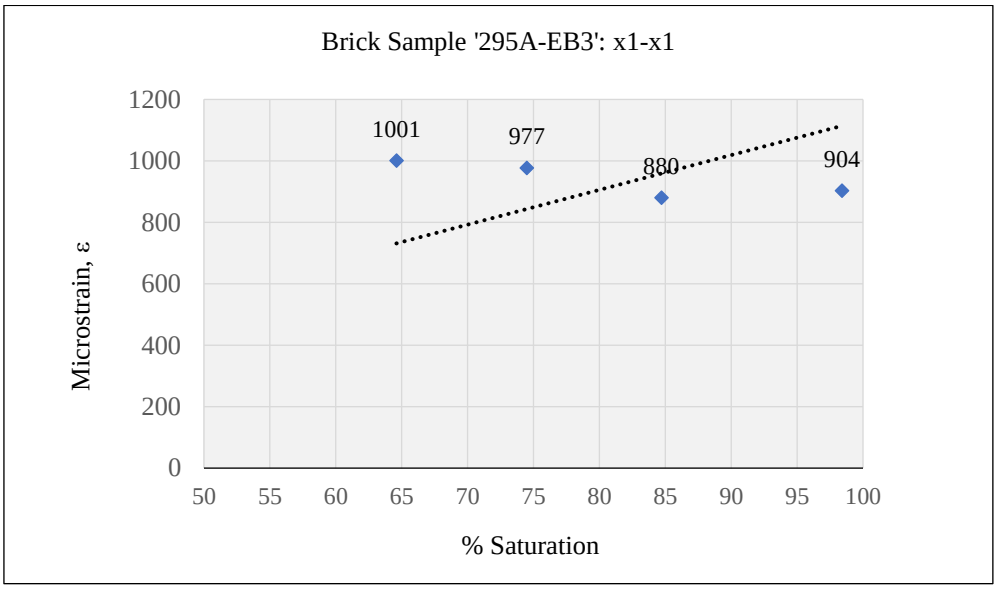

APPENDIX A 23: STRAINS ALONG THE X1-X1 AXIS

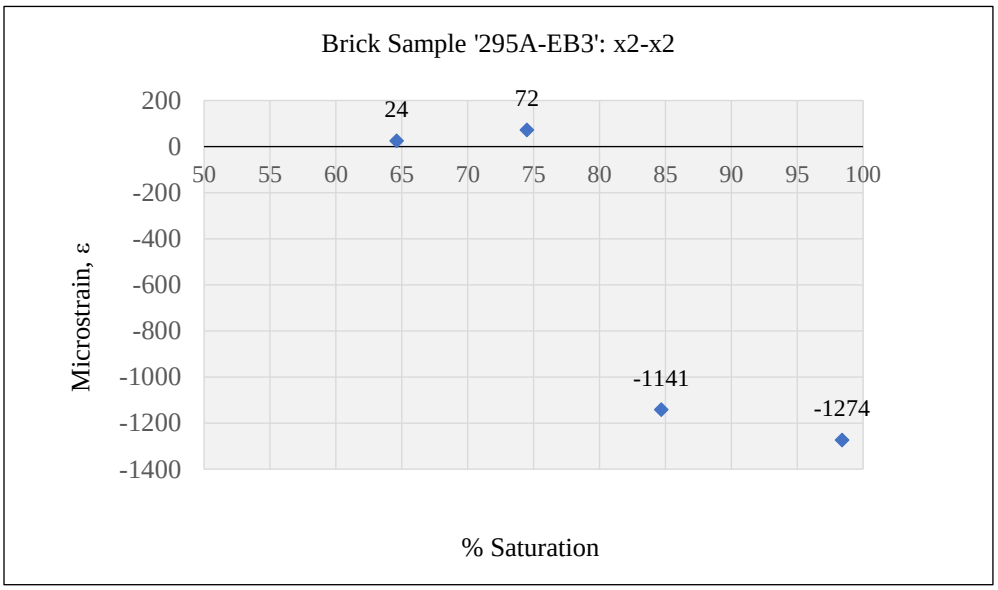

APPENDIX A 24: STRAINS ALONG THE X2-X2 AXIS

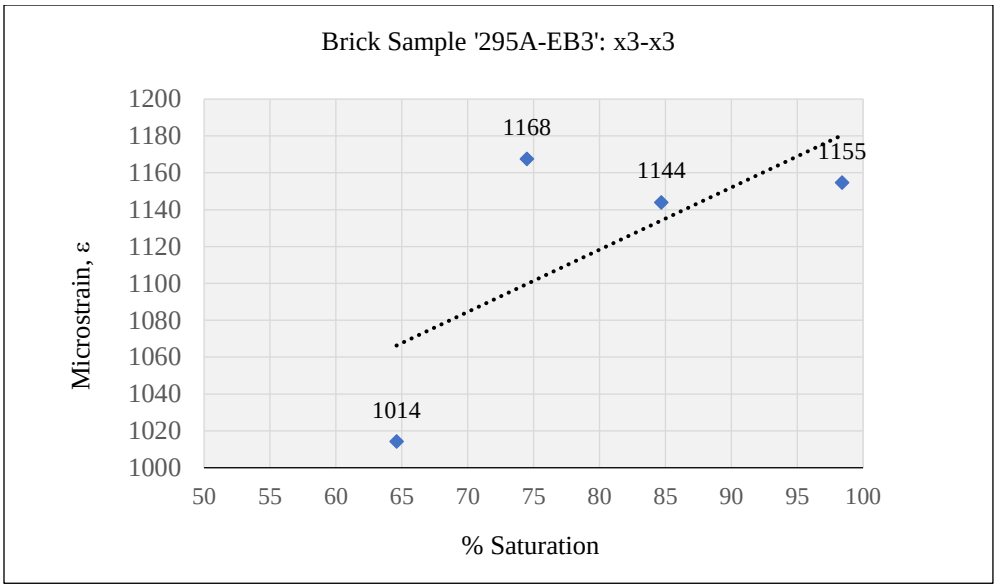

APPENDIX A 25: STRAINS ALONG THE X3-X3 AXIS

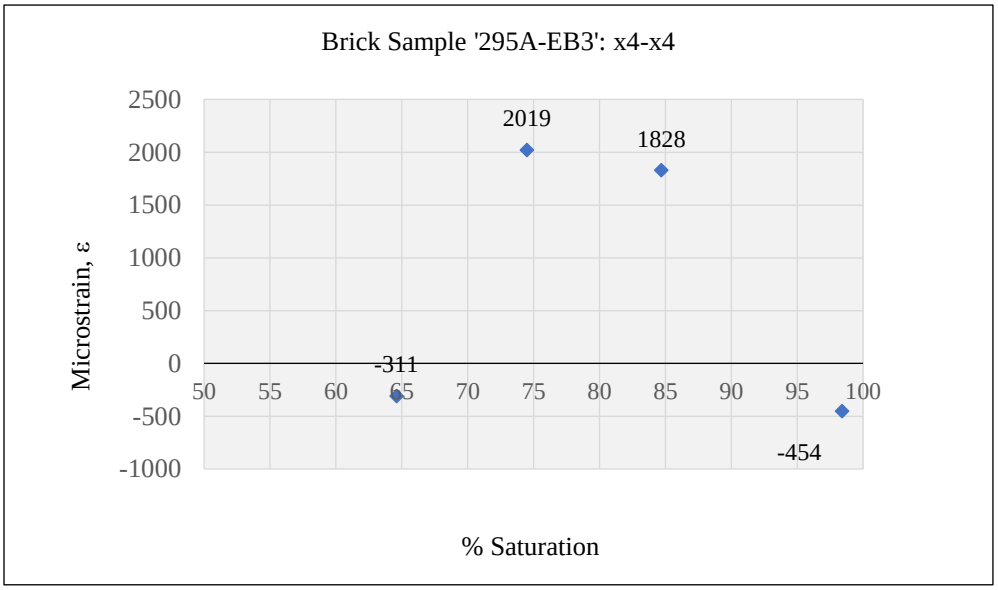

APPENDIX A 26: STRAINS ALONG THE X4-X4 AXIS

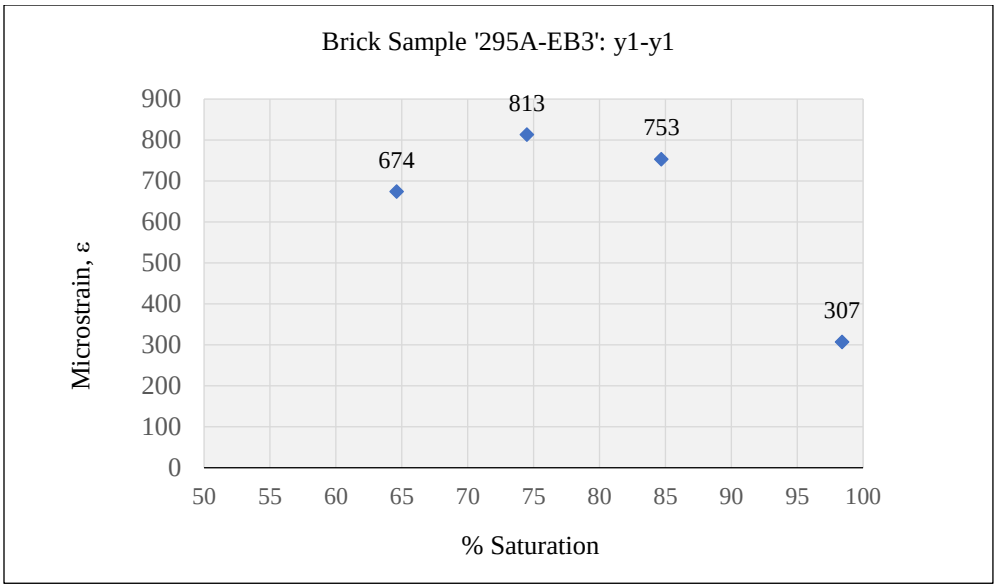

APPENDIX A 27: STRAINS ALONG THE Y1-Y1 AXIS

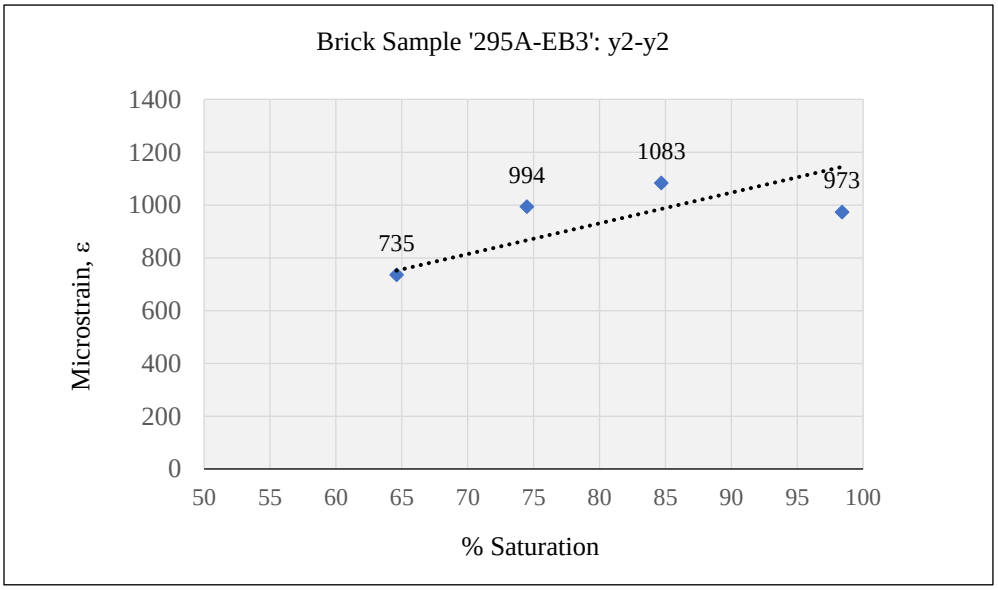

APPENDIX A 28: STRAINS ALONG THE Y2-Y2 AXIS

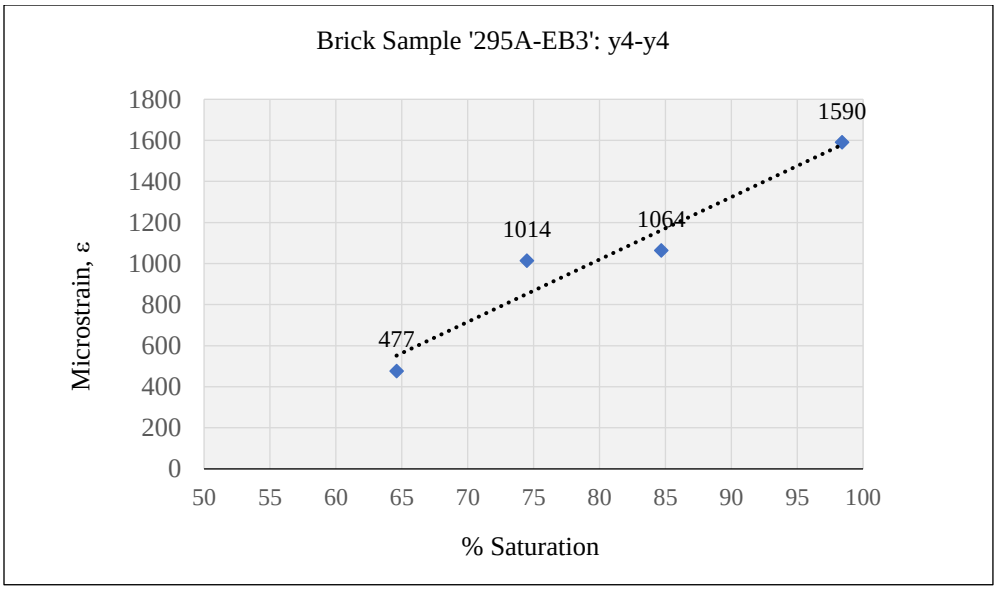

APPENDIX A 29: STRAINS ALONG THE Y4-Y4 AXIS

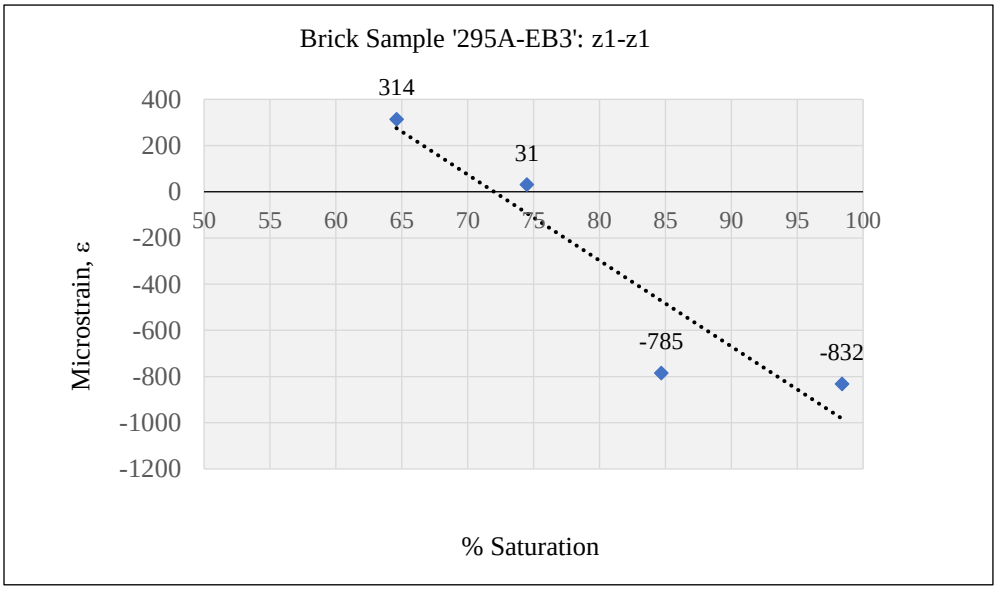

APPENDIX A 30: STRAINS ALONG THE Z1-Z1 AXIS

A 5 TYPE 305-EB4

A5.1 STRAINS ALONG THE X, Y AND Z-AXES

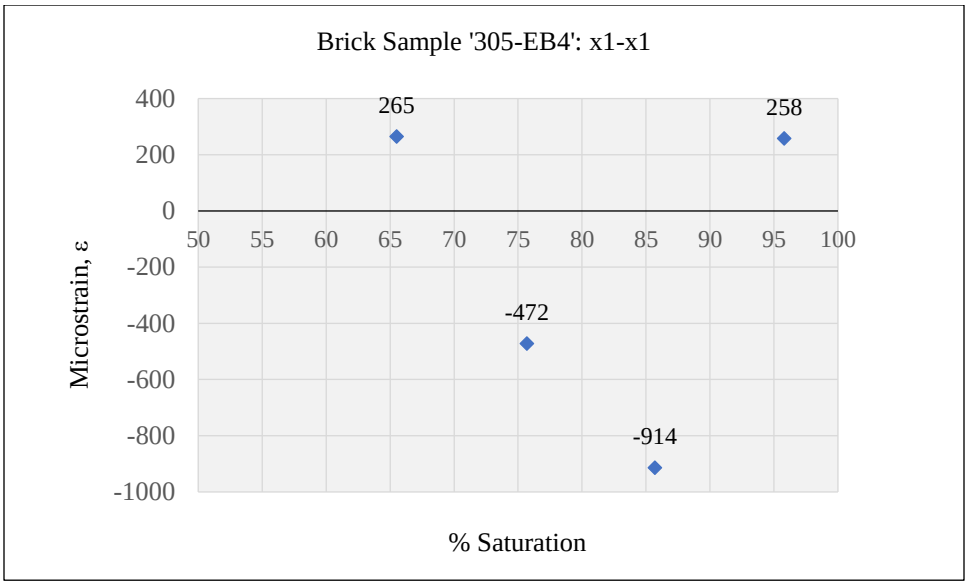

APPENDIX A 31: STRAINS ALONG THE X1-X1 AXIS

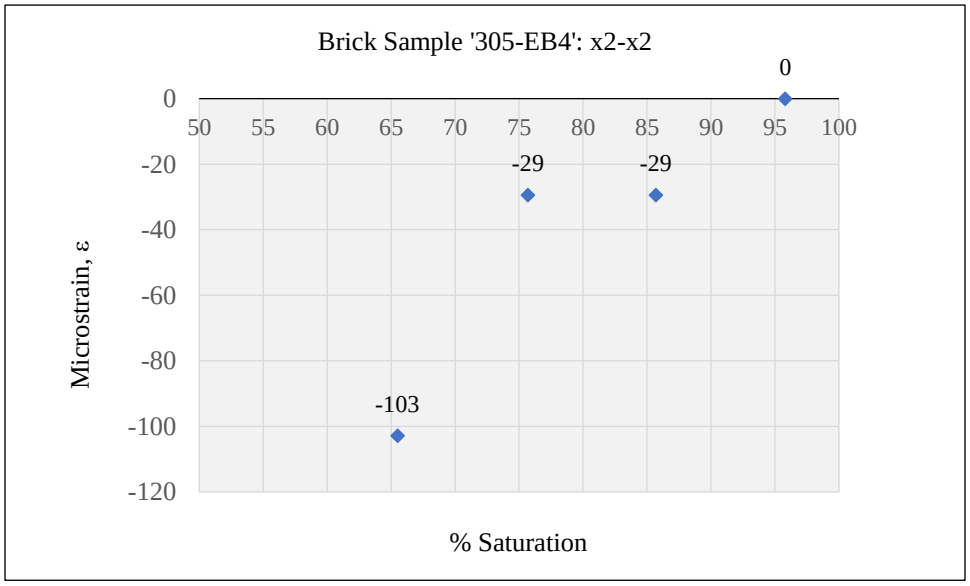

APPENDIX A 32: STRAINS ALONG THE X2-X2 AXIS

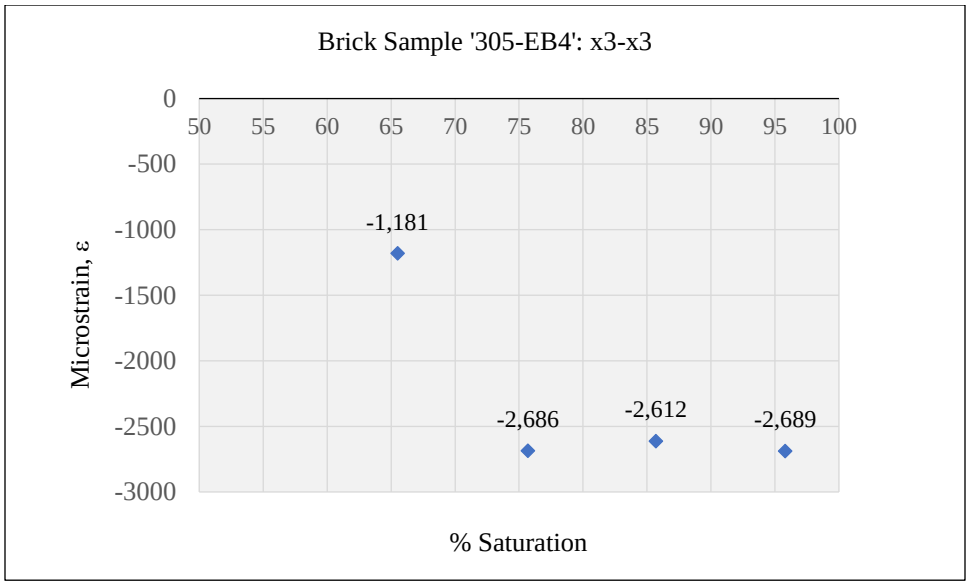

APPENDIX A 33: STRAINS ALONG THE X3-X3 AXIS

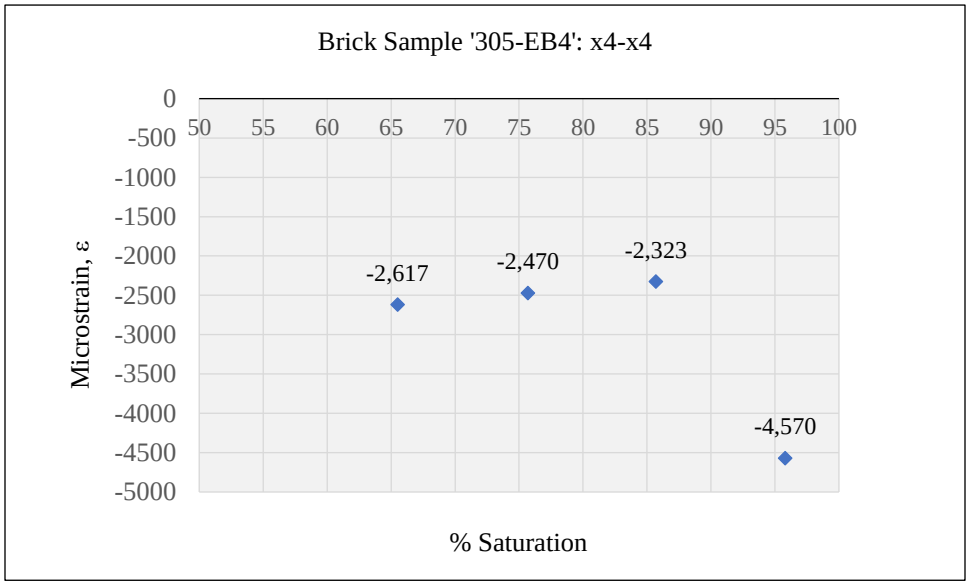

APPENDIX A 34: STRAINS ALONG THE X4-X4 AXIS

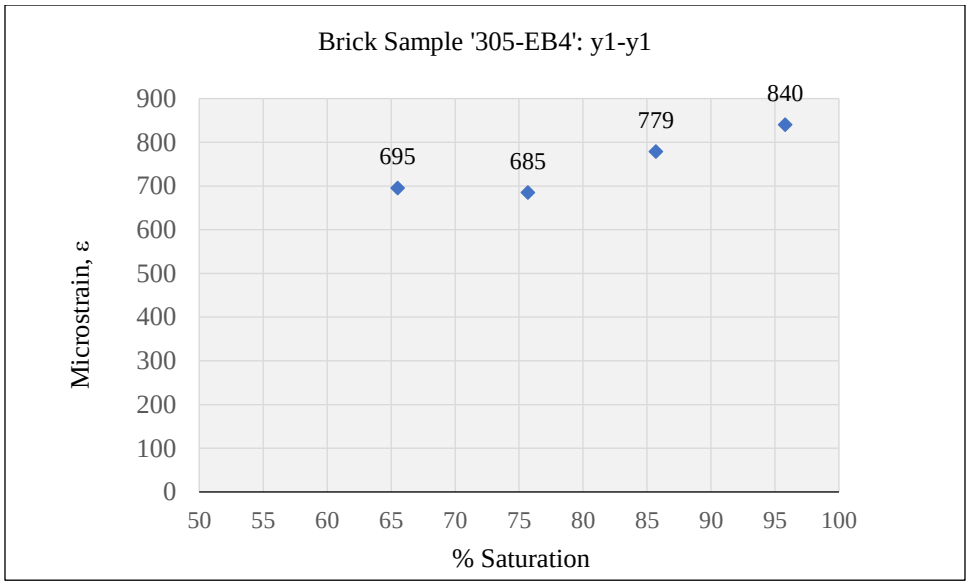

APPENDIX A 35: STRAINS ALONG THE Y1-Y1 AXIS

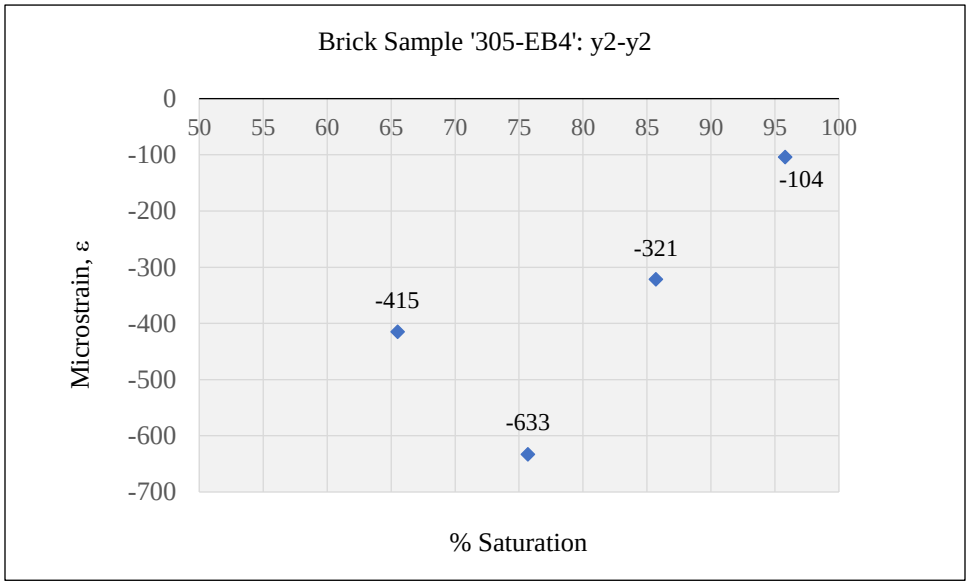

APPENDIX A 36: STRAINS ALONG THE Y2-Y2 AXIS

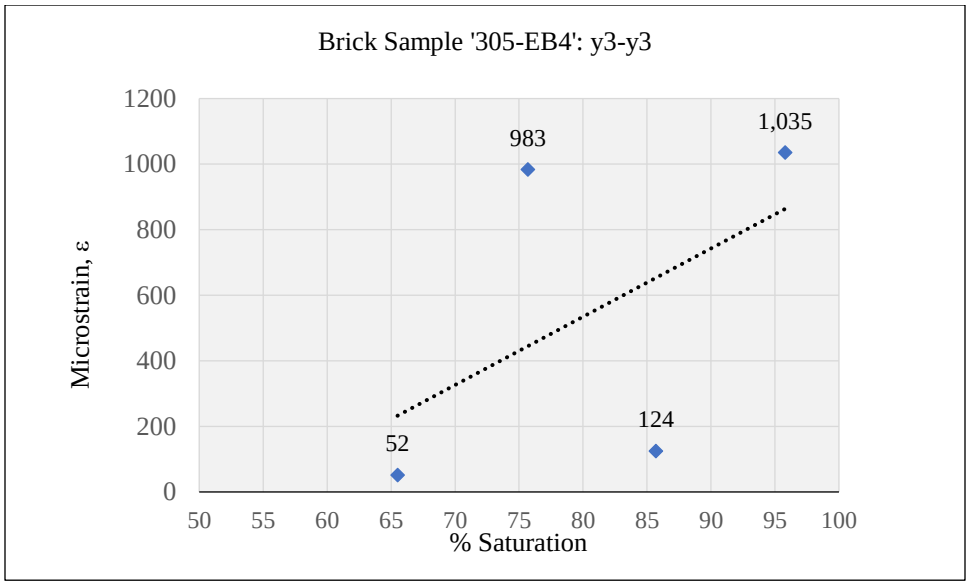

APPENDIX A 37: STRAINS ALONG THE Y3-Y3 AXIS

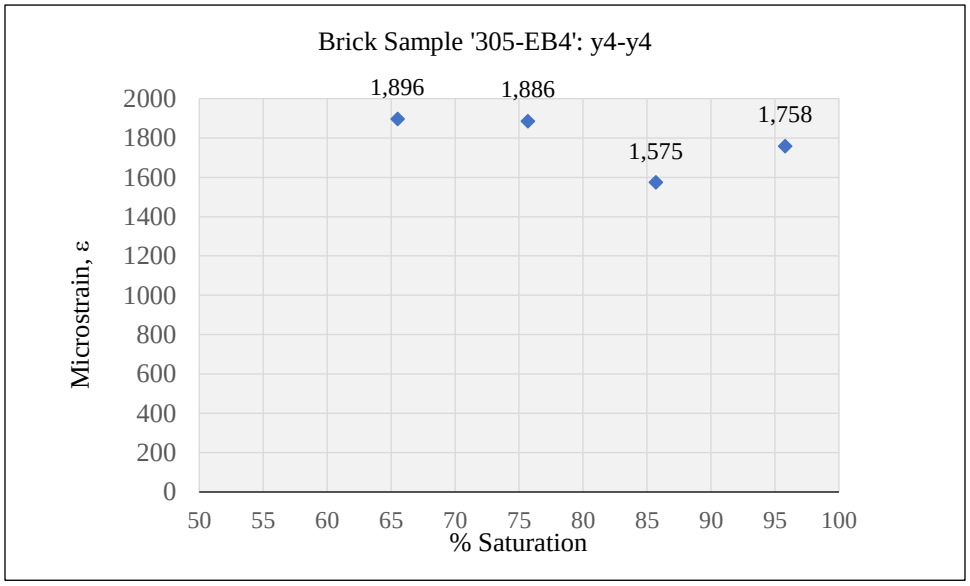

APPENDIX A 38: STRAINS ALONG THE Y4-Y4 AXIS

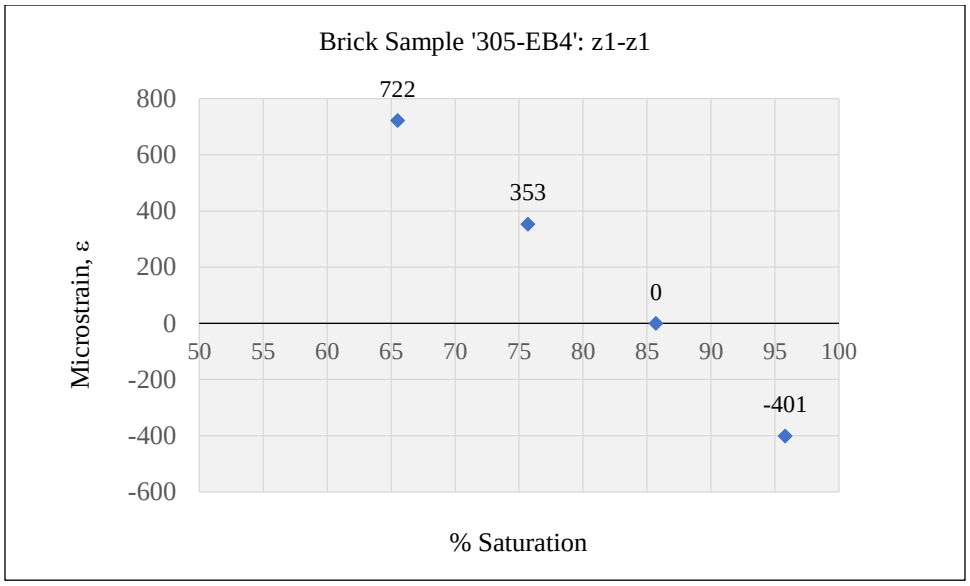

APPENDIX A 39: STRAINS ALONG THE Z1-Z1 AXIS

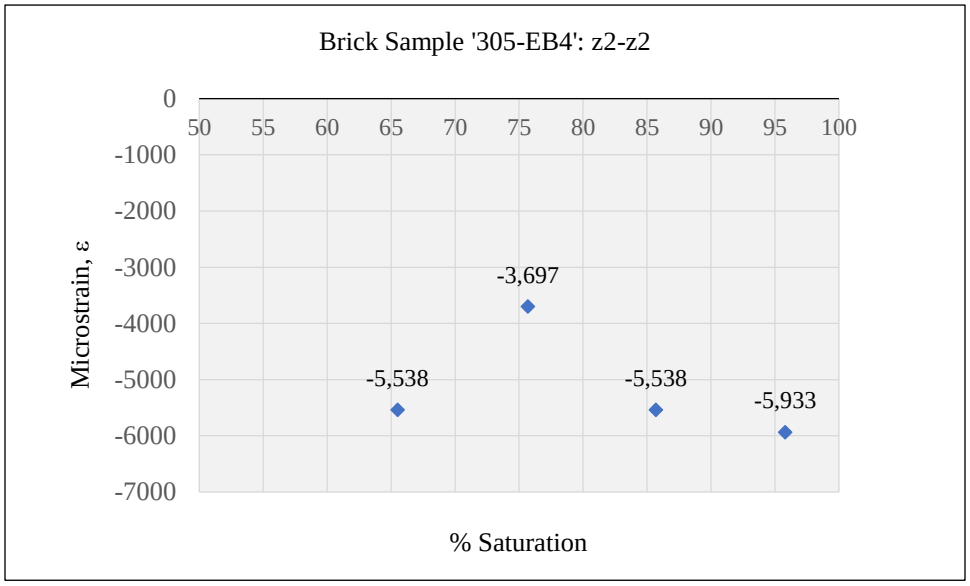

APPENDIX A 40: STRAINS ALONG THE Z2-Z2 AXIS

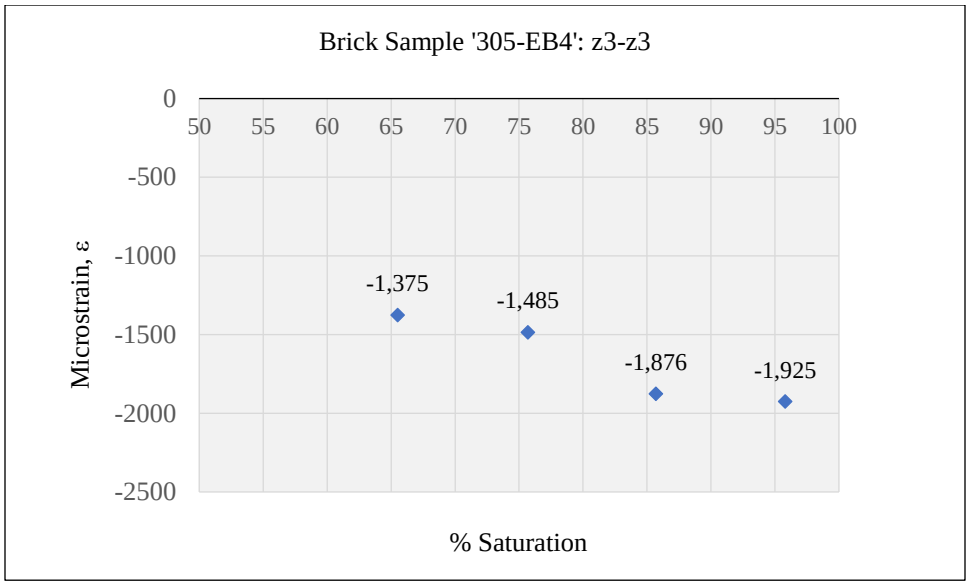

APPENDIX A 41: STRAINS ALONG THE Z3-Z3 AXIS

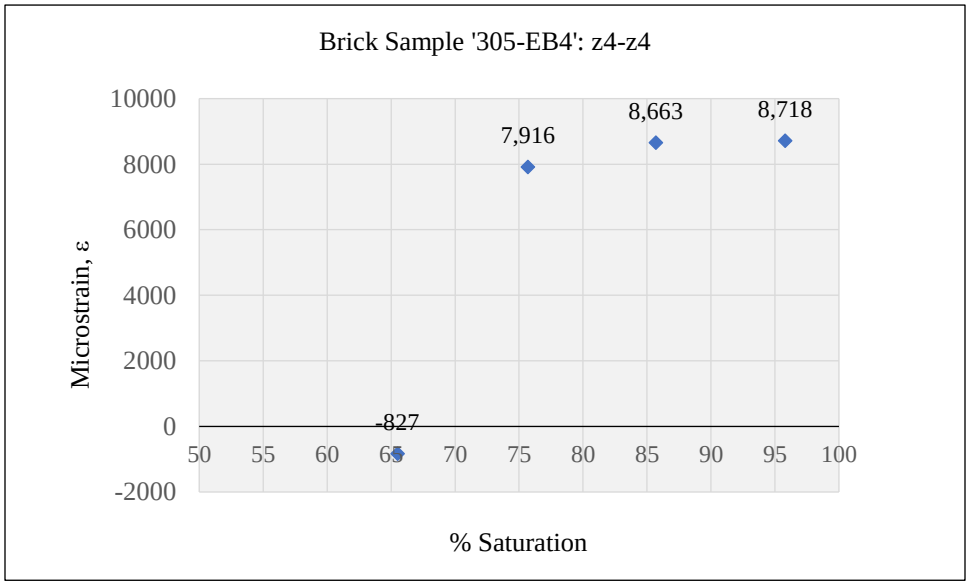

APPENDIX A 42: STRAINS ALONG THE Z4-Z4 AXIS

A 6 TYPE 297-EB2

A6.1 STRAINS ALONG THE X, Y AND Z- AXES

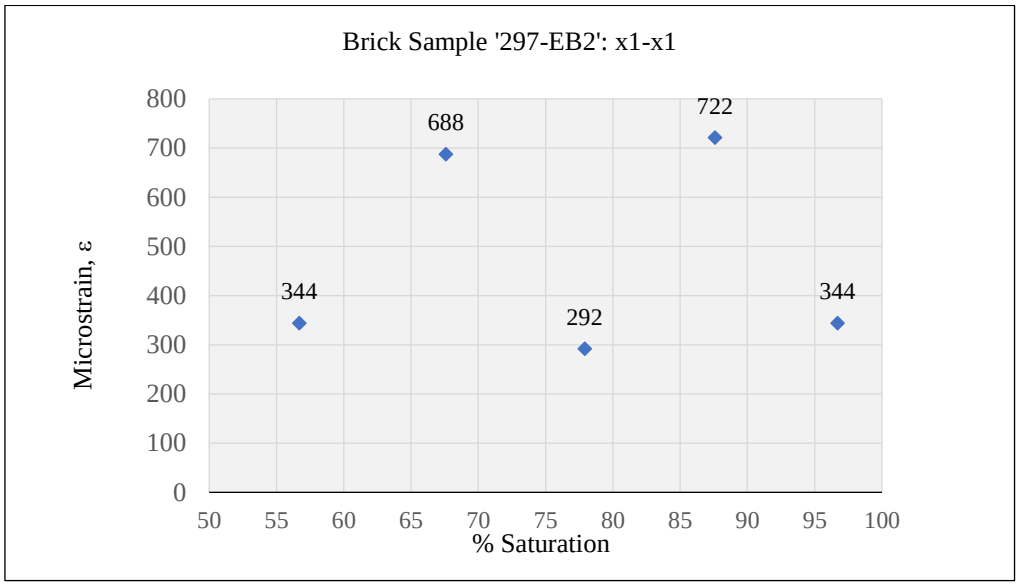

APPENDIX A 43: STRAINS ALONG THE X1-X1 AXIS

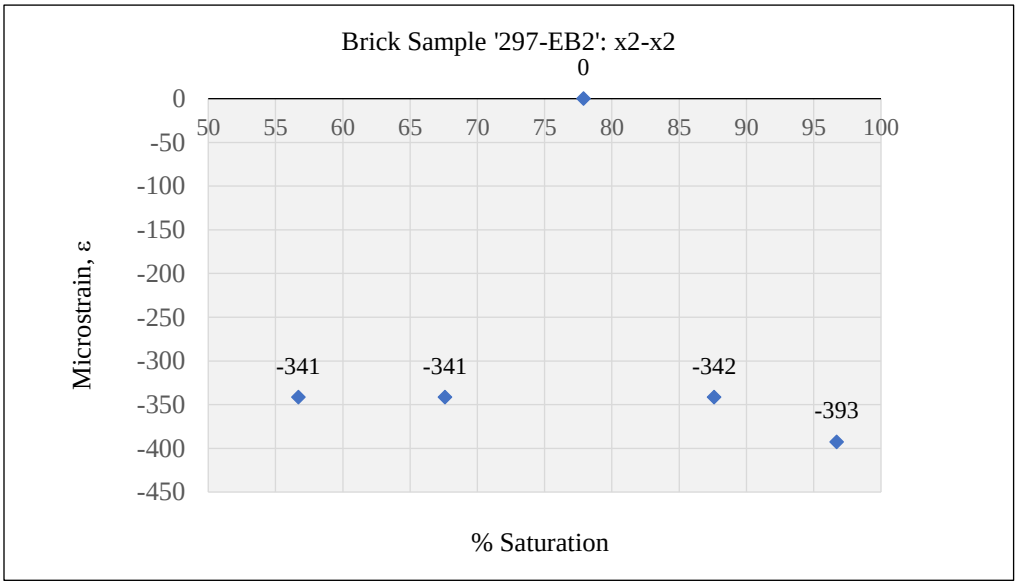

APPENDIX A 44: STRAINS ALONG THE X2-X2 AXIS

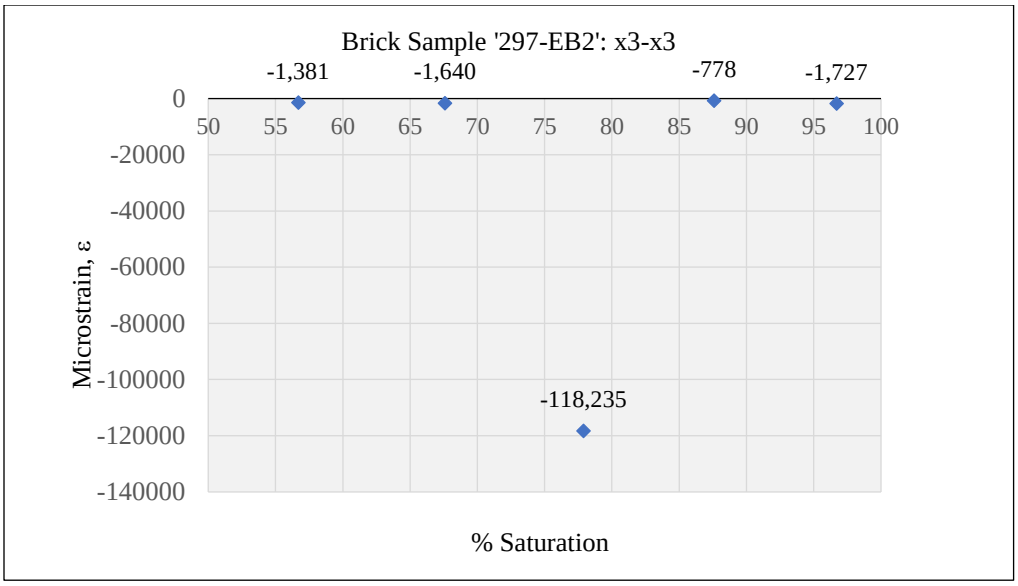

APPENDIX A 45: STRAINS ALONG THE X3-X3 AXIS

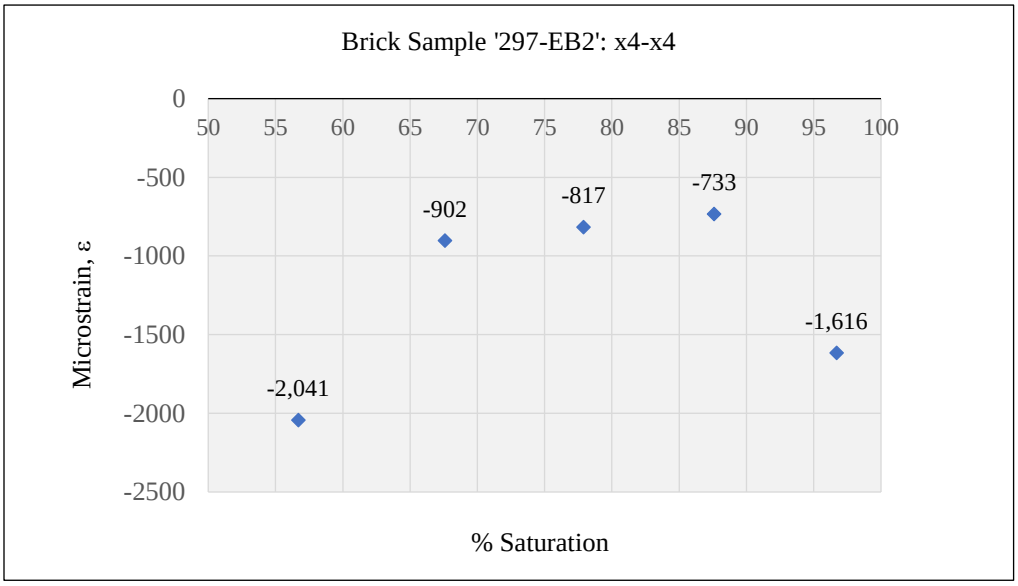

APPENDIX A 46: STRAINS ALONG THE X4-X4 AXIS

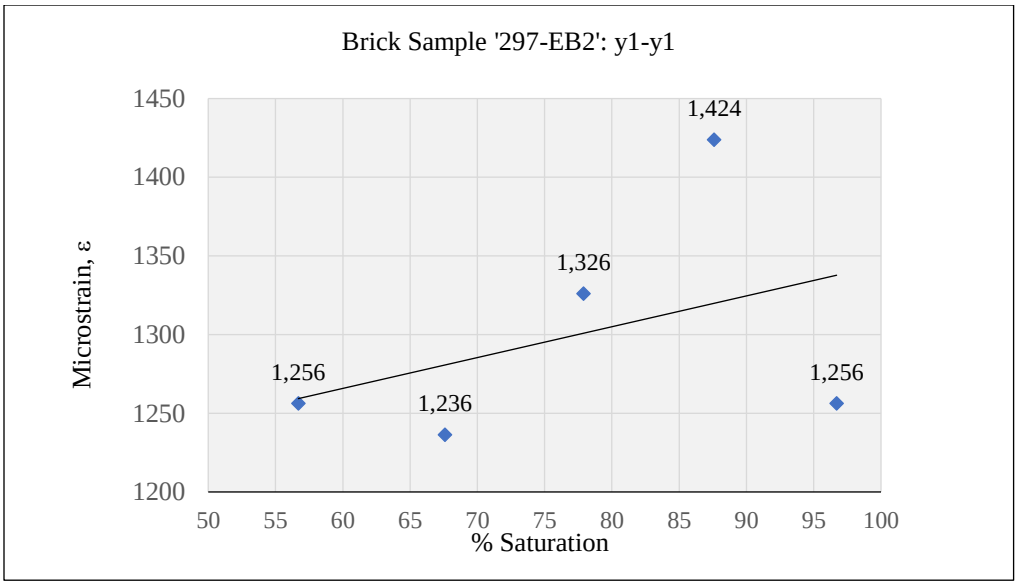

APPENDIX A 47: STRAINS ALONG THE Y1-Y1 AXIS

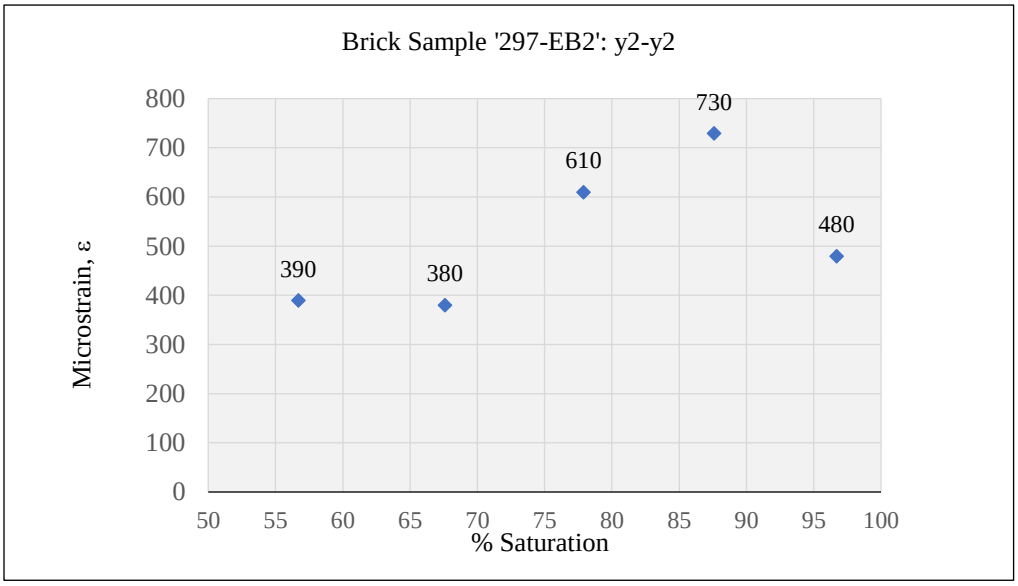

APPENDIX A 48: STRAINS ALONG THE Y2-Y2 AXIS

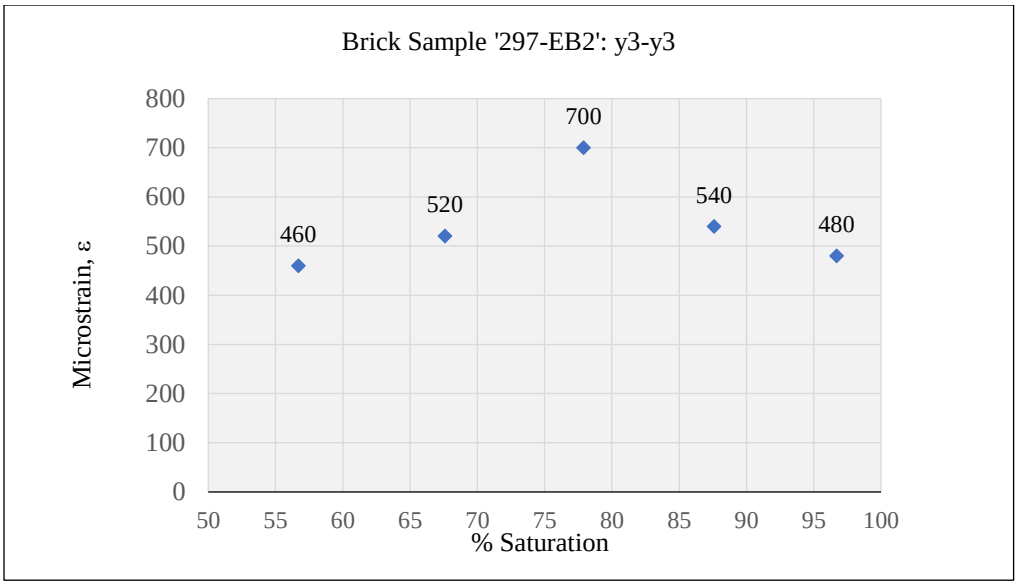

APPENDIX A 49: STRAINS ALONG THE Y3-Y3 AXIS

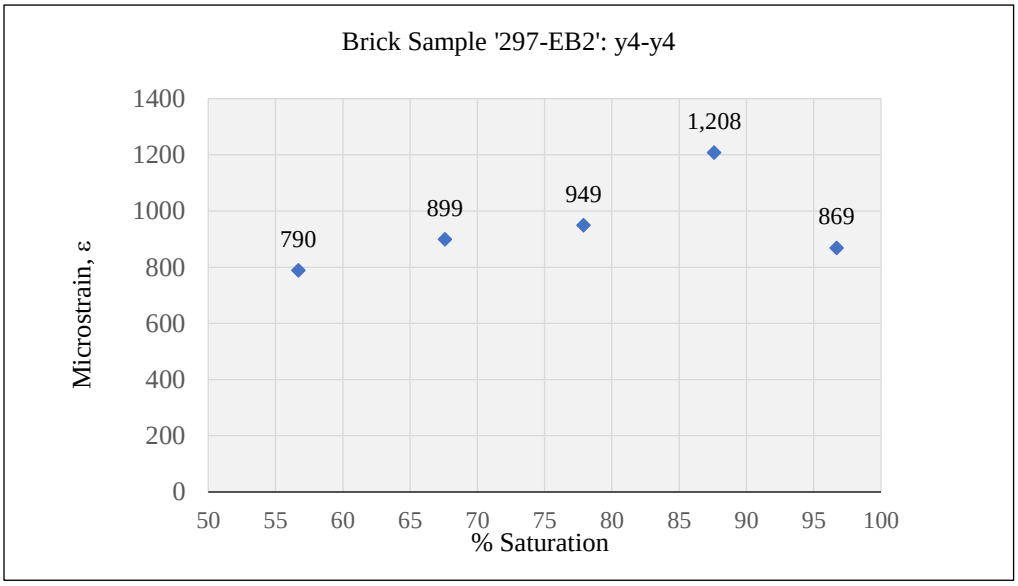

APPENDIX A 50: STRAINS ALONG THE Y4-Y4 AXIS

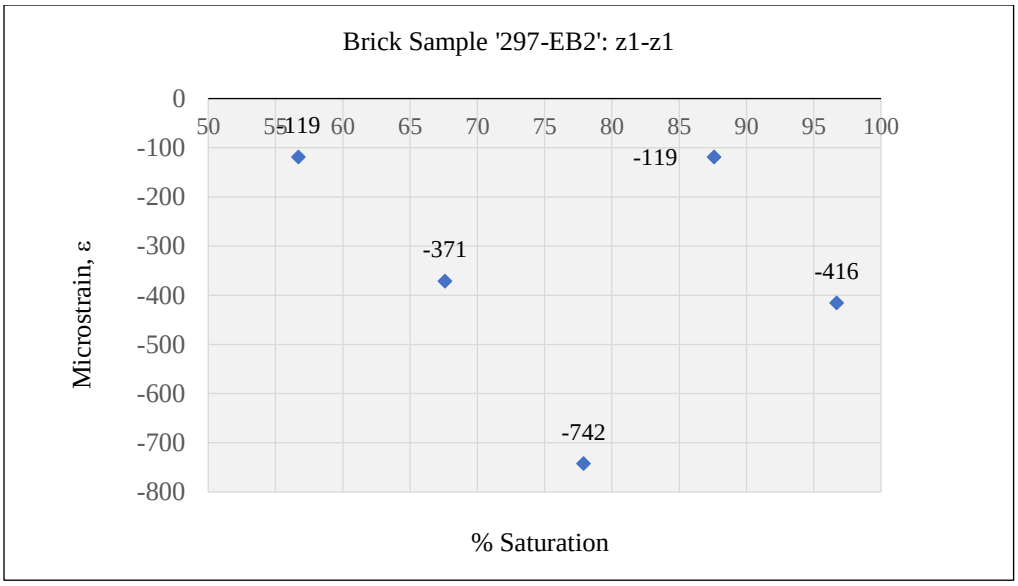

APPENDIX A 51: STRAINS ALONG THE Z1-Z1 AXIS

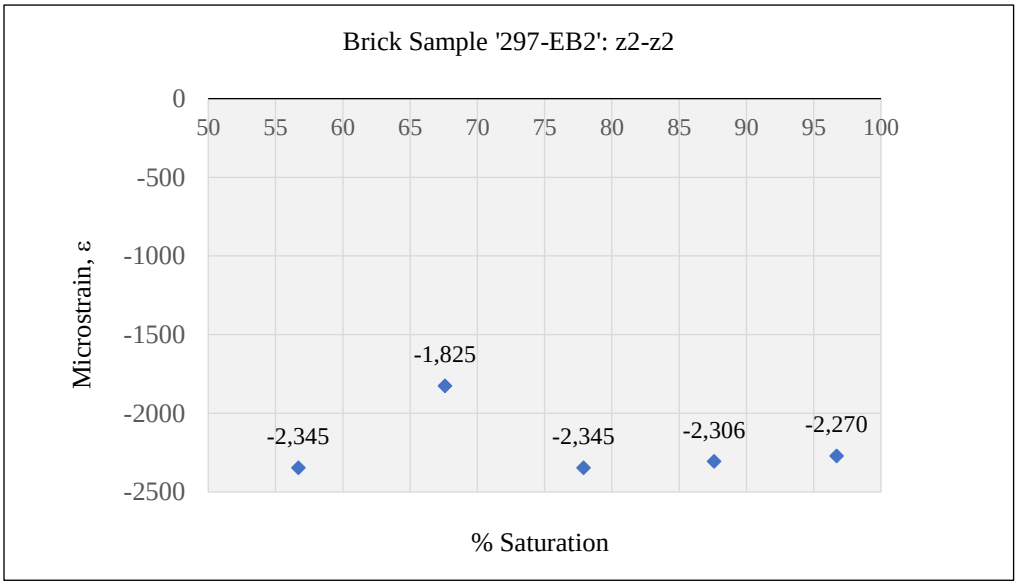

APPENDIX A 52: STRAINS ALONG THE Z2-Z2 AXIS

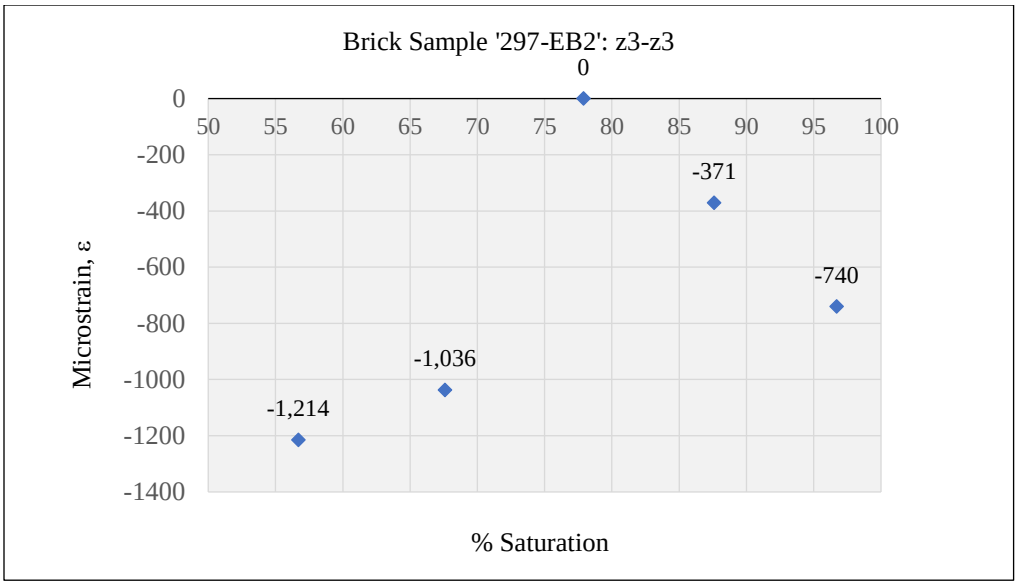

APPENDIX A 53: STRAINS ALONG THE Z3-Z3 AXIS

A 7 TYPE 295A-F4

A7.1 STRAINS ALONG X, Y AND Z-AXES

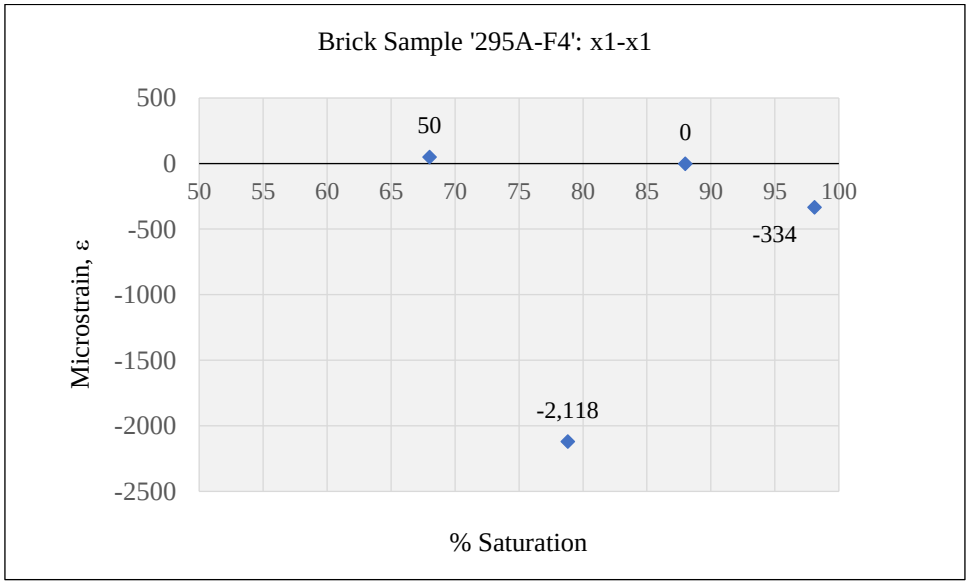

APPENDIX A 54: STRAINS ALONG THE X1-X1 AXIS

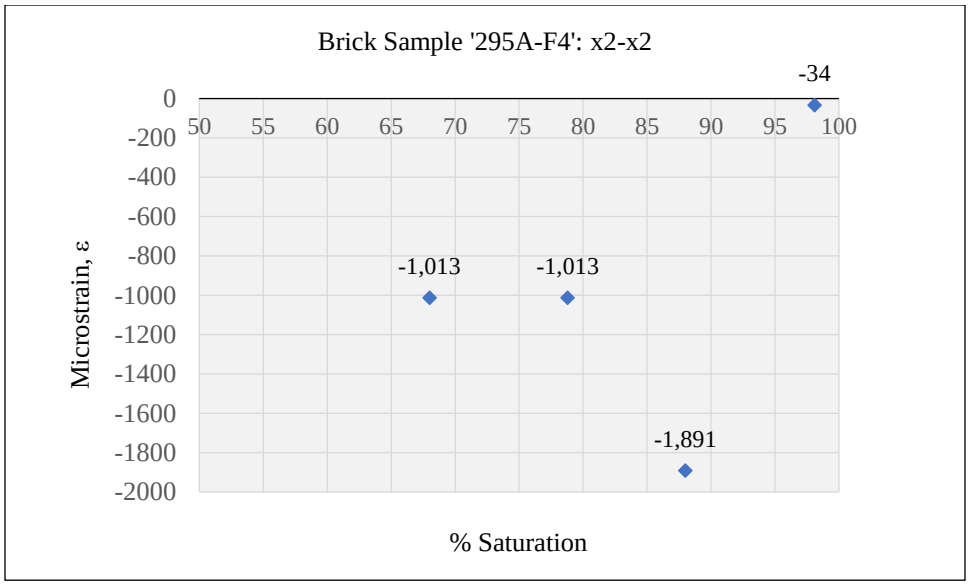

APPENDIX A 55: STRAINS ALONG THE X2-X2 AXIS

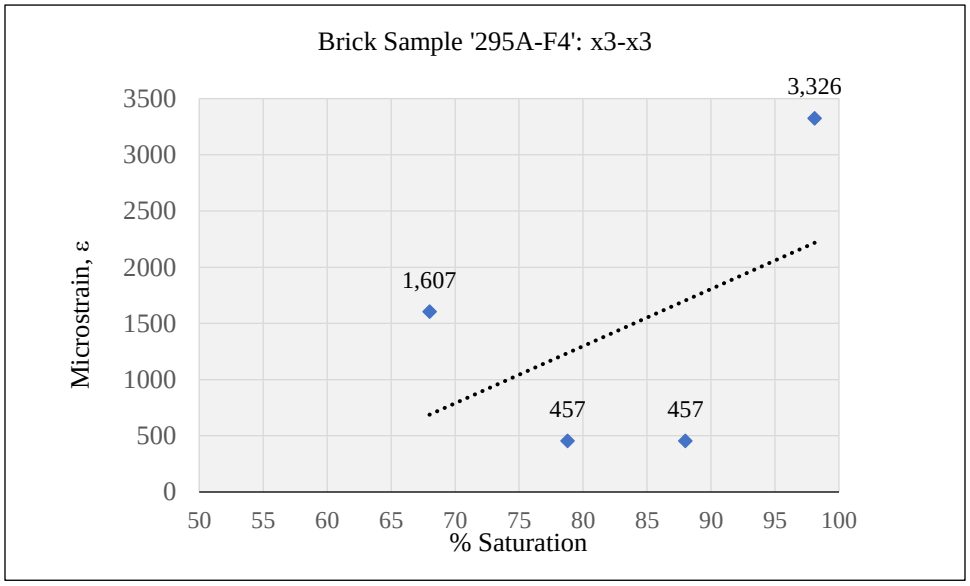

APPENDIX A 56: STRAINS ALONG THE X3-X3 AXIS

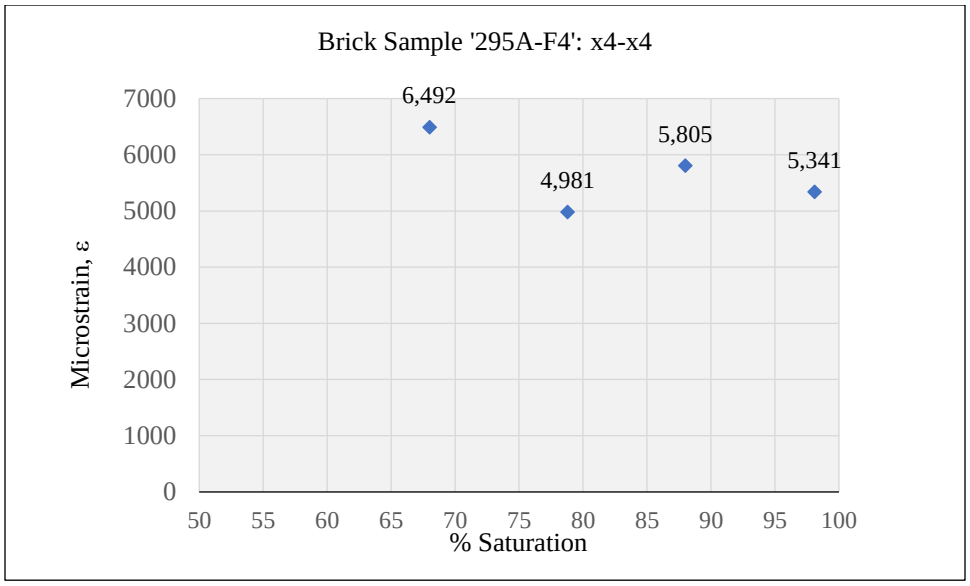

APPENDIX A 57: STRAINS ALONG THE X4-X4 AXIS

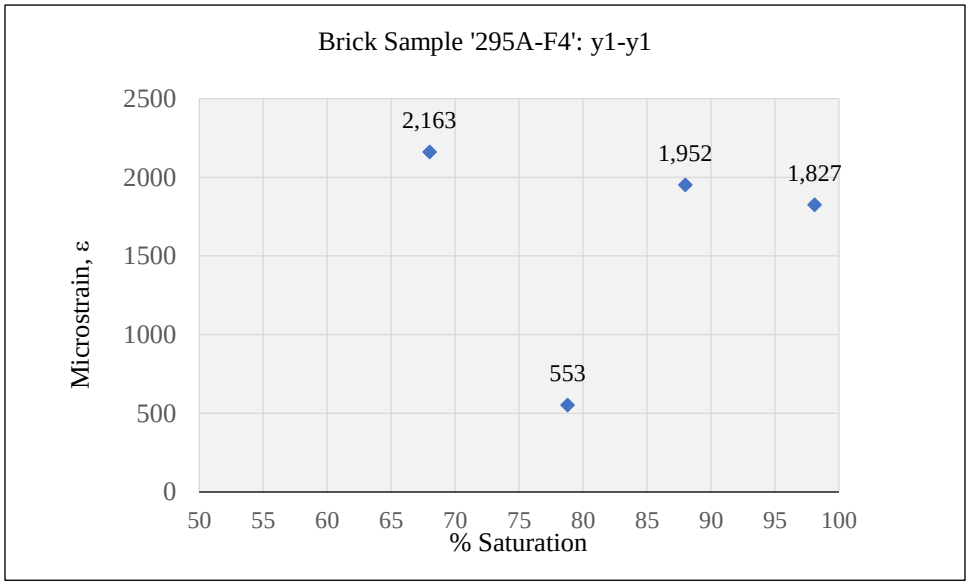

APPENDIX A 58: STRAINS ALONG THE Y1-Y1 AXIS

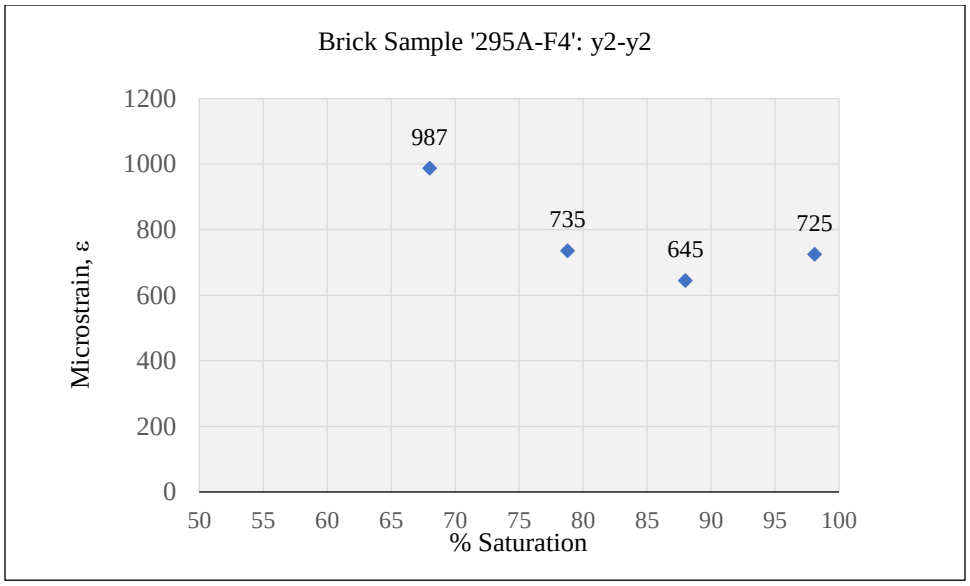

APPENDIX A 59: STRAINS ALONG THE Y2-Y2 AXIS

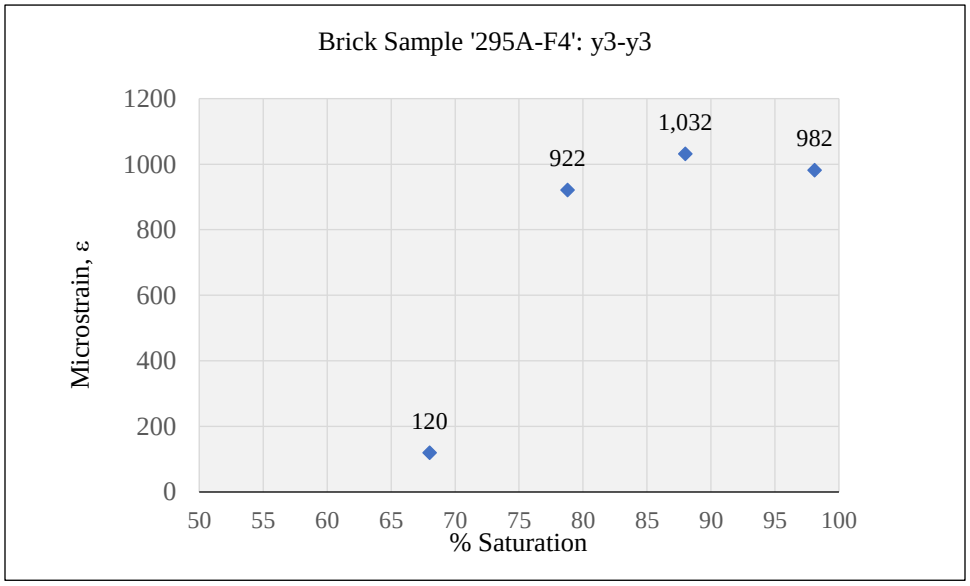

APPENDIX A 60: STRAINS ALONG THE Y3-Y3 AXIS

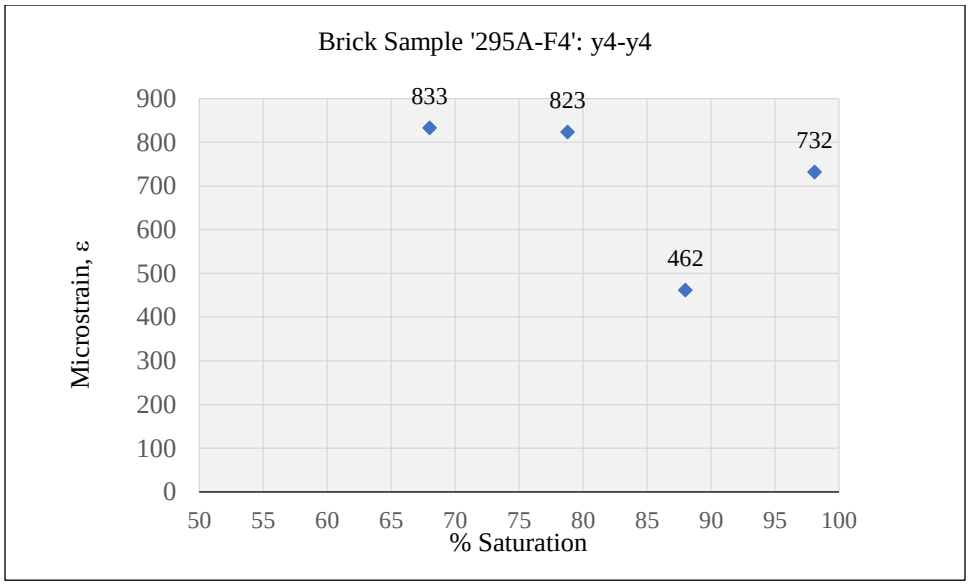

APPENDIX A 61: STRAINS ALONG THE Y4-Y4 AXIS

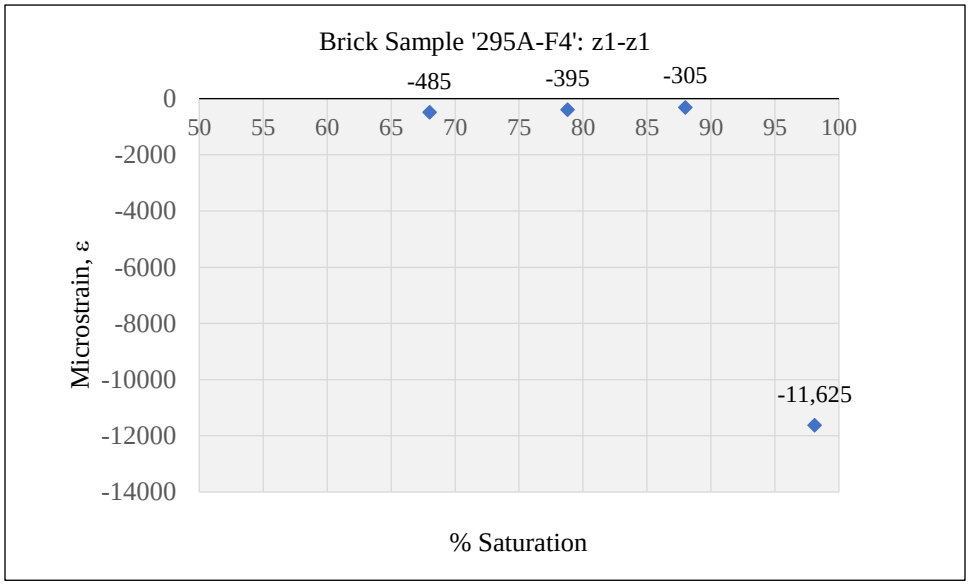

APPENDIX A 62: STRAINS ALONG THE Z1-Z1 AXIS

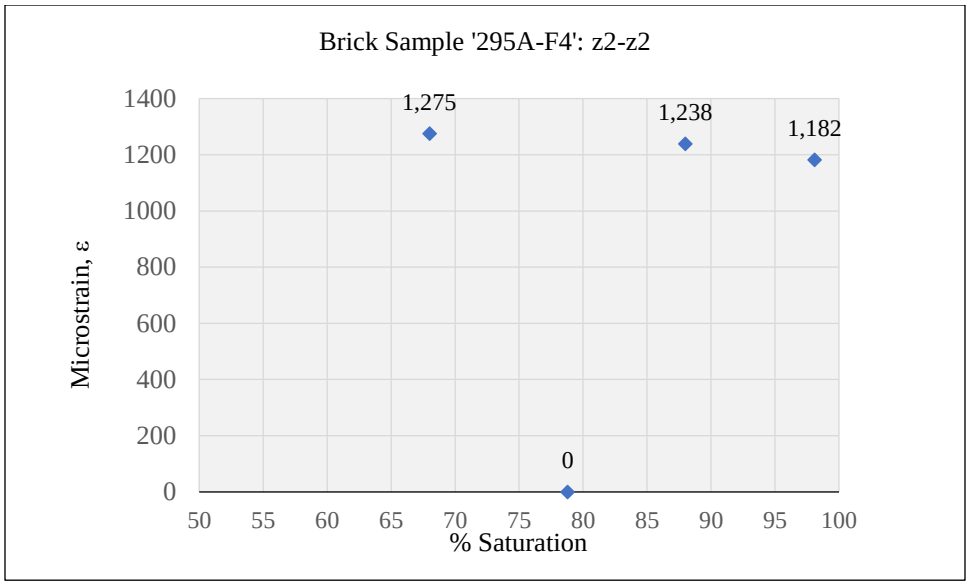

APPENDIX A 63: STRAINS ALONG THE Z2-Z2 AXIS

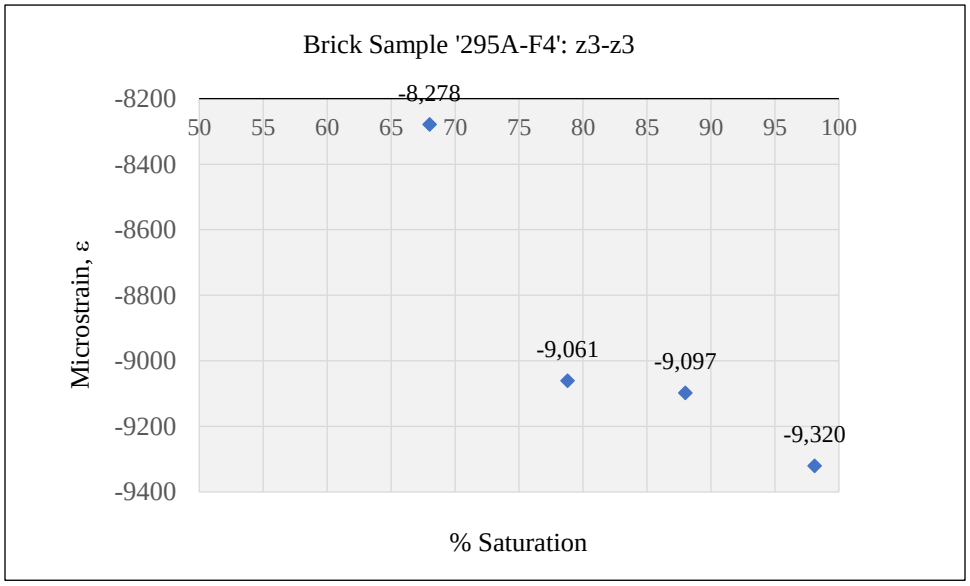

APPENDIX A 64: STRAINS ALONG THE Z3-Z3 AXIS

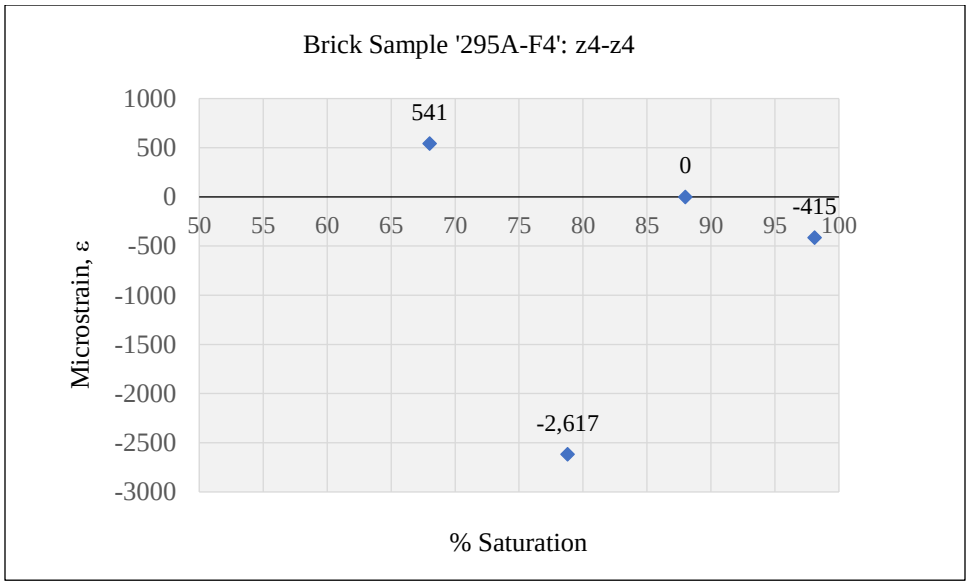

APPENDIX A 65: STRAINS ALONG THE Z4-Z4 AXIS

A 8 TYPE 349-ER1

A8.1 STRAINS ALONG THE X, Y AND Z-AXES

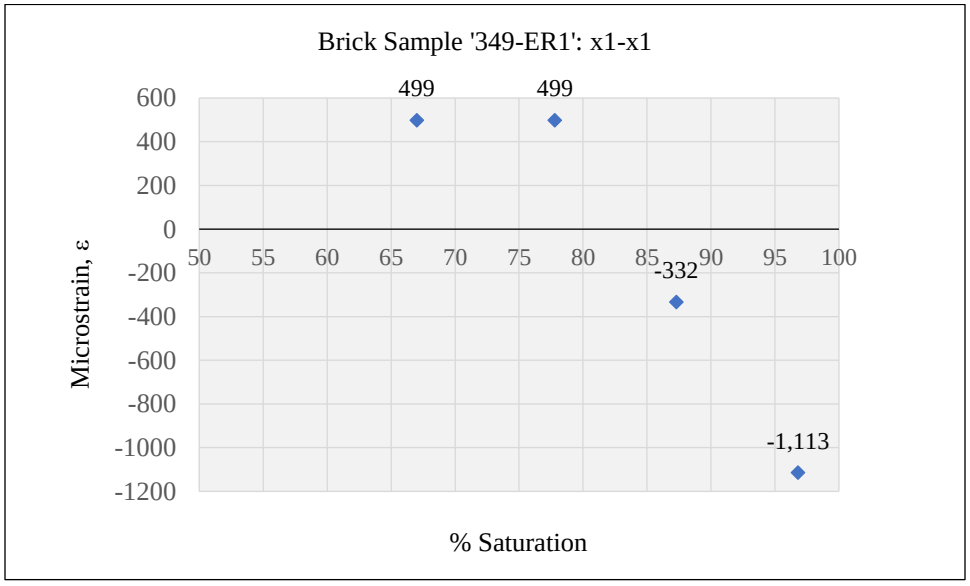

APPENDIX A 66: STRAINS ALONG THE X1-X1 AXIS

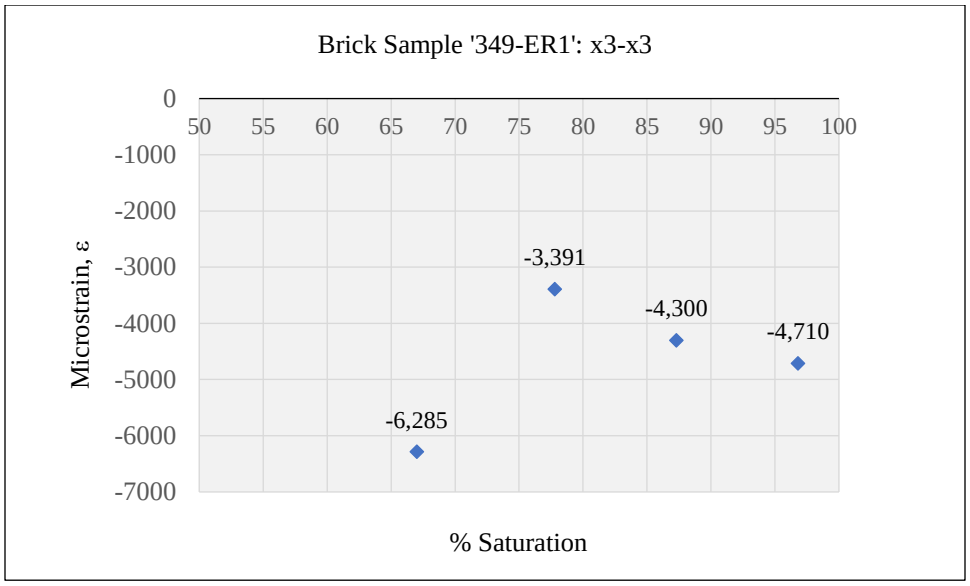

APPENDIX A 67: STRAINS ALONG THE X3-X3 AXIS

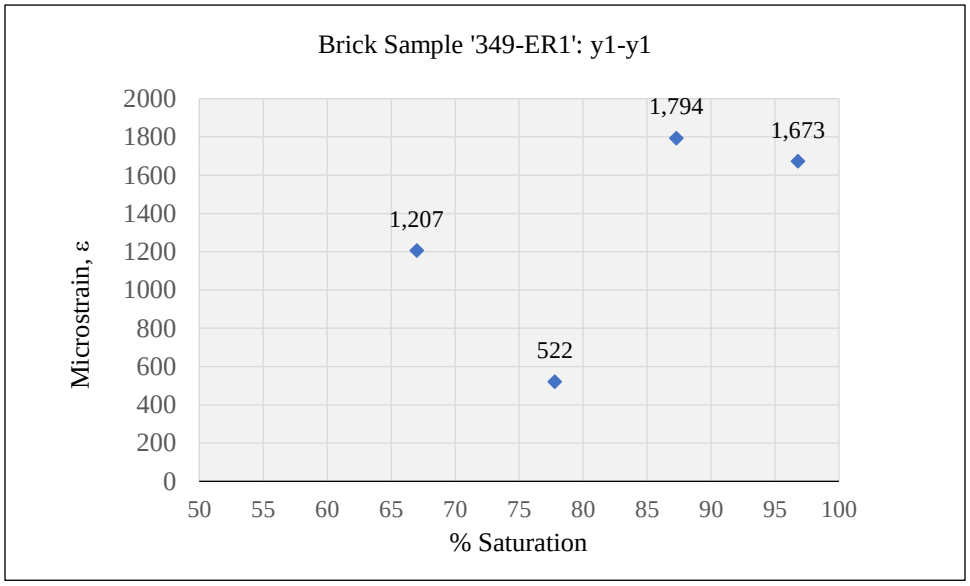

APPENDIX A 68: STRAINS ALONG THE Y1-Y1 AXIS

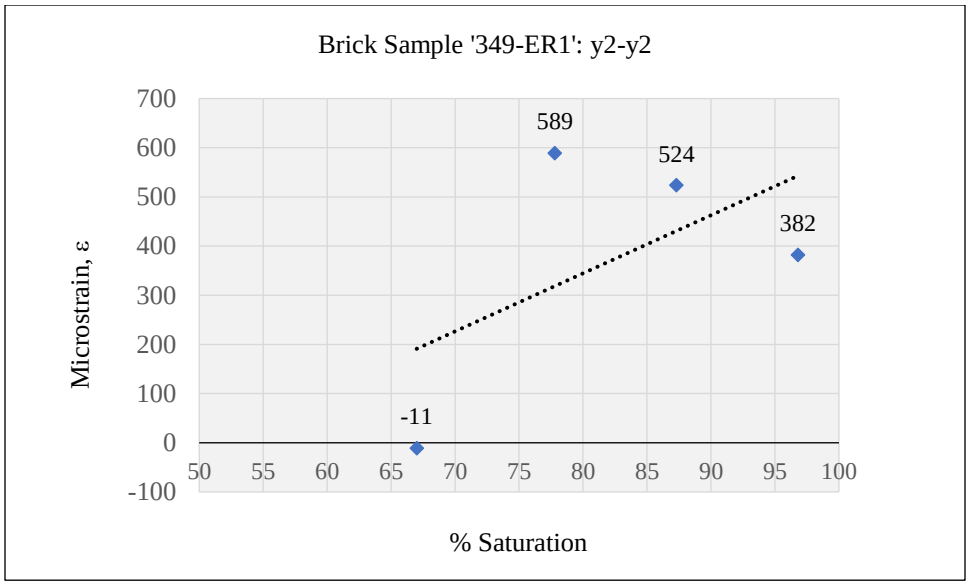

APPENDIX A 69: STRAINS ALONG THE Y2-Y2 AXIS

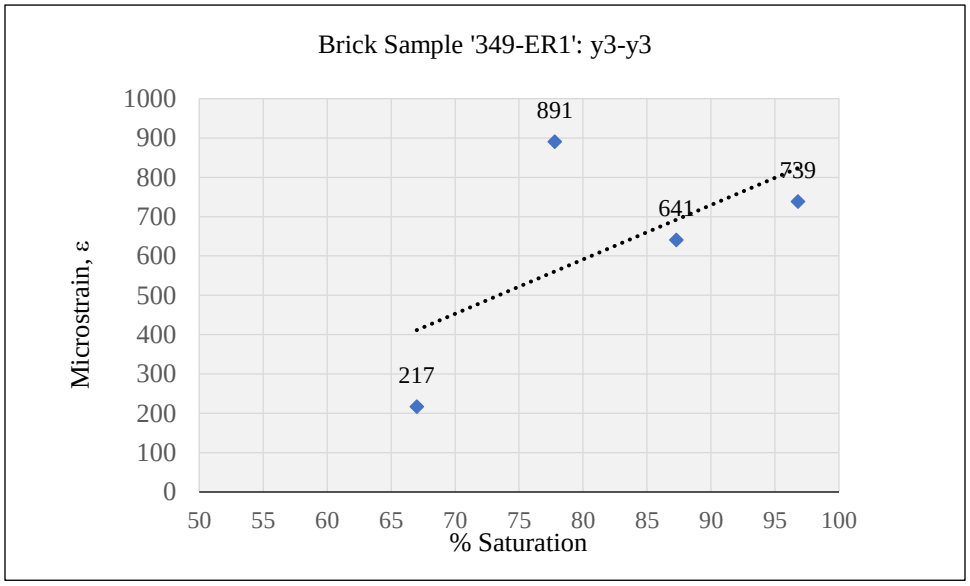

APPENDIX A 70: STRAINS ALONG THE Y3-Y3 AXIS

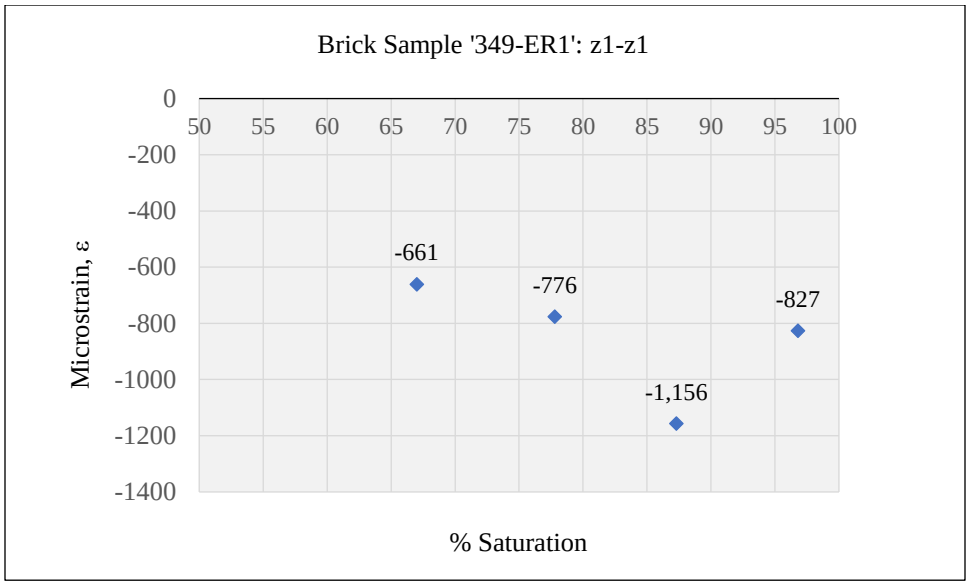

APPENDIX A 71: STRAINS ALONG THE Z1-Z1 AXIS

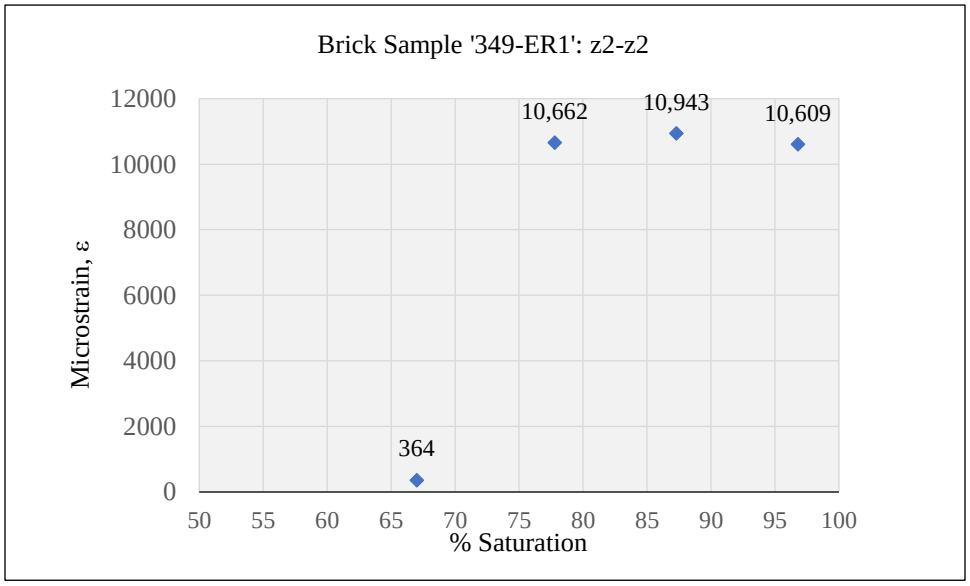

APPENDIX A 72: STRAINS ALONG THE Z2-Z2 AXIS

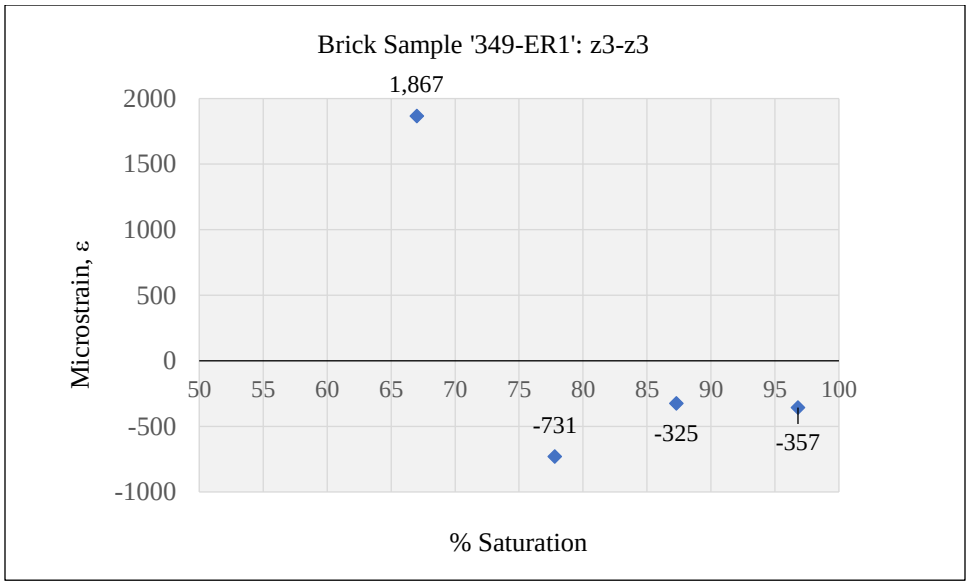

APPENDIX A 73: STRAINS ALONG THE Z3-Z3 AXIS

APPENDIX B – LENGTH MEASUREMENTS OF SPECIMENS

B 1 IN THE DRY STATE, BEFORE BEING SUBJECTED TO FREEZE-THAW CYCLES

TABLE 13: LENGTH MEASUREMENTS ALONG DIFFERENT AXES (BRICK SAMPLES ARE IN THE DRY STATE)

Brick nomenclature	X-axes (mm)				Y-axes (mm)				Z-axes (mm)				Average		
	x1-x1	x2-x2	x3-x3	x4-x4	y1-y1	y2-y2	y3-y3	y4-y4	z1-z1	z2-z2	z3-z3	z4-z4	x-avg	y-avg	z-avg
295C-F2	79.586	82.491			98.228	97.614	98.265		62.950				81.038	98.035	62.950
309-EF2	80.835	77.246			94.391	93.850	96.238		62.968	63.840			79.040	94.826	63.404
60	77.986	79.832	78.051	76.093	92.693	93.087	92.607	93.018	57.200	60.063	57.035	59.365	77.990	92.851	58.416
305-EB4	67.815	68.065	67.765	68.018	96.334	96.434	96.618	96.503	62.363	63.560	63.978	62.910	67.916	96.472	63.203
295A-EB3	82.919	83.232	84.790	83.697	100.867	100.612	100.582	100.582	63.663				83.660	100.661	63.663
297-EB2	58.168	58.583	57.910	58.783	100.303	100.016	99.953	100.061	67.363	67.388	67.535		58.361	100.083	67.428
295A-F4	59.960	59.215	59.133	58.225	99.408	99.261	99.793	99.614	55.685	54.915	54.963	55.408	59.133	99.519	55.243
349-ER1	60.155	60.003	60.463		91.955	91.676	92.031		60.530	60.493	61.585		60.207	91.887	60.869

B 2 AFTER THE FIRST SET OF FREEZE THAW CYCLES

TABLE 14: LENGTH MEASUREMENTS ALONG DIFFERENT AXES (AFTER THE FIRST SET OF FREEZE-THAW CYCLES)

Brick nomenclature	X-axes (mm)				Y-axes (mm)				Z-axes (mm)				Average		
	x1-x1	x2-x2	x3-x3	x4-x4	y1-y1	y2-y2	y3-y3	y4-y4	z1-z1	z2-z2	z3-z3	z4-z4	x-avg	y-avg	z-avg
295C-F2	79.507	82.399			98.196	97.616	98.187		62.553				80.953	98.000	62.754
309-EF2	80.874	77.224			94.417	93.878	96.168		62.815	64.438			79.049	94.821	63.626
60	78.049	79.782	78.046	75.997	92.706	93.135	92.732	93.036	57.085	60.035	57.363	59.290	77.969	92.902	58.443
305-EB4	67.833	68.058	67.685	67.840	96.401	96.394	96.623	96.686	62.408	63.208	63.890	62.858	67.854	96.526	63.091
295A-EB3	83.002	83.234	84.876	83.671	100.935	100.686		100.630	63.683				83.696	100.750	63.740
297-EB2	58.188	58.563	57.830	58.663	100.429	100.055	99.999	100.140	67.355	67.230	67.453		58.311	100.156	67.346
295A-F4	59.963	59.155	59.228	58.603	99.623	99.359	99.805	99.697	55.658	54.985	54.508	55.438	59.237	99.621	55.147
349-ER1	60.185	59.360	60.083		92.066	91.675	92.051	92.125	60.490	60.515	61.700		59.942	91.979	60.902

B 3 AFTER THE SECOND SET OF FREEZE THAW CYCLES

TABLE 15: LENGTH MEASUREMENTS ALONG DIFFERENT AXES (AFTER THE SECOND SET OF FREEZE-THAW CYCLES)

Brick nomenclature	X-axes (mm)				Y-axes (mm)				Z-axes (mm)				Average		
	x1-x1	x2-x2	x3-x3	x4-x4	y1-y1	y2-y2	y3-y3	y4-y4	z1-z1	z2-z2	z3-z3	z4-z4	x-avg	y-avg	z-avg
295C-F2	79.509	82.376			98.200	97.624	98.127		62.538				80.943	97.984	62.736
309-EF2	80.927	77.229			94.414	93.884	96.153		63.088	64.440			79.078	94.817	63.764
60	78.032	79.766	78.078	75.990	92.704	93.133	92.595	92.999	57.303	60.003	57.330	59.308	77.967	92.858	58.486
305-EB4	67.783	68.063	67.583	67.850	96.400	96.373	96.713	96.685	62.385	63.325	63.883	63.408	67.819	96.543	63.250
295A-EB3	83.000	83.238	84.889	83.866	100.949	100.712		100.684	63.665				83.748	100.782	63.718
297-EB2	58.208	58.563	57.815	58.730	100.427	100.054	100.005	100.151	67.338	67.265	67.465		58.329	100.159	67.356
295A-F4	59.833	59.155	59.160	58.515	99.463	99.334	99.885	99.696	55.663	54.915	54.465	55.263	59.166	99.595	55.076
349-ER1	60.185	60.005	60.258		92.003	91.730	92.113		60.483	61.138	61.540		60.132	91.994	61.053

B 4 AFTER THE THIRD SET OF FREEZE THAW CYCLES

TABLE 16: LENGTH MEASUREMENTS ALONG DIFFERENT AXES (AFTER THE THIRD SET OF FREEZE-THAW CYCLES)

Brick nomenclature	X-axes (mm)				Y-axes (mm)				Z-axes (mm)				Average		
	x1-x1	x2-x2	x3-x3	x4-x4	y1-y1	y2-y2	y3-y3	y4-y4	z1-z1	z2-z2	z3-z3	z4-z4	x-avg	y-avg	z-avg
295C-F2	79.443	82.380			98.222	97.597	98.174		62.460				80.912	97.998	62.681
309-EF2	80.884	77.204			94.421	93.834	96.236		62.608	64.378			79.044	94.830	63.493
60	78.029	79.767	78.045	75.986	92.658	93.034	92.412	93.223	57.688	59.368	57.318	59.318	77.957	92.832	58.423
305-EB4	67.753	68.063	67.588	67.860	96.409	96.403	96.630	96.655	62.363	63.208	63.858	63.455	67.816	96.524	63.221
295A-EB3	82.992	83.137	84.887	83.850	100.943	100.721		100.689	63.613				83.717	100.7843	63.671
297-EB2	58.185	58.583	51.063	58.735	100.436	100.077	100.023	100.156	67.313	67.230	67.535		56.641	100.173	67.359
295A-F4	59.960	59.103	59.160	58.563	99.602	99.325	99.896	99.660	55.668	54.983	54.463	55.408	59.196	99.621	55.130
349-ER1	60.135	60.015	60.203		92.120	91.724	92.090		60.460	61.155	61.565		60.094	92.045	61.060

B 5 AFTER THE FOURTH SET OF FREEZE THAW CYCLES

TABLE 17: LENGTH MEASUREMENTS ALONG DIFFERENT AXES (AFTER THE FOURTH SET OF FREEZE-THAW CYCLES)

Brick nomenclature	X-axes (mm)				Y-axes (mm)				Z-axes (mm)				Average		
	x1-x1	x2-x2	x3-x3	x4-x4	y1-y1	y2-y2	y3-y3	y4-y4	z1-z1	z2-z2	z3-z3	z4-z4	x-avg	y-avg	z-avg
295C-F2	79.426	82.333			98.192	97.626	98.249		62.388				80.880	98.022	62.624
309-EF2	80.702	77.416			94.426	93.821	96.221		62.503	64.983			79.059	94.823	63.743
60	78.03	79.740	78.033	75.975	92.642	93.036	92.404	92.988	57.685	59.385	57.163	59.285	77.945	92.768	58.379
305-EB4	67.8325	68.065	67.583	67.708	96.415	96.424	96.718	96.673	62.338	63.185	63.855	63.458	67.797	96.558	63.209
295A-EB3	82.994	83.126	84.888	83.659	100.898	100.71		100.742	63.610				83.667	100.783	63.669
297-EB2	58.21	58.563	57.865	58.74	100.446	100.089	100.007	100.182	67.355	67.233	67.510		58.344	100.181	67.366
295A-F4	59.94	59.213	59.33	58.538	99.59	99.333	99.891	99.687	55.038	54.980	54.455	55.385	59.255	99.625	54.964
349-ER1	60.088	59.960	60.18		92.109	91.711	92.099		60.480	61.135	61.563		60.076	92.040	61.059

B 6 AFTER THE FIFTH SET OF FREEZE THAW CYCLES

TABLE 18: LENGTH MEASUREMENTS ALONG DIFFERENT AXES (AFTER THE FIFTH SET OF FREEZE-THAW CYCLES)

Brick nomenclature	X-axes (mm)				Y-axes (mm)				Z-axes (mm)				Average		
	x1-x1	x2-x2	x3-x3	x4-x4	y1-y1	y2-y2	y3-y3	y4-y4	z1-z1	z2-z2	z3-z3	z4-z4	x-avg	y-avg	z-avg
295C-F2	79.436	82.344			98.238	97.637	98.586		62.085				80.890	98.154	62.335
309-EF2	80.855	77.171			94.445	93.959	96.228		62.388	64.360			79.013	94.877	63.374
60	78.037	79.776	78.028	75.973	92.697	93.13	92.701	92.998	57.685	59.98	57.205	59.255	77.954	92.882	58.531
297-EB2	58.188	58.560	57.81	58.688	100.429	100.064	100.001	100.148	67.335	67.235	67.485		58.311	100.161	67.352

REFERENCES

Anderson, L. M. (1999). Spalling brick—Material, design or construction problem? *Journal of Performance of Constructed Facilities*, *13*(4), 163–171.

Brocken, H. J. P. (1998). Moisture transport in brick masonry: the grey area between bricks, (1998), 172. https://doi.org/10.6100/IR519159

Charola, A. E., & Wendler, E. (2015). Editorial Note. *Restoration of Buildings and Monuments*, *21*(1), 55–65. https://doi.org/10.1515/rbm-2015-0006

Chen, Z., Chen, H., Li, J., Li, H., & Ma, W. (2019). Study on the Changing Rules of Silty Clay's Pore Structure under Freeze-Thaw Cycles. *Advances in Civil Engineering*, *2019*. https://doi.org/10.1155/2019/7493872

Crawford, C. B. (1984). Frost durability of clay bricks - Evaluation criteria and quality control. In *Proceedings of the CBAC/DBR Manufacturer's Symposium*. Ottawa: NRCC.

Cultrone, G., Elert, K., Jose, M., Sebastia, E., Cazalla, O., & Navarro, C. R. (2004). Influence of mineralogy and firing temperature on the porosity of bricks, *24*, 547–564. https://doi.org/10.1016/S0955-2219(03)00249-8

Davison, J. I., & Sereda, P. J. (1978). Measurement of linear expansion in bricks due to freezing. *Journal of Testing and Evaluation*, *6*(2), 144–147.

De Kock, T., Boone, M. A., De Schryver, T., Van Stappen, J., Derluyn, H., Masschaele, B., … Cnudde, V. (2015). A pore-scale study of fracture dynamics in rock using X-ray micro-CT under ambient freeze-thaw cycling. *Environmental Science and Technology*, *49*(5), 2867–2874. https://doi.org/10.1021/es505738d

Everett, D. H. (1961). The thermodynamics of frost damage to porous solids. *Transactions of the Faraday Society*, *57*, 1541–1551. https://doi.org/10.1039/TF9615701541

Fagerlund, G. (1975). Critical degrees of saturation at freezing of porous and brittle materials. *Conf. on Durability of Concrete, ACI STP, Atlantic*, *17*, 13–65.

https://doi.org/10.14359/17604

Fagerlund, G. (1977). The critical degree of saturation method of assessing the freeze/thaw resistance of concrete. *Materials and Structures*, *10*(58), 217–229.

Funk, M. (2014). Hysteretic moisture properties of porous materials: Part II. Condensation potentials. *Journal of Building Physics*, *39*(3), 207–241. https://doi.org/10.1177/1744259114527809

Gummerson, R. J., Hall, C., & Hoff, W. D. (1980). Water movement in porous building materials-II. Hydraulic suction and sorptivity of brick and other masonry materials. *Building and Environment*, *15*(2), 101–108. https://doi.org/10.1016/0360-1323(80)90015-3

Hall, C. (1977). Water movement in porous building materials-I. Unsaturated flow theory and its applications. *Building and Environment*, *12*(2), 117–125. https://doi.org/10.1016/0360-1323(77)90040-3

Hall, C., & Hoff, W. D. (2009). *Water Transport in Brick , Stone and Concrete*. Boca Raton, Florida: CRC Press.

Hughes, R. E., & Bargh, B. L. (1982). The Weathering of Brick: Causes, Assessment and Measurement, (December).

Hutcheon, N. B., & Handegord, G. O. P. (1995). Building science for a cold climate . Institute for Research in Construction . Retrieved from http://ryerson.summon.serialssolutions.com/2.0.0/link/0/eLvHCXMwfV3JCsIwEB1cLooHV6wbAc-VmtVeFcUP8C5tk4AgPfn_OKlpLUI9hsAwSYbMy5D3BoDRXRT-3Ak8VogUtMUAM1pZzgxjVGUZS1VkpbRNtO6qhFGW4DwQresnUS4Oioo2tEQR6EfXyhGRecyZlBH1KjvlWH2Bbi2RXIbQceSCEbRMPoZ-TQxwAtuj71BNfFY

Litvan, G. G. (1973). Pore structure and frost susceptibility of building materials. In *International Symposium on Pore Structure and Properties of Materials* (p. 1132). Prague: NRCC.

Maage, M. (1984). Frost resistance and pore size distribution in bricks. *Matériaux et Construction*, *17*(5), 345–350. https://doi.org/10.1007/BF02478706

Mallidi, S. R. (1996). Application of mercury intrusion porosimetry on clay bricks to assess freeze-thaw durability - a bibliography with abstracts. *Construction and Building Materials*, *10*(6), 461–465.

Mensinga, P. (2009). *Determining the Critical Degree of Saturation of Brick Using Frost Dilatometry*. University of Waterloo. Retrieved from https://uwspace.uwaterloo.ca/bitstream/handle/10012/4638/Mensinga_Peter.pdf;sequence=1

Raimondo, M., Dondi, M., Gardini, D., Guarini, G., & Mazzanti, F. (2009). Predicting the initial rate of water absorption in clay bricks. *Construction and Building Materials*, *23*(7), 2623–2630. https://doi.org/10.1016/j.conbuildmat.2009.01.009

Ritchie, T. (1968). *Factors Affecting Frost Damage to Clay Bricks*. *Building Research Note* (Vol. 62). Ottawa. https://doi.org/10.1039/B910216G

Robinson, G. C. ., & Holman, J. R. . (1977). Relation Between Physical Properties and Durability of Commercially Marketed Brick. *American Ceramic Society Bulletin*, *56*(2), 1071–1077.

Scherer, G. W. (1999). Crystallization in pores. *Cement and Concrete Research*, *29*(8), 1347–1358. https://doi.org/10.1016/S0008-8846(99)00002-2

Straube, J., & Burnett, E. F. P. (2005). *Building Science for Building Enclosures*. Westford, Massachusetts: Building Science Press.

Straube, J., Schumacher, C., & Mensinga, P. (2010). Assessing the freeze-thaw resistance of clay brick for interior insulation retrofit projects. *Proceedings of the Performances of Envelopes of Whole Buildings XI*, 1–8. https://doi.org/10.1081/E-EEE2-120046011

Torraca, G. (2006). *Porous Building Materials* (3rd ed.). Rome, Italy: ICCROM (International Centre for the Study of the Preservation and Restoration of Cultural Property).

Uranjek, M., & Bokan-Bosiljkov, V. (2015). Influence of freeze-thaw cycles on mechanical properties of historical brick masonry. *Construction and Building Materials*, *84*, 416–428. https://doi.org/10.1016/j.conbuildmat.2015.03.077

Van Straaten, R. (2014). Improving Access To the Frost Dilatometry Methodology for Assessing Brick Masonry Freeze Thaw Degradation Risk, 79–88.

Van Straaten, R., Trainor, T., & Schumacher, C. (2016). Critical freeze/thaw saturation measurement of in-service masonry. *Thermal Performance of the Exterior Envelopes of Whole Buildings*, *2016-Decem*, 177–186.

Washburn, E. W. (1921). *Note on a Method of Determining the Distribution of Pore Sizes in a Porous Material*. https://doi.org/10.1103/PhysRev.17.273

Williams, B. E. (2015). *Assessment of Load Bearing Clay Brick Masonry for Analyzing Long-Term Durability Through Field Measurement and Visual Review*. Ryerson University.

Williams, B., & Richman, R. (2017). Laboratory dilatometry and field test to assess durability of masonry. *Journal of Building Physics*, *40*(5), 425–443. https://doi.org/10.1177/1744259116649364